Wavelength Stabilisation for High Power CO_2 Slab Waveguide Lasers using Waveguide Surface Patterning

Thesis presented for the degree of

Doctor of Philosophy

Paul A. Field

Department of Physics

Heriot-Watt University

Edinburgh

September 2001

Contents

Acknowledgements

Abstract

Bibliography

1: Introduction 9

2: RF Excited CO_2 Slab Waveguide Lasers 18

2.1 Introduction

2.2 CO_2 Laser Spectroscopy

2.3 Basic Waveguide Principles

2.4 Optical Resonators for Slab Waveguide Lasers

2.5 RF Excitation

2.6 Conclusions

2.7 References

3: Laser Wavelength Filtering Techniques 46

3.1 Introduction

3.2 Diffraction Grating Tuning

3.3 Fabry-Perot Etalons

3.4 Thin Film Coatings

3.5 Bragg Cavities DFB Lasers

3.6 Photonic Band Gap Filters

3.7 Tuning a CO_2 Slab Waveguide – A Possible Solution

3.8 Conclusions

3.9 References

4: Precision laser processing of optical filters with slab waveguide CO_2 lasers 63

4.1 Introduction

4.2 Possible construction techniques

4.3 Micro-machining workstation

4.4 Laser Beam Parameters

4.5 Shot to Shot Pointing Fluctuations

4.6 Direct Writing in Aluminium

4.7 Aluminium Removal from Pre-coated Mirrors

4.8 Machining of Laser Electrodes

4.9 Conclusions

4.10 References

5: Wavelength Selective Waveguide Transmission 88

5.1 Introduction

5.2 Material Dependence on Scattering and Reflection

5.3 Pattern Dependence on Scattering and Reflection

5.4 Incidence Angle Dependence Scattering

5.5 Horizontal Angle Dependence

5.6 Waveguide Transmission

5.7 Conclusions

6. Line Selective Slab Waveguide Laser 106

6.1 Introduction

6.2 Laser and Beam Analysing Apparatus

6.3 Wavelength Characteristics During Standard Operation

6.4 10P20 Selection in a Slab Waveguide Laser

6.5 10R20 Selection in a Slab Waveguide Laser

6.6 Conclusions

6.7 References

7: Conclusions + Further Work 130

To

My Anne and My Mum

Acknowledgements

My thanks must go to many people, I will try to list them here, but any I miss out, please accept my apologies.

Firstly thanks must go to Prof. Howard Baker and Prof. Denis Hall for allowing me to undertake this research, and to Howard for his guidance in his role as my supervisor.

Thanks must go to all the guys in the lab, to Pancho, Gavin, Paul, Cao, Jason, Adrian, Dave, Krystof and Michael, for there for frequently lightening up of the atmosphere during tense moment and making the lab an enjoyable place to be, (most of the time). Extra thanks must go to Gavin, Paul and Pancho for there help and advise when things were going well and not so well.

This leads me to the guys in the office, to Andy, Richard, Sean, Brian and Henni, thanks for anything and everything. Peter, Alan and Graeme also deserve a mention, mostly for putting up with me through many lunchtimes.

Thanks must also go to Anne, Mum and David for nagging and supporting me as I prepared this manuscript for submission. Special thanks must go to my Mum and David for patient proof reading of the final text.

Abstract

RF excited CO_2 slab waveguide lasers are now developed as compact, highly efficient, cost-effective high power laser sources, suitable for a large number of uses. However a major problem remains in that the output power, wavelength and beam shape are unstable in time, leading to restrictions in their use in high precision and wavelength dependent work.

A new method of wavelength control has been explored, using 2-D periodic patterns machined directly onto the waveguide surface of one of these lasers. These grating structures have been produced using a laser micro-machining technique which has been developed to allow for accurate and repeatable feature periodicity, along with fast prototyping. Several geometries of gratings, both one and two dimensional, have been machined from a number of materials compatible with IR hollow waveguide use, with feature spacings ranging from 80-150 μm.

Sensitive techniques developed to measure the wavelength dependent transmission of these waveguides out with a laser cavity, have shown a 2-3% loss selectivity using 50mm long patterns.

The inclusion of the two dimensional grating in the unstable resonator of an industrial slab laser device is shown to stabilise the output wavelength to the 10.59 μm transition and maintain a constant spatial mode.

Bibliography

CONFERENCE PAPERS

"Precision laser optical microstructures with slab waveguide CO2 lasers" H J Baker, G A J Markillie, P Field, Q Cao, C Janke, D R Hall, International Conference of Laser Ablation, Osaka (1999)

"Enhancement of the Micromachining Capabilities of CO_2 Planar Waveguide Lasers", F Villarreal, P R Murray, Q Cao, P A Field, G A J Markillie, H J Baker, D R Hall, ICALEO `99, San Diego

"Rapid prototyping of Refractive micro-optics using slab waveguide CO2 Lasers" H.J.Baker, G.A.J.Markillie, F. Villarreal, Q. Cao, P.R. Murray, P.A.Field, K. Nowak, C. Janke and D.R.Hall, Cleo Europe 2000

Chapter 1

Introduction

Currently CO_2 lasers are used to perform numerous tasks, from cutting metal to date stamping food packages. Wide ranges of laser configurations are manufactured, each offering different operational characteristics, some with high average powers, some with excellent beam quality, some with wavelength selection capabilities

Commercially a wide range of different CO_2 lasers is available, all with different resonator geometries, varying beam shapes, power outputs and levels of output stability. At the lower end of the power scale are glass tube lasers with a similar resonator geometry to the first helium-neon lasers. Lasers of this type frequently allow for wavelength selection with powers ranging between 1 and 20W. These lasers are often used in a research environment as well as for the pumping of far infra red laser cavities. For extension to industrial laser power levels several glass tubes are commonly placed in series to form one resonator, with each tube electrically excited individually. Such multi-tube lasers are commercially available, often with the tubes arranged in a zig zag geometry to reduce overall laser size, capable of producing up to 1.5 kilowatts of power. These lasers are used for, among other applications, metal cutting, drilling and welding.

This multiple tube approach has several problems, they are often very large, require high voltages (several kilovolts) for gas excitation, and have limited pulsing capabilities. Various manufacturers produce RF excited Waveguide lasers, capable of addressing these issues. Products are available producing from a few tens of watts to a few kilowatts of output power. Some devices are air-cooled, others water cooled, operating

with electrical excitation of only a few hundred volts, generally in a compact device, when compared with the glass tube equivalent. These lasers often work in a pulsed mode, operating with repetition rates of up to tens of kilohertz.

Two other common types of CO_2 laser include the transversely excited atmospheric (TEA) laser and the fast flow laser. The TEA laser can produce many MW of power in a pulse of around 1μs, firing at a rate of less than 50Hz. Fast flow lasers continually move the gas mixture through the laser cavity to allow for gas cooling.

Over the past 15 years research has been carried out at Heriot-Watt University in the field of RF excited CO_2 slab waveguide lasers. This work has led to numerous advancements in this patented [1.1,1.2] laser technology. The research undertaken has led to commercially available lasers, produced by Rofin-Sinar, Coherent and Lumonics, with output powers from 100W to 4KW [1.5], excellent beam quality ($M^2 < 1.2$ [1.6]) and very long working lifetimes. This design of laser has found numerous uses in both industry and research applications.

These lasers are now very compact devices capable of delivering multi-kilowatt output powers with a high beam quality. For their size, larger output powers can be obtained with the slab geometry compared with more traditional designs, as power is dependent upon the area of the device, not the length. The use of RF excitation allows for larger stable regions of discharge, enabling greater areas to be used and consequently higher power levels.

A hybrid resonator design is now used in these devices. In the waveguide direction the cavity is formed by two plane mirrors and light guided through a waveguide. In the other direction, the lateral direction, an unstable resonator is employed. If a positive branch resonator is used then a large proportion of the waveguide gain volume is used, if a negative branch is utilised then the cavity is relatively insensitive to misalignment.

The edge coupled output from the laser is rectangular in shape, which is considered undesirable when compared to a circular Gaussian beam available from many glass tube lasers. To overcome this problem a set of circularising optics has been developed which allows for a Gaussian beam of very high quality to be produced.

Other advances within the university have led to the development of array lasers, producing numerous output beams with an total power in excess of 2kW[1.3]. In addition super pulsing has now been demonstrated by the slab waveguide laser, producing 2.5-3.5 kW in a pulse of duration 12-120 μs [1.4].

However accomplished these laser systems are, the majority of devices are still unable to operate consistently on a single line. They generally scan around in operating wavelength and mode in a characteristic way for each laser device, often referred to as the laser signature. The CO_2 molecule is capable of emitting radiation at many discrete wavelengths between 8 and 18 μm. More commonly the CO_2 molecule is used to produce many wavelengths between 9 and 12 μm with transitions occurring in the regular band of the molecular spectrum. The line at which the laser operates depends upon a combination of the gain available in each of these transitions and the length of the cavity. When the laser oscillator switches to resonate at another wavelength this can

often be linked to a change in the beam mode/shape. This can lead to a number of undesirable effects when the laser is used for machining:

- poor beam quality: the optics used to circularise the beam emitted from the laser are specifically aligned for one laser output mode, if the signature of the laser scans to another mode the output beam from the circularising optics will change. The quality (M^2) of the beam may be reduced, a non-circular spot may be produced or the direction of the output beam could be altered. This could lead to pointing errors and spot size alterations, causing errors in micro-machining systems or holes being drilled with incorrect diameters.

- change in wavelength: many cutting/welding operations are wavelength dependent, more so in polymers than metals, where a small change in emitted wavelength can have a significant change in absorption.

- change in power: as the mode changes, the power is also likely to change, in a machining process this could lead to an increased/decreased removal of material.

- change in polarisation: as the mode changes the polarisation of the output beam can switch, possibly leading to a decreased transmission through an optical path and subsequently less power reaching the work piece.

In many applications this signature scanning is of little significance:

- many uses of these lasers involve cutting, keyhole welding or drilling of metals which is generally unaffected by signature scanning. In these applications power levels used are often several times higher than need be, thus the drop in power associated with signature scanning is unlikely to cause the process to fail. Metals are generally highly reflective at the operating wavelengths of CO_2 (thus high power levels are required to machine such materials), a small change in wavelength has little or no effect on the absorption. If very exact cuts are required as in micromachining, then change in beam shape may be undesirable; on larger scale metal cutting, e.g. car body parts, it is unlikely that beam mode changes would cause the work piece to be cut out with tolerances.

However there are applications where this signature scanning is of great importance:

- drilling blind holes (i.e. not all the way through a material), where depth is dependent upon power, could be adversely effected by power/wavelength variations.

- via drilling in printed circuit board (PCB) has to be very accurately controlled. A drop in power or directional pointing error could cause a hole in a PCB to be too deep, not deep enough or in the wrong place, which could cause an entire product to fail.

- a pointing error in a marking machine could cause characters to be misrepresented; an "E" may appear as a "F".

- if cutting polymers, a slight variation in wavelength can lead to a significant variation in absorption, thus if the polymer were being cut it may only by marked, or if the product were being marked then a change in wavelength/power could lead to that product being cut.

This thesis aims to address some of these issues as part of the Engineering and Physical Sciences Research Council's, Second Generation of Slab Lasers Project. As well as being supported by the EPSRC this work has been supported by sponsorship from ROFIN-SINAR UK Ltd, one of the manufacturers of the CO_2 slab waveguide laser, who hope to produce lasers with greater output mode stability.

We propose to introduce a filter into the aluminium waveguide wall of a CO_2 slab waveguide laser. This will cause the laser resonator to oscillate on one particular wavelength and correspondingly one particular output mode. This could open up new application avenues for the Slab Waveguide Laser, especially where precision and repeatability is critical.

Several designs of CO_2 laser can have some degree of wavelength selection/mode control incorporated into them; many of them incorporate a grating in place of one of the resonator mirrors. The CO_2 slab waveguide laser has curved mirrors at both ends and inclusion of a grating on one of these curved surfaces would not only be very hard to achieve but be prohibitively expensive. Any grating on these mirrors would have to be able to cope with the high power densities present in this design of laser, again adding to the cost.

Any solution to this wavelength stabilisation problem would be required to meet a number of criteria. It must be able to be easily incorporated into an existing manufacturing process, ideally providing a low cost solution, without requiring increased accuracy for cavity alignment. The effect of these filters would have to be great enough to fix the cavity to one wavelength, without a dramatic reduction in output power.

To realise our proposed optical filters, we will incorporate a grazing incidence two-dimensional grating, not into the mirrors, but in one of the walls of the waveguide. This will allow for wavelength stabilisation, and thus mode control, by favouring transmission through the waveguide at certain wavelengths.

This approach can be compared with research carried out in many other fields of work. If reflections vertically across the cavity are considered, this filter could be thought of as a three dimensional crystal lattice, allowing comparison in both the field of crystallography and photonic band gap structures [1.7,1.8,1.9]. Without considering such reflections, comparisons can be drawn with two-dimensional photonic band gap structures [1.11] and with some aspects of solid state waveguide lasers in particular with distributed feedback (DFB) [1.11,1.12] lasers.

In order to allow for rapid prototyping of many different filter designs, altering size, pattern and material, a laser micro-machining rig will be designed and constructed. This rig, described more in chapter 4, utilises the high beam quality and the high repetition rate of a commercially availableCO_2 slab waveguide laser, to produce patterns in a

number of different materials. One and two-dimensional gratings will be produced in aluminium, ceramic, quartz glass and silica, with feature sizes ranging from 20-50 μm, and periods of between 80 and 150 μm. Gratings produced by this rig will be used to determine, initially, if the proposed filters will indeed have some degree of wavelength dependence on transmission; and once this is established what pattern, materials, feature sizes should be used to produce a filter for inclusion within a laser cavity. Chapter 5 contains details of the experiments carried out to determine these parameters

The final filters constructed for inclusion into the laser cavity will be produced directly in aluminium, in one of the walls of the waveguide. Two filters will be designed, the first aiming to lock the laser to its fundamental mode (10P20) of operation and the second to cause the laser to operate at another wavelength, the 10R20 mode, this is discussed in greater detail in chapter 6.

1.1 REFERENCES

1.1 US Patent no. 4,719,639 "Carbon dioxide slab laser" Inventor Tulip; John (Alberta, CA) Jan 1987

1.2 US Patent no. 5,123,028 "RF Excited CO2 Slab Waveguide Laser" Assignee: Coherent Inc., Palo Alto, Calif. June 1992

1.3 F.J. Villarreal, H.J. Baker, R.H. Abram, D.R. Jones and D.R. Hall "Beam Reformatting of One- and Two-Dimensional Arrays of CO_2 Waveguide Lasers", IEEE Journal of Quantum Electronics Vol 35 No 2 pp267 (1999)

1.4 F. Villarreal, P.R. Murray, H.J. Baker and D.R. Hall, "Enhanced peak power and short pulse operation of planar waveguide CO_2 lasers", Applied Physics Letters, Vol 78 No 16 2276 (2001)

1.5 ROFIN-SINAR Gmbh, Hamburg, Laser Datasheet, DC Series Lasers

1.6 H J Baker, G A J Markillie, P Field, Q Cao, C Janke, D R Hall, "Precision laser optical microstructures with slab waveguide CO_2 lasers" International Conference on Laser Ablation, Osaka (1999)

1.7 Eli Yablonovitch, "Inhibited Spontaneous Emission in Solid-State Physics and Electronics", Physical Review Letters, Vol 58 No. 20, 2059 (1987)

1.8 Greg Parker and Martin Charlton, "Photonic Crystals", Physics World, Vol 13 Issue 8, (2000)

1.9 M.M. Sigalas, C.T. Chan, K.M. Ho and C.M. Soukoulis, "Mettalic photonic band-gap materials", Physical Review B, Vol 52, No. 16, 11744 (1995)

1.10 D. Labilloy, H. Benisty, C. Weisbuch, T.F. Krauss, D. Cassagne, C. Jouanin, R. Houdre, U. Oesterle and V. Bardinal "Diffraction Efficiency and Guided Light Control by Two-Dimensional Photonic-Bandgap Lattices" IEEE Journal of Quantum Electronics Vol 35, No 7 July 1999

1.11 Han and J J Coleman, "Two Dimensional Rectangular Lattice Distributed Feedback Lasers: A Coupled-Mode Analysis of TE Guided Modes", IEEE J. of Quantum Electronics, vol. 31, pp 1947-1954, 1995

1.12 Amnon Yariv, "Quantum Electronics" 3rd Edition, Oxford University Press

Chapter 2

RF Excited CO_2 Slab Waveguide Lasers

2.1 INTRODUCTION

The carbon dioxide (CO_2) laser is one of the most widely used lasers today, offering a very high efficiency, an order of magnitude higher than for many other gas discharge lasers. A small laser can produce tens of watts where as larger examples are capable of producing hundreds of kilowatts of power in CW mode or gigawatts of power in under pulsed operating conditions. The CO_2 laser has proved to be one of the most useful and studied lasers discovered to date. Tasks performed by this laser are almost limitless in number, including date stamping, metal cutting and welding, kevlar cutting, resistor trimming, surgery, weaponry and laser fusion.

Since the CO_2 laser was first demonstrated in the 1960's many different configurations have been made and tested. The first set-up employed a traditional DC excited lasing medium held within a glass tube resonator, similar to that commonly used in helium neon lasers. Other variations of the CO_2 laser have been discussed in chapter 1.

Mercatili and Schmeltzer [2.1] first postulated waveguide lasers in 1964. They suggested utilising a small bore hollow glass tube as a waveguide containing a medium for optical amplification. The first such laser was demonstrated by Smith [2.2] in 1971, where a laser was constructed in a glass capillary tube containing a helium and neon mixture.

Since then numerous other variations of waveguide laser have been demonstrated. These have used various different waveguide geometries and excitation media. Of particular interest here slab (rectangular) waveguide geometries have been shown to produce very output powers with excellent beam quality. Excitation for these lasers has been provided by a number of amplifying media, including carbon dioxide, carbon monoxide, xenon, Nd:GLASS, & Nd:YAG.

Waveguide CO_2 lasers were first demonstrated by Bridges et al [2.3] in 1972. Their system used a 1mm diameter, 30cm long glass capillary tube. This was excited by a longitudinal DC discharge, and contained a flowing gas mixture of CO_2, He and N_2. Since then considerable work has been undertaken in the field of the CO_2 waveguide laser, changing the shape and layout of the waveguide, the resonator configurations and the excitation source. The CO_2 waveguide laser can also be operated at substantially higher pressure and exhibits significantly higher gain than more traditional CO_2 lasers

In the 1970's and 80's CO_2 waveguide construction changed from capillary tubes (initially glass and then materials with higher thermal conductivity e.g. BeO), to a square/rectangular bore geometry. This new four-sided configuration was considerably easier to manufacture, to the accuracy required for low loss optical propagation.

Transverse radio frequency (RF) excitation has largely replaced the longitudinal direct current (DC) excitation commonly used in early CO_2 waveguide lasers. This DC excitation was easily implemented for short low power devices where the voltage required to establish the E/N (ratio of electric field strength to molecular density) required for optimal laser excitation was low. Demands for increased power led to an

increase in the length of the waveguides and consequently higher voltages to maintain the E/N. This voltage could be significantly reduced if the gas mixture were excited transversely, perpendicular to the resonator optical axis. A DC discharge is not suitable for this type of excitation, owing to the small distances between cathode and anode. In this case the majority of the power would be dissipated at the cathode leading to a non-uniform excitation of the laser amplification medium. However if the amplification medium is excited by an RF (1-200MHz) supply, stability can be maintained over a wide range of operating conditions (electrode spacing and gas pressure). This allows for far larger input power densities than are attainable from DC discharges and as a consequence far narrower laser output pulses. The impedance characteristics of the RF field generated by these lasers, remove the need for ballast resistors which are required to maintain a stable discharge for DC excited lasers. This leads to a higher overall efficiency as additional power is not dissipated in heating a series of ballast resistors.

Typically RF excited CO_2 slab waveguide lasers are constructed from two polished water cooled aluminium electrodes, providing the upper and lower waveguide walls. Two insulating ceramic spacers are used to define the remaining walls. These are housed inside a vacuum box along with the resonator mirrors and mounts. The two aluminium electrodes, as well as acting as waveguide walls, provide two further functions. Firstly they provide a route to introduce the RF excitation to the amplification medium, and secondly they provide adequate diffusion cooling of the discharge. In the lasers described later in the this thesis, the laser electrodes are spaced by between 1 and 2mm. It can be shown using equation 2.15 that a spacing of this order will introduce a significant loss for modes with $m \geq 2$, but still allow the fundamental

mode (m=1), to propagate with a low loss. Therefore a waveguide with this electrode spacing will preferentially transmit the fundamental mode. Other higher order modes will be present, but these will experience higher transmission losses than the fundamental, and will generally be depleted. Many modes are able to propagate in the lateral direction, where in our case the side walls are removed and propagating modes are controlled purely by the mirror curvatures in an unstable resonator configuration, (see section 2.4).

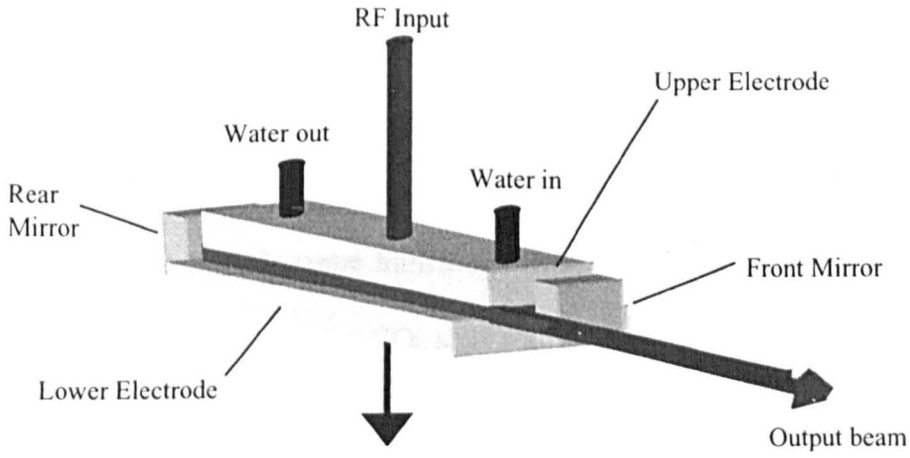

Figure 2.1 Internal Laser Schematic of a RF excited CO_2 Slab Waveguide Laser

One major advantage provided by the configuration of the RF excited slab waveguide is that the power output is proportional to the area of the electrode, rather than the length of the discharge region. This leads to the possibility of increasing power by either increasing the width or length of the discharge region. Thus power output can be increased significantly with only a small increase in overall laser size. RF excitation allows a stable and uniform discharge to be maintained whilst increasing the electrode area. An internal schematic of this type of laser is shown in figure 2.1

2.2 CO_2 LASER SPECTROSCOPY

In this section the spectroscopic processes seen in the CO_2 laser are discussed. The CO_2 laser is a molecular laser with energy transferred between different rotational-vibrational lines of the CO_2 molecule. There are over 200 allowable transitions between vibrational-rotational energy states of the CO_2 molecule, leading to photons being emitted over a wide range (from 8 μm -18μm) of wavelengths.

The majority of the possible laser transitions attainable in the CO_2 spectrum are caused by transitions in the so called regular band which are described below. However recent work at Heriot-Watt University, and previous work by Reid and Siemsen [2.4], has shown a requirement to include some transitions from the hot band region of the CO_2 spectrum in the gain spectrum of the CO_2 slab waveguide lasers used throughout this thesis. This is also described in later in this section.

The laser amplification medium of CO_2, He and N_2, used in the CO_2 slab waveguide laser is excited via an electrical discharge, which is used either directly or indirectly to raise the energy of the CO_2 molecule to the 001 state as shown in figure 2.2.

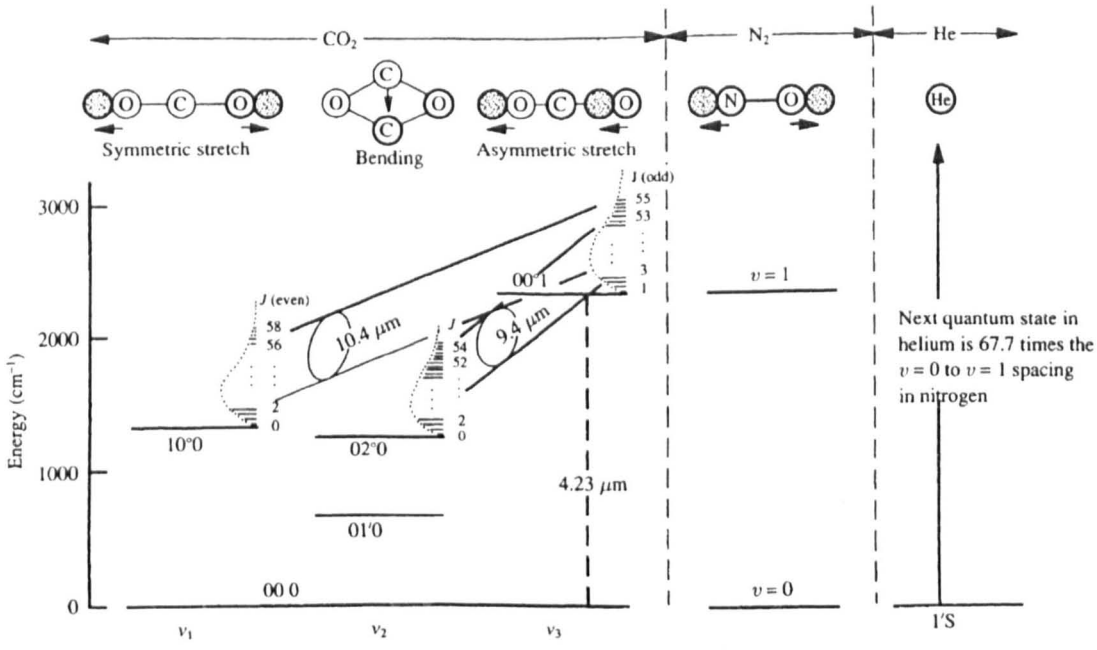

Figure 2.2 Energy Diagram for the Laser Amplification Medium in CO_2 Laser showing the Regular Bands only[2.5]

There are three main means of reaching this excited upper lasing level. The first is achieved by direct electron collision with the CO_2 molecule, the second by transfer from the v=1 excited state of the CO molecule and the third by transfer from the v=1 state of the N_2 molecule.

Transfer of energy from the N_2 molecule provides the majority of excitation in this system. The v=1 state of N_2 is metastable, as transition directly back to the ground state is forbidden. The only way for the N_2 molecule to return to its ground state is either by transfer of energy to the CO_2 molecule or via collisions with the sidewalls. The energy of the v=1 N_2 state is within $18cm^{-1}$ of the CO_2 (001) asymmetric stretch mode. Energy is transferred according to the energy equation

$$N_2\,(v{=}1) + CO_2\,(000) \rightarrow N_2\,(v{=}0) + CO_2\,(001) - 18cm^{-1} \qquad (2.1)$$

Excitation is also provided via energy transfer from CO. Although there is no CO in the original laser amplification medium, CO_2 dissociates into CO in the discharge. As much as 50-70% [2.6,2.7] of the CO_2 dissociates into CO and O_2, during the discharge process. This remains in the laser until it either recombines to form CO_2 or the gas mixture in the laser is refreshed. The first vibrational level v=1 of CO is excited via electron impact, but it can, unlike N_2, decay back to the ground state without need for collisions with CO_2 or the cavity wall. If an excited CO molecule collides with a CO_2 molecule a transfer of energy as described in equation 2.2 occurs. The energy difference in this case is greater than that for the case of N_2, and thus pumping via CO is less effective than via N_2.

$$CO\ (v=1) + CO_2\ (000) \rightarrow CO\ (v=0) + CO_2\ (001) - 206cm^{-1} \qquad (2.2)$$

Once pumped to the 001 state the lifetime (as determined by collisions with other molecules) of the excited molecule in pure CO_2 is around 30μs, at 100 torr. However if the excited molecule is in a mixture of gases containing 3 parts He, 1 part N_2 and 1 part CO_2 at a pressure of 100torr, along with the presence of the dissociated CO, the upper state lifetime is extended by a factor of 3 to around 100μs [2.8]. In pulsed lasers the length of this upper state can lead to a delay in the switching off of the optical pulse, which can cause the optical pulses to merge. This merging effect can be reduced by increasing the pressure of the gas mixture.

Xenon is added to the gas mixture (5%) as it has been observed [2.9,2.10] to increase the laser output power and efficiency. Xenon has an ionisation potential of 12.1eV, which is lower than the other species present in the mixture, thus aiding in the production of new electrons. The presence of these electrons increases the number of

available electrons with a suitable energy to excite either the CO_2, CO or N_2 molecules required for population of the upper laser level.

The lower laser levels, the $CO_2(020)$ bending mode and the $CO_2(100)$ symmetric stretch mode quickly de-excite down to the lowest bending mode, the 010 mode. This mode however has an exceptionally long lifetime, far longer than that of the upper lasing level. This level must be depopulated for the lower lasing levels to be able to de-excite and consequently for a population inversion to be established. In order to depopulate this levels helium is added to this gas mixture. The addition of helium has two effects, firstly it de-excites the 010 level via gas collisions, and secondly it promotes thermal energy transfer to the waveguide walls. A reduction in the concentration of helium has the effect of reducing the gain as the population in the lower level builds up reducing the population inversion, and hence the gain of the laser. The addition of helium has very little effect on the lifetime of the upper lasing level [2.11], it does however, if present in sufficient quantities, reduce the lifetime of the lower levels to the order of a few μs.

The allowed transitions that occur in the CO_2 molecule during lasing are governed by the following conditions

$$\Delta v = \pm 1 \quad (\Delta v = \pm 2 \text{ can occur but are much weaker}) \tag{2.3}$$

$$\Delta J = \pm 1 \tag{2.4}$$

Where v corresponds to the vibrational level and J the rotational level. When $\Delta J = +1$ then the family of transitions is called the R branch and when $\Delta J = -1$ it is said to be the P branch. (If $\Delta J = 0$ then transitions are in the Q branch however these transitions are forbidden for the CO_2 molecule.) When transitions occur from the 001 state to the 020

the resultant wavelengths that are emitted are around 9.4 μm, this is generally referred to as the 9-micron branch. Similarly, transitions from 001 to 100 are generally referred to as the 10-micron branch as wavelengths emitted are around 10.4μm.

If a transition occurs in the 9 micron branch between say the 001, J=21 state, and the 020, J=20 state, then the line would be referred to as 9P20. The 9 signifying the 001-020 transition the P signifying $\Delta J = -1$ and the 20 being the final J state in the lower level. Similarly a transition from the 001, J=43 state to the 100, J=44 state would be referred to as 10R44.

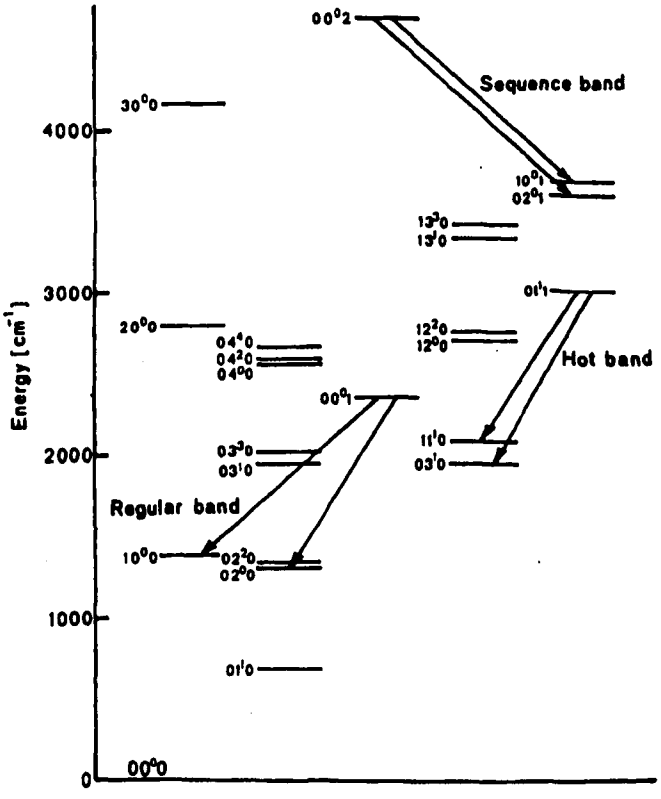

Figure 2.3 Low-lying Vibration Levels of CO2 including Regular, Hot and Sequence Bands [2.7]

Other bands of the CO_2 spectrum can also give rise to lasing, namely the hot band and the sequence band. These are shown in figure 2.3. The transitions that occur as a result

of these bands have a significantly lower gain than those in the regular band. However the wavelengths corresponding to some of these transitions match very closely to those associated with regular band transitions [2.4]. Recent work at Heriot-Watt [2.12] has produced the laser gain coefficients shown in figure 2.4, where it can be seen that there is a significant increase in laser gain at the 10.59μm, 10P20 lasing transition. This is caused by the summation of both the 10P20 line in the regular band and a line from the hot band.

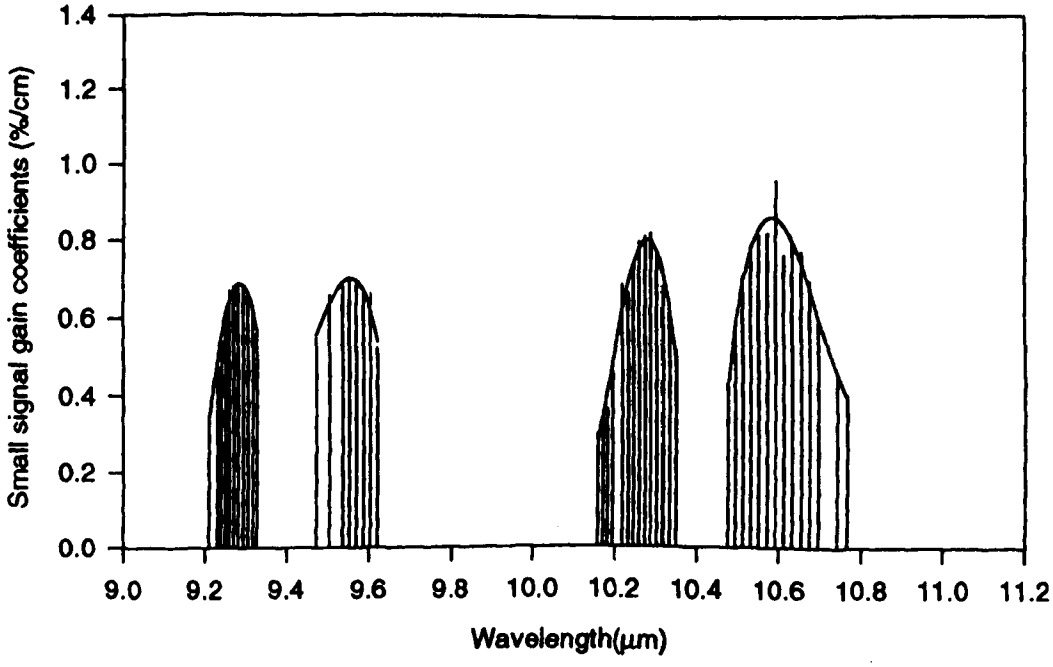

Figure 2.4, Gain of CO_2 Slab Waveguide Laser showing additional gain from Hot Band transitions [2.12]

One method commonly used to alter the operating wavelength of a CO_2 laser device is to replace the CO_2 in the mixture with a CO_2 gas containing non-standard isotopes carbon or oxygen. The available frequencies available when using alternative isotopes have been extensively researched [2.7 and references therein]. Tables of their lasing frequencies are given by Bradley et al [2.13,2.14] for the regular band transitions for nine isotopes.

It has been shown previously in this section that many lines or wavelengths can be obtained from a CO_2 laser. Generally only one line/transition is expected to lase at any one time. Once a particular transition, say 10P20, starts to lase, the upper level population available for that transition will reduce. To produce lasing, molecules excited in the upper level must release energy and transfer to the lower lasing level, reducing the population inversion and subsequently the gain. If this upper level population is not replenished then lasing on the 10P20 transition would cease as gain on other neighbouring transitions would be stronger. This is not the case. As the population inversion decreases, to maintain a steady state, energy is transferred to the upper lasing level for the 10P20 transition via elastic collisions with other excited molecules (effectively changing their "j" value). This prevents the gain for the 10P20 transition falling and reduces the gain for the states that have provided the excited molecules from which the energy has been transferred.

Each of the lines available for lasing has a frequency range $\Delta\nu$, over which it emits radiation, known as the linewidth. At the pressures of interest in this thesis the linewidth depends upon homogeneous broadening. The line shape above a gas pressure of 50 torr in a CO_2 laser is primarily defined by collisional processes, either limiting the lifetime of excited states, modulating energy levels of excited molecules or interrupting the phase of the wavefronts. All of these affect the frequency of the radiation emitted. The higher the pressure of the gas excitation media, the higher the number of collisions and consequently the broader the linewidth. The normalised line shape function of interest here is shown in equation 2.5 [2.7].

$$s(\nu-\nu_{12})=\frac{\Delta\nu_p}{2\pi}\left[(\nu-\nu_{12})^2+(\frac{\Delta\nu_p}{2})^2\right]^{-1} \tag{2.5}$$

where ν is the frequency, ν_{12} is the central line frequency, and $\Delta\nu_p$ is the pressure-broadened linewidth [2.7]. The latter is given be

$$\Delta\nu_p=7.58(\psi_{CO_2}+0.73\psi_{N_2}+0.64\psi_{He})\rho\left(\frac{300}{T}\right)^{\frac{1}{2}}MHz \tag{2.6}$$

Where T is the temperature, ψ is the fraction of gas component and ρ is the total gas pressure in torr.

Figure 2.5 shows a series of lineshapes (as described by equation 2.5) for 5 different CO_2 transitions (i.e. j values). The first (upper) line shows the gain available when not lasing, ie the small signal gain. Once lasing starts on one of the allowed resonator modes, shown by the vertical dotted lines and as described later by equation 2.9, the gain in that transition reduces. The gain continues to reduce until it reaches the loss line for the cavity, shown by the solid horizontal in figure 2.5. At this point in order to continue with steady state lasing the gain for that transition must be increased. As previously described this occurs by neighbouring transitions giving gain to that line, in effect reducing the gain for all values of j, whilst maintaining the relative magnitude of the gain between the transitions. This steady state condition, when cavity loss equals gain, is shown at t=0 in figure 2.5. Now if the cavity length begins to alter the allowed resonator modes will change, this is shown by the movement of the dotted lines to the right at t = 1,2 and 3, see equation 2.9. The frequency of the laser output has now moved further away from the peak of the first lineshape at t=1, however the gain at that

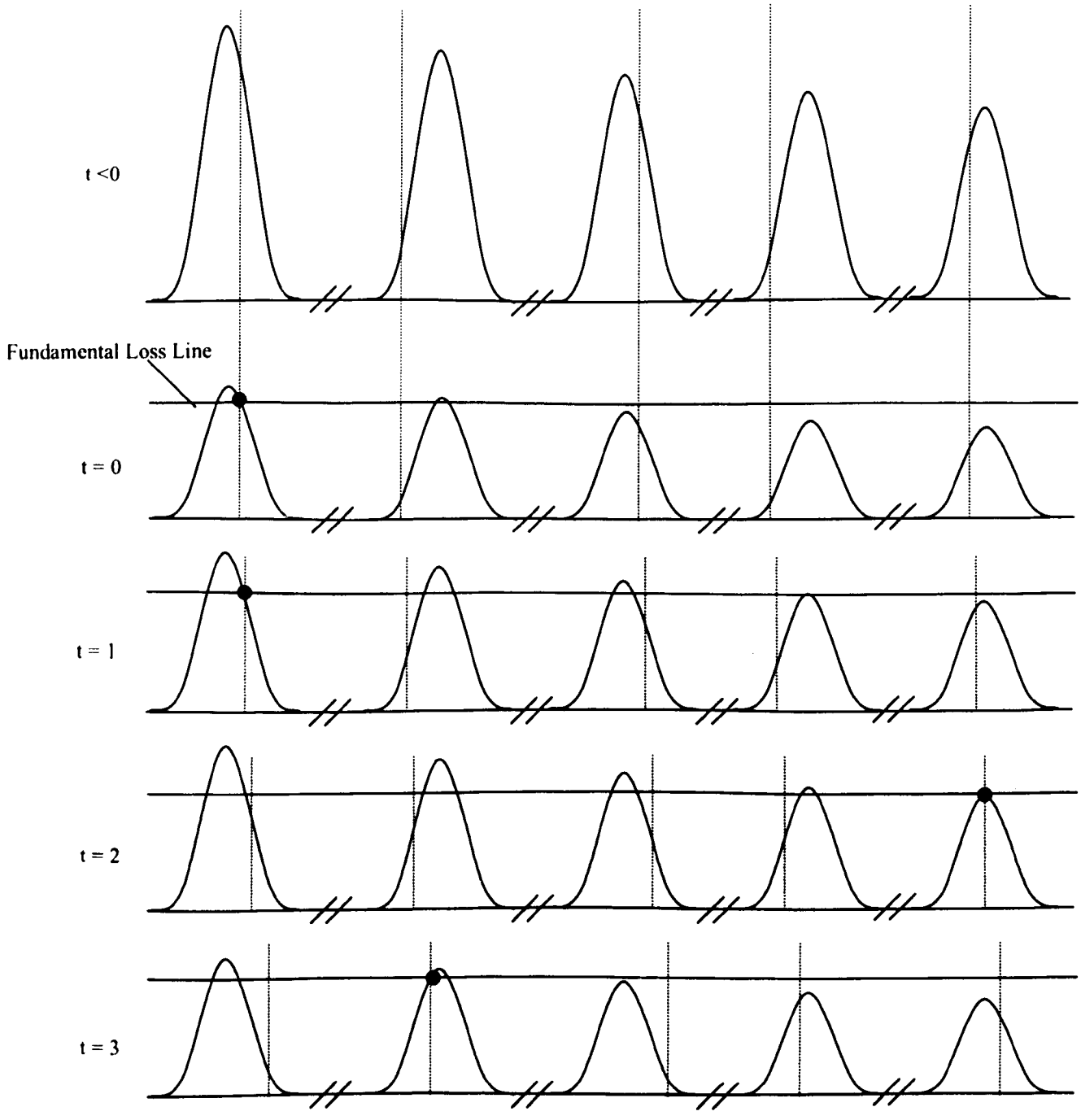

Figure 2.5 Small signal Gain vs Frequency, for t<0, and saturated gain vs frequency vs gain, at $t \geq 0$, for various CO_2 transitions at various times. Also shown are the fundamental loss lines (solid horizontal line) and the longitudinal mode positions (dotted vertical lines, shown moving to the right with time.)

point, shown by the red dot, is still higher than for any of the other resonator modes shown. Thus, the laser output is still occurring on the same transition. The gain

available to all transitions will alter (maintaining ratios between gain for all transitions) so that the gain at the laser output frequency is equal to the losses present (as shown by the loss line). By time t=2 the resonator modes have moved further to the right and the maximum gain seen by any of the transitions is seen by the right most line, again shown by the red dot. Thus lasing will cease at the first transitions and begin at the frequency of the right most transition. The laser will switch to lase on a different line. The gain available to all transitions will alter to restore a steady state, loss equal to gain. In the final time shown t=3 the maximum gain has again moved this time to the second line from the left, and the line lasing will again switch. From this it can be seen that a small alteration in gain is all that is needed to cause the laser to operate on a different line, at a different wavelength.

It is also possible for the laser to switch to operate on other lines described by higher order transverse modes, with frequencies as described in equation 2.9. This condition would occur when the highest gain available to any one of the resonator modes occurred at the loss line associated with the higher order mode as opposed to the loss line associated to the fundamental mode.

The non-sequential pattern of wavelengths (and output beam shapes) that a device scans through during the warm up process, whilst the cavity/resonator length is altering, is often referred to as signature scanning.

2.3 BASIC WAVEGUIDE PRINCIPLES

If the walls of laser cavity are such that they obstruct the standing waves of the optical resonator, then the output mode will be different from that of a free space resonator. The allowed propagating modes of this waveguiding resonator will be dependent on the shape of the cavity.

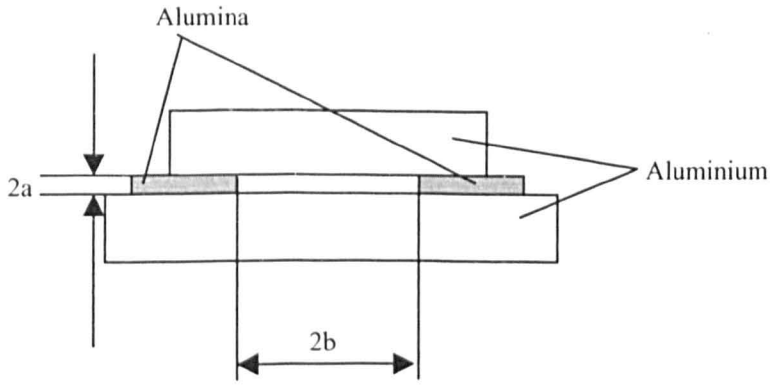

Figure 2.6 Cross Section of Slab Waveguide consisting of two aluminium and 2 alumina walls

Propagating modes allowed within waveguides can be calculated by solving the standard wave equation in free space but with dielectric boundary conditions. Instead of falling away to zero at infinity the field components are matched to the waveguide walls. Expressions for these allowed propagating modes were first calculated by Marcatili and Schmeltzer [2.1], who solved the wave equation for a hollow dielectric waveguide. In 1976, Krammer [2.15] developed similar expressions for E, the electric field and the propagation vector for a two material rectangular waveguide, as shown in figure 2.6. These expressions which were simplified by substituting a metal for one of the two materials in the rectangular waveguide, are shown in equation 2.7 [2.16]. In equation 2.7E represents the electric field amplitude in the x direction, and m and n the transverse and lateral mode numbers. These equations make use of two main

assumptions, firstly that the waveguide gap, 2a, is considerably larger than the wavelength and secondly that there is perfect reflection at the waveguide wall. Using these approximations the waveguide modes can be thought of as a set of four plane waves which propagate through the guide at a small defined angle to the waveguide axis. Two in the lateral and two in the transverse direction

$$E_{mn}(x,y) = (ab)^{-\frac{1}{2}}\left[\cos\left(\frac{m\pi x}{2a}\right)\right]\left[\cos\left(\frac{n\pi x}{2b}\right)\right]; m,n = odd$$
$$E_{mn}(x,y) = (ab)^{-\frac{1}{2}}\left[\sin\left(\frac{m\pi x}{2a}\right)\right]\left[\sin\left(\frac{n\pi x}{2b}\right)\right]; m,n = even \qquad (2.7)$$

In order for a particular device to act as a waveguide, as a general rule it must have N<1 [2.17], where N is the Fresnel number as defined below

$$N = \frac{a^2}{\lambda L} \qquad (2.8)$$

where λ is the wavelength and L is the length of the guide.

The frequency of the allowed modes in a resonator is given by equation 2.9. This is calculated from the requirement that the phase shift for a round trip of cavity length 2L is equal to an integer number times 2π, [2.16]

$$\nu_{mnq} = \frac{qc}{2L} + \frac{\lambda c}{32}\left(\frac{m^2}{a^2} + \frac{n^2}{b^2}\right) \qquad (2.9)$$

where c is the velocity of light in a vacuum and q is in the longitudinal mode number.

The propagation constants for EH_{mn} modes are expressed below [2.18]

$$\kappa_{mn} = \beta_{mn} + i\alpha_{mn} \tag{2.10}$$

where the attenuation α is given by equation 2.11 for light polarised vertically in the waveguide and equation 2.13 for light polarised horizontally. β the phase is given by equation 2.10 for both polarisations

$$\alpha_{mn} = \frac{1}{a}\left(\frac{m\lambda}{4a}\right)^2 \mathrm{Re}\left[\frac{\varepsilon_a}{\varepsilon_o}\left(\frac{\varepsilon_a}{\varepsilon_o}-1\right)^{-\frac{1}{2}}\right] + \frac{1}{b}\left(\frac{n\lambda}{4b}\right)^2 \mathrm{Re}\left[\left(\frac{\varepsilon_b}{\varepsilon_o}-1\right)^{-\frac{1}{2}}\right] \tag{2.11}$$

$$\beta_{mn} = \frac{2\pi}{\lambda}\left[1-\frac{1}{2}\left(\frac{m\lambda}{4a}\right)^2-\frac{1}{2}\left(\frac{n\lambda}{4b}\right)^2\right] \tag{2.12}$$

$$\alpha_{mn} = \frac{1}{a}\left(\frac{m\lambda}{4a}\right)^2 \mathrm{Re}\left[\left(\frac{\varepsilon_a}{\varepsilon_o}-1\right)^{-\frac{1}{2}}\right] + \frac{1}{b}\left(\frac{n\lambda}{4b}\right)^2 \mathrm{Re}\left[\frac{\varepsilon_b}{\varepsilon_o}\left(\frac{\varepsilon_b}{\varepsilon_o}-1\right)^{-\frac{1}{2}}\right] \tag{2.13}$$

where ε_a is the relative dielectric constant of the aluminium section of the waveguide, ε_b refers to the alumina side walls and ε_o the surrounding material. In this case ε_o=1 and expressions for ε_a and ε_b are given in equation 2.14.

$$\varepsilon_a = (n_a - ik_a) \qquad \varepsilon_b = (n_b - ik_b) \tag{2.14}$$

where n_a and n_b are the refractive indices, and k_a and k_b are the extinction coefficients (all positive real numbers).

In the case of the waveguide design used in this thesis, there are no side walls present. Therefore the ε_b term is zero, simplifying expressions 2.11-2.13. This type of resonator generally favours the horizontally polarised modes over the vertically polarised ones, (mainly owing to loss factors related to the metal). This allows the attenuation part of the propagation constant to be simplified to

$$\alpha_{mn} = \frac{1}{a}\left(\frac{m\lambda}{4a}\right)^2 \mathrm{Re}\left[(\varepsilon_a - 1)^{-\frac{1}{2}}\right]. \qquad (2.15)$$

2.4 OPTICAL RESONATORS FOR SLAB WAVEGUIDE LASERS

In a generic waveguide laser resonator (shown in figure 2.7) round trip losses are higher than those in a more conventional "glass tube" laser. Radiation must pass from the waveguide to a free space region (between mirror and waveguide) and back into the

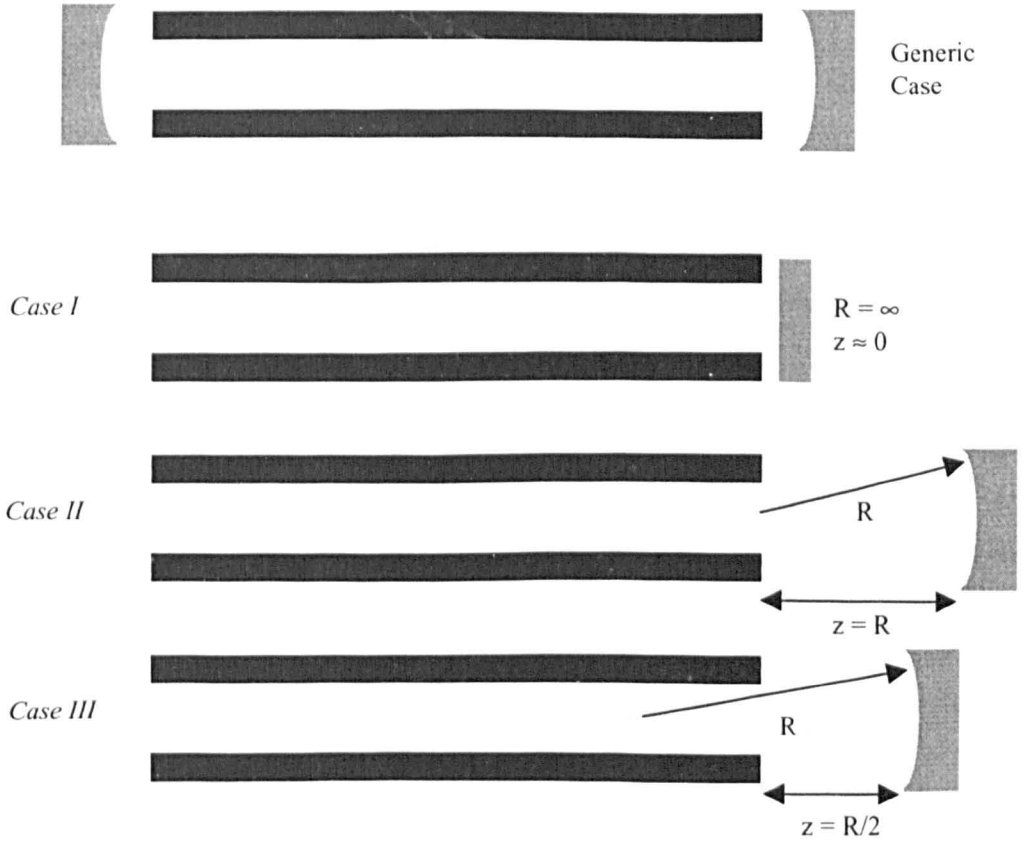

Figure 2.7 Low coupling loss resonator configurations

waveguide twice per round trip. This coupling from waveguide to free space to waveguide introduces losses into the optical system, and this is an important consideration during the optical design of a waveguide laser. Degnan and Hall [2.19] found three types of resonator which provide a means of achieving this waveguide-free

space-waveguide coupling whilst maintaining a low optical loss in the resonator. *Case I, II and III* as defined by Degnan and Hall differ in the mirror to waveguide spacing, Z, and the radius of curvature of the mirror, R, as shown in figure 2.8. A Dual *Case I* configuration is the most commonly used design as it offers the highest coupling efficiency and consequently highest power output. In the ideal case when both end mirrors are very close to the end of the waveguide the single round trip is very close to that of an undistorted guide of length 2l, (l is the waveguide length). This low loss is possible, as the light has no room to diffract or scatter from the ends of the waveguide.

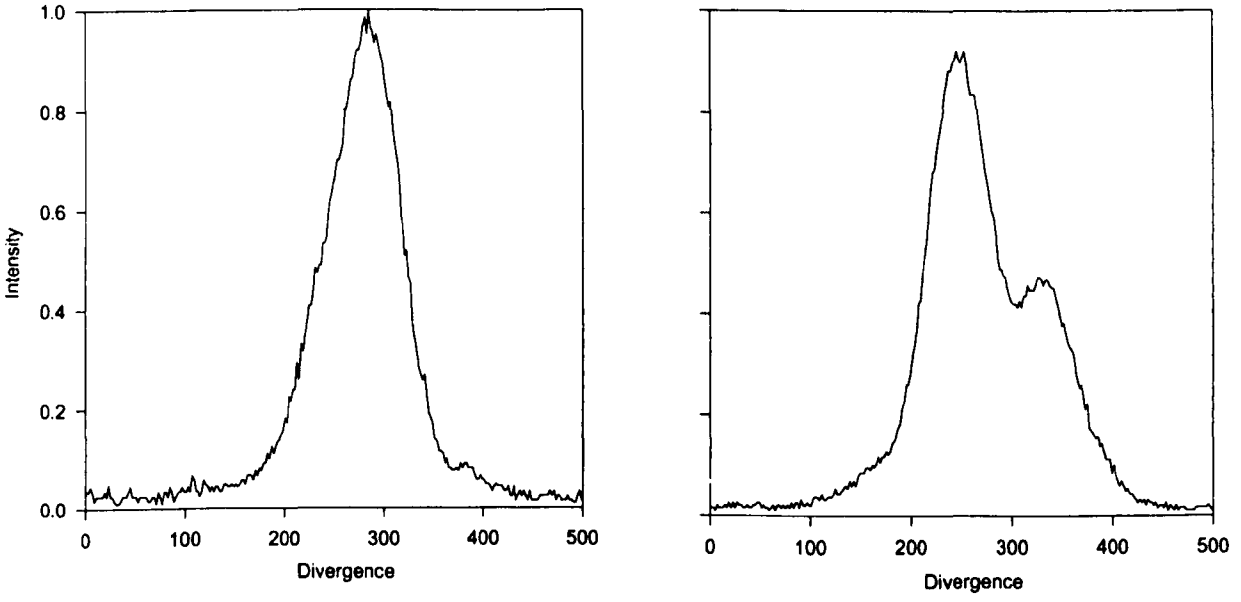

Figure 2.8 (a) & (b) Examples of far field intensity of the waveguide mode of a slab waveguide laser, showing (a) a fundamental mode and (b) fundamental mode with some higher order modes present.

Generally the resonator will be designed such that the fundamental mode is preferentially transmitted in the waveguide direction, see figure 2.8(a). This is accomplished by selecting a narrow waveguide gap (1-2mm) and by alignment of the cavity mirrors. However it is also possible that higher order modes will be present in

the cavity. A second, or subsequent, resonator mode may visibly effect the far field pattern by producing a shoulder on the plot or these may be so weak that they can only be detected by measuring the beat frequency or frequencies. An example of such a shoulder can be seen in figure 2.8 (b) which shows a beam profiles measured from the laser described in chapter 6.

In the case of a slab waveguide laser the two dimensions of the guide are very different, in lateral direction the width may be up to 100mm whereas in the transverse direction the gap is in the range of 0.3-2mm. The asymmetry allows, in the transverse direction, a waveguide mode to form and in the lateral direction, many possible modes of propagation. Consequently a hybrid resonator allowing a waveguide mode to propagate in the transverse direction and one of a number of possible modes to propagate in the lateral direction would be advantageous.

The hybrid resonator commonly used in the slab waveguide, employs a dual *Case I* type resonator in the waveguide direction, and in the lateral direction, an unstable free space confocal resonator. This confocal resonator can either be a positive (focal point outside the cavity) or negative (focal point inside the cavity) branch resonator, as shown in figure 2.9. In this case the positive or negative is determined by the product g_1g_2 where g_1 and g_2 are given by

$$g_1 = 1 - \frac{L}{R_1}$$
$$g_2 = 1 - \frac{L}{R_2} \qquad (2.16)$$

where L is the cavity length, R_1 and R_2 are the radii of the mirrors. Generally these resonators have a lower power extraction and operate with a lower efficiency than an all-waveguide resonator would, This is a result of the non-uniform flux density created in the waveguide by the unstable resonator. The waveguide gain volume is not efficiently utilised. The positive branch resonator offers a greater power extraction than the negative branch, however it is extremely sensitive to misalignment. The negative branch is relatively insensitive to misalignment but is more prone to thermal instability of the discharge as there is an intracavity focus.

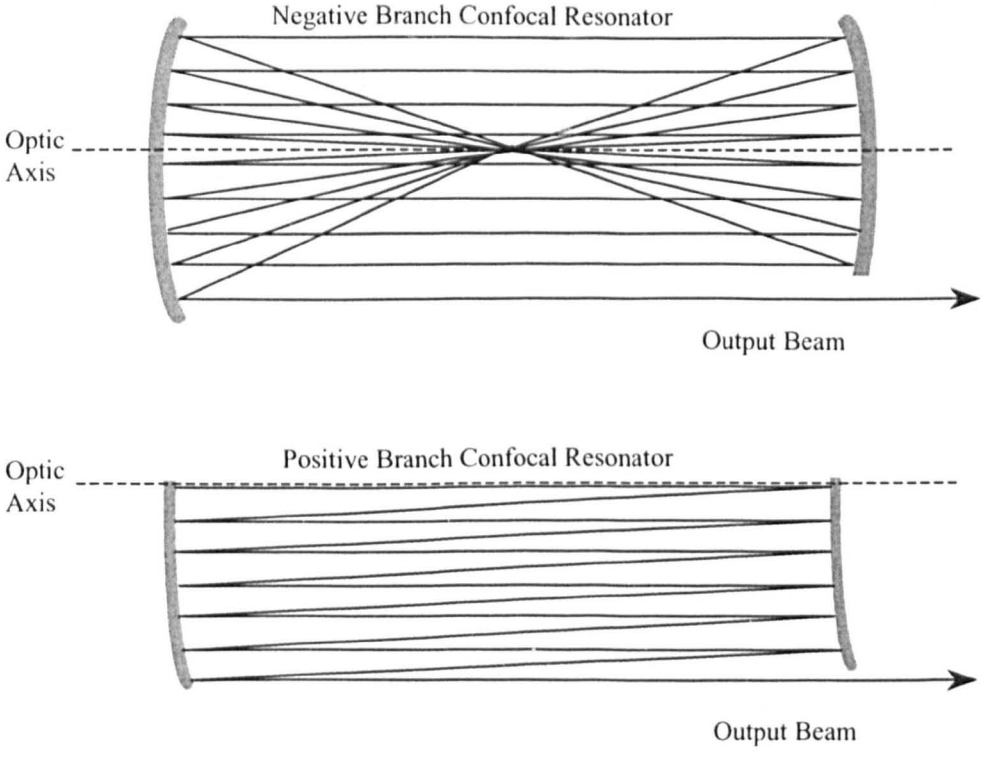

Figure 2.9 Confocal Unstable Resonators

The resonators used throughout this work have utilised a dual *case I* type resonator design in the waveguide direction, and a negative branch unstable free space confocal resonator in the lateral direction.

2.5 RF EXCITATION

As previously mentioned RF discharge pumping of a laser amplification medium has several advantages over the more traditional longitudinal DC discharge pumping. This section will outline the RF processes used in pumping of the CO_2 laser discharge.

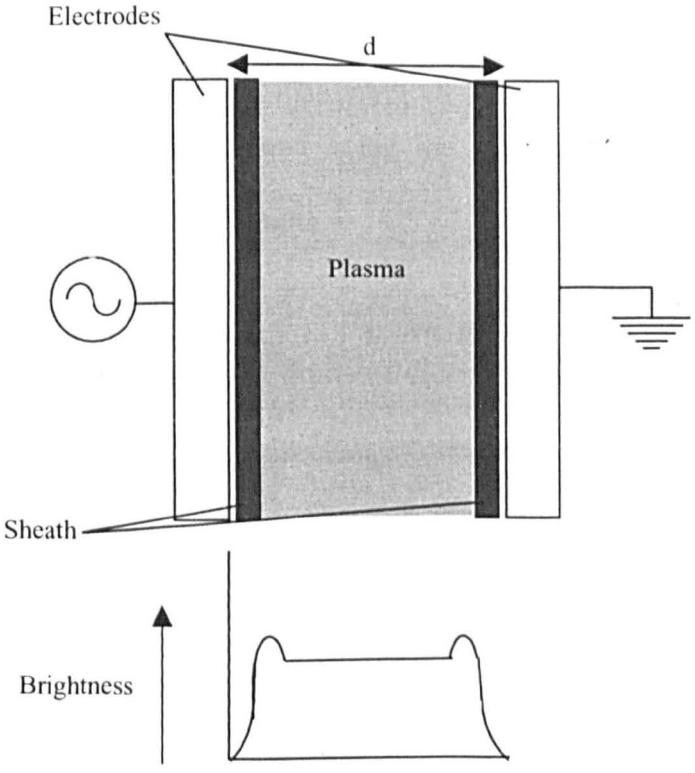

Figure 2.10 Cross section of the visible light emission from a transversely pumped alpha discharge between to parallel plate electrodes

Levitski [2.20] first recognised that there are two stable forms of RF discharge, which he named as alpha (α) and gamma (γ). These forms of discharge have both been studied for their use in exciting laser amplification media [2.21]. However as the electron energies in the γ discharge are too high for effective excitation of molecular energy levels, only the α discharge is suitable for excitation of molecular gain media lasers (i.e.

CO_2). Although unsuitable for CO_2 excitation, the γ discharge cannot be overlooked as transition from α to γ discharge demonstrates an instability in the α discharge and thus we must be understand the γ discharge mechanisms to avoid occurrence.

Figure 2.10 shows a schematic of the cross section of the visible light emitted from a transversely pumped α discharge between two parallel plate electrodes. Two differing and distinct regions can be seen. The first being the central plasma region, in which the laser excitation occurs. The second being the pair of bright regions next to each electrode referred to as plasma sheaths.

In a DC discharge electrons move from one electrode to the other. However in an AC discharge the motion of the electrons changes once every half cycle. If the frequency of the excitation, ω, current is low enough (<100kHz) electrons will continue to move from one electrode to the other before the current reverses. After the current has reversed, they will move in the opposite direction between electrodes. This low frequency case can still be modelled as having DC characteristics. However if ω is greater than say 1MHz the electrons will no longer reach the opposite electrode before the current, and consequently electrode, direction changes. Electrons towards the centre of the discharge will oscillate back and forth. This central plasma region exhibits some similar characteristics to that of a DC discharge in that it has a neutral charge, i.e. the number of positive ions is balanced out by the number of electrons. These positive ions have a considerably larger mass than the electrons and can be thought of as stationary when compared to the electrons. Resulting from this high electron mobility, electrons close to the electrodes will reach the electrodes during the half current cycle and will be lost to the excitation process. Consequently there will be a lower concentration of electrons in

the regions adjacent to the electrodes, and the positive ion sheaths shown in figure 2.3 will form. These sheath regions form a natural capacitive ballast to the highly conducting plasma in the central region and are primarily responsible for the net positive impedance characteristic of the entire transverse RF discharge [2.22]. This provides a similar stability to the RF discharge as ballast resistors do to a DC discharge.

If the power in an α discharge is raised to a critical value, a transition to a γ discharge will occur. In this case the voltage provided is high enough to break down the sheath regions. The γ discharge is similar in many ways to a DC discharge, in that it will tolerate very high power densities and is sustained by wall ionisation processes. These ionisation processes can lead to significant damage of the electrodes. In a γ discharge the boundary sheaths are very thin, and the displacement and conduction currents are far higher than for the α discharge case.

These sheaths are of particular interest in this thesis as we propose to include a grating pattern in or on the waveguide wall where these sheaths are formed. One main area of concern is whether any patterned area on the electrodes will cause a breakdown of the sheath, leading to a γ discharge. If the gratings are machined directly into the electrodes, with depths of the order of a few tens of μm, the sheath will not be effected. However if the gratings are formed by the inclusion of a secondary material, i.e. an alumina block, then the possibility of γ discharge must be assessed further.

In order to couple the power generated by the RF power supply efficiently into the laser head the input impedance of the laser head must match the that of the RF power supply, usually 50Ω. To achieve matching between supply and laser a matching circuit is

employed. This alters the magnitude of the load (laser head) impedance to that of the supply. Figure 2.11 shows the matching circuit utilised during the work reported in

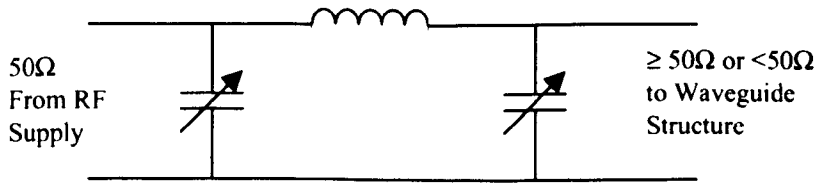

Figure 2.11 Circuit diagram for matching circuit

chapter 6 of this thesis. The circuit allows for almost any load impedance to be matched to the 50Ω supply impedance. Thus reducing any reflected power to a minimum and ensuring maximum power is transferred to the discharge region. The ability to tune the matching circuit (via variable capacitors) aids in the process of striking (lighting) of the discharge. Once matched, the RF power is fed to the waveguide structure, inside the vacuum box of the laser, via a copper feed through. This feed through is insulated from the laser casing by a ceramic disc spacer.

The electrode length is a significant proportion of the wavelength of the incoming RF power, thus the voltage across the entire length of the electrode will not be constant. This will lead to non-uniformities in the discharge, with some regions being brighter than others. In order to ensure that the discharge is homogeneous the difference in voltage applied to all parts of the electrode must be minimised. This can be achieved using resonance transmission techniques. A set of coils is placed in parallel with the capacitance of the electrode structure (i.e. between upper and lower electrodes). The inductance of this set of coils is chosen to match the requirements for parallel resonance at the frequency of the RF generator. The relationship between inductance and frequency is given in equation 2.17, where f is the RF generator frequency, and L and C

are the waveguide structures inductance and capacitance respectively of the waveguide structure.

$$f = \frac{1}{2\pi\sqrt{LC}} \tag{2.17}$$

2.6 CONCLUSIONS

Numerous variations of the RF excited CO_2 slab waveguide laser, are now commercially available, one such commercially available laser is detailed in chapter 4.

Lasers are available with widely varying output powers, from tens of Watts to several kilowatts. They are used for many purposes, from machining materials such as aluminium and kevlar, to surgery for cutting tissue and bone. The high PRF available from this laser allows it to excel in the field of high speed marking. When used in conjunction with a beam scanning system the CO_2 slab waveguide laser can produce an output similar to that produced by a dot matrix printer [2.23, 2.24].

CO_2 lasers are available that operate at wavelengths other than the fundamental lasing wavelength of 10.6μm. These alternate wavelengths are selected by using CO_2 gas with non-standard isotopes of either carbon or oxygen, and/or by using wavelength selective coatings in the mirrors. However, these lasers still are not able to operate exclusively on a single wavelength or in a single mode.

2.7 REFERENCES

2.1 E A Mercatili and R A Schmeltzer "Hollow Metallic and Dielectric Waveguides for Long Distance Optical Transmission and Lasers", Bell Syst. Tech. J. **43**, 1783 (1964)

2.2 P W Smith "A Waveguide Laser", Appl. Phy. Lett. **19**, No. 5, 132 (1971)

2.3 T J Bridges, E G Burkhardt and P W Smith, "CO_2 Waveguide Lasers", J. Appl. Phys. Lett. **20**, pp 403-405 (1972)

2.4 John Reid and Klaus J. Siemsen "Gain of High-Pressure CO2 Lasers", IEEE Journal of Quantum Electronics, Vol QE-14 No 4 (1978)

2.5 Joseph T. Verdeyen, "Laser Electronics" Third Edition

2.6 G C R Williams and A L S Smith, "Plasma Chemistry of RF Discharges in CO_2 Laser Gas Mixtures", J Phys D: Appl Phys **18**, 335 (1985)

2.7 W.J.Witterman "The CO2 Laser" Springer-Verlag

2.8 P.K.Cheo, "relaxation of CO2 Laser Levels by Collisions with Foreign Gases", IEEE J Quantum Electronics QE-4, 587 (1968)

2.9 P O Clark and J Y Wade, "The influence of Xenon on Sealed-Off CO_2 Lasers", IEEE J Quantum Electron **QE-4**, 263 (1968)

2.10 D He and D R Hall, "The influence of Xenon on Sealed-Off Operation of RF-Excited CO_2 Waveguide Lasers", J Appl Phys **56**, 856 (1984)

2.11 S De Benedictis, G Dilecce and A Raino, "Diagnostics of CO2 Radiofrequency Waveguide Laser Active Medium", J Phys D: Appl Phys **26**, 920 (1993)

2.12 F. Villereal, Q Cao, Work still to be published 2001

2.13 C Freed, L.C. Bradley, R.G. O'Donnell, IEEE J QE-6 1195 (1980)

2.14 L.C.Bradley, K.L. Soohov, C. Freed, IEEE J QE-22 234 (1986)

2.15 H Krammer "Field Configuration and Propagation Constants of Modes in Hollow Rectangular Dielectric Waveguides", IEEE J. Quantum Electronics, **QE-12**, 505 (1976)

2.16 C A Hill "Transverse Modes of Plane-Mirror Waveguide Resonators", IEEE J. Quantum Electronics **24**, No 9, 1937 (1988)

2.17 D R Hall and C A Hill "Handbook of Molecular Lasers", Ed P K Cheo (New York and London: Mercel Dekker) 3.2 (1987)

2.18 C.A. Hill "Physics and Technology of Laser Resonators" Chapter 3, Ed D.R. Hall, P.E. Jackson (Bristol: Adam Hilger) (1989)

2.19 J J Degnan and D R Hall, "Finite Aperture Waveguide Laser Resonators", IEEE J Quantum Electron **QE-9**, 901, (1973)

2.20 S M Levitskii, "An Investigation of the Breakdown Potential of a High-Frequency Plasma in the Frequency and Pressure Transition Regions", J. Sov. Phys.-Tech. Phys. No **2**, 887 (1957)

2.21 V I Myshenkov and N A Yatsenko, "Prospects for using High-Frequency Capacitive Discharges in Lasers", Sov. J. QE-**11**, 1297, (1981)

2.22 P P Vitruk, H J Baker and D R Hall, "The Characteristics and Stability of High Power Transverse RF Discharges for Waveguide CO2 Slab Lasers", J Phys D: Appl Phys **25**, 1767, (1992)

2.23 Lumonics XYMark Data Sheet

2.24 Rofin-Sinar Technologies Blazar Flexscan® Data Sheet

Chapter 3

Laser Wavelength Selection Techniques

3.1 INTRODUCTION

Many commercially available lasers can operate over a range of wavelengths. Some lasers can have their lasing wavelength altered by the user, some come pre-set to a predetermined wavelength, others alter wavelength apparently at random.

Several techniques are employed in the quest to lock a laser to one operating wavelength. Possibly the most common is the inclusion of a diffraction grating where one of the cavity mirrors would usually sit. By altering the angle of this grating it can be possible to tune the laser over a range of available wavelengths. Wavelengths can also be chosen and locked onto by varying the length of the cavity so that the length coincides with one of the resonant modes for the given wavelength. Other lasers are locked to a wavelength by applying wavelength selective coatings to internal cavity optics, only allowing certain wavelengths to propagate. Some modern semi-conductor lasers, such as DFB lasers, are now grown such that only one wavelength can be emitted,. Another more fundamental method used for wavelength tuning in gas lasers, is to vary the isotopes of the constituent gases in the excitation medium, as mentioned in chapter 2.

During this chapter we shall look at some of the techniques currently used for wavelength selection in lasers, discussing in particular whether each method would be suitable for wavelength selection in a hollow slab waveguide device.

The final section discusses a possible approach for tuning the CO_2 slab waveguide laser described in chapter 2. A few constraints have been put on to any possible solution, primarily to allow for commercial exploitation, these are listed below.

1 The resonator layout should not have to be extensively altered, keeping additional manufacturing costs to a minimum.

2 The attainable power should not drop more than say ten percent.

3 The ability to select one specific wavelength is required, and to have the laser operate only on that wavelength (i.e. wavelength stabilised.), not over a few wavelengths around a central wavelength.

3.2 DIFFRACTION GRATING TUNING

One of the most widely used methods for wavelength tuning is to incorporate a diffractive grating in place of one of the mirrors used to form the resonator cavity. Figure 3.1 shows an example of such a laser containing a Littrow grating. The Littrow

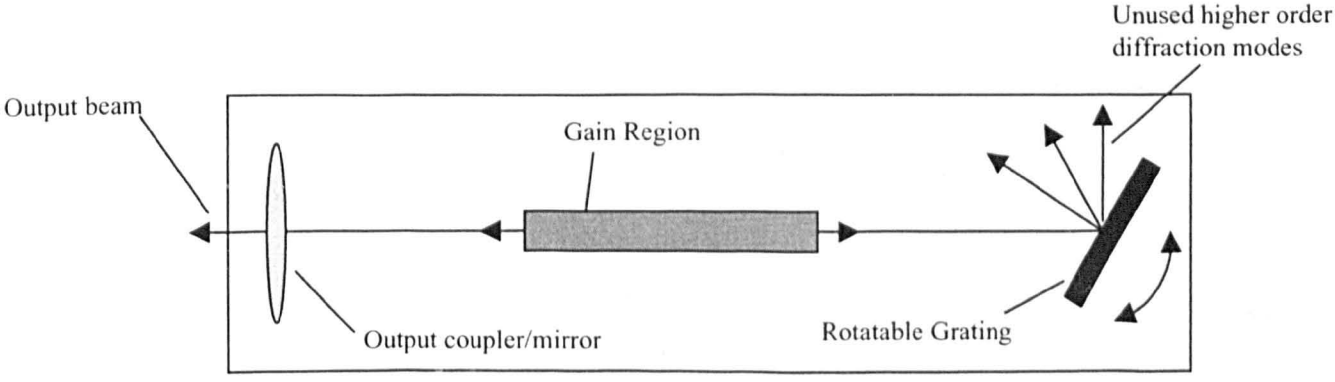

Figure 3.1 Layout of typical grating tuned laser cavity

configuration is a special case of grating where the light is reflected back towards the direction from which it came.

If monochromatic light is incident on a diffraction grating, it is diffracted into discrete modes propagating in specific directions. If each line in a diffraction grating is envisaged as a source of light (as stated by the Huygens-Fresnel diffraction principle [3.1]) light diffracted from each slit will form a diffracted wavefront. From this wavefront there exists a unique set of discrete angles from which the light from all the slits is in phase, consequently they combine constructively to form diffraction modes.

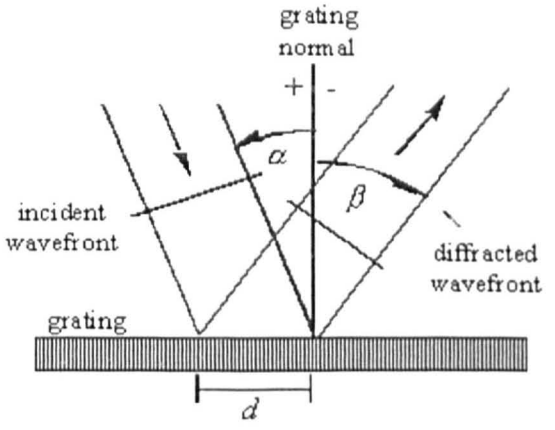

Figure 3.2 Diffracted light paths from a diffraction grating

The angle at which these diffraction modes propagate is given by equation 3.1 the grating equation [3.2]

$$\sin\alpha + \sin\beta_m = \frac{m\lambda}{d} \tag{3.1}$$

If a grating is used to replace one the mirrors in a laser cavity as in figure 3.1, the wavelength permitted to resonate in the cavity can be selected by rotating the grating. Rotation of the grating alters α in equation 3.1 and consequently β will change. At a certain input angle α, for one specific wavelength, the reflected beam will return along the same path as it entered, for a different value of α a different wavelength will be reflected back along the same path. Thus a resonant cavity will be established for just

one wavelength, all other wavelengths will encounter significant cavity losses, vastly reducing the possibility of lasing at any wavelength other than that chosen by the angle of the grating. This configuration of laser is frequently used for the design of tuneable CO_2 lasers. The Edinburgh Instrument Tuneable Lasers described later in this thesis are of this design

In 1999 Ralf Michael Hocke [3.3] incorporated a Littrow grating into an RF excited CO_2 slab waveguide laser to allow for line selection. Figure 3.3 shows his set-up Hocke used a grating in place of one of the resonator mirrors, with the first diffraction order aligned back along the waveguide and the zeroth order used to couple radiation from the resonator.

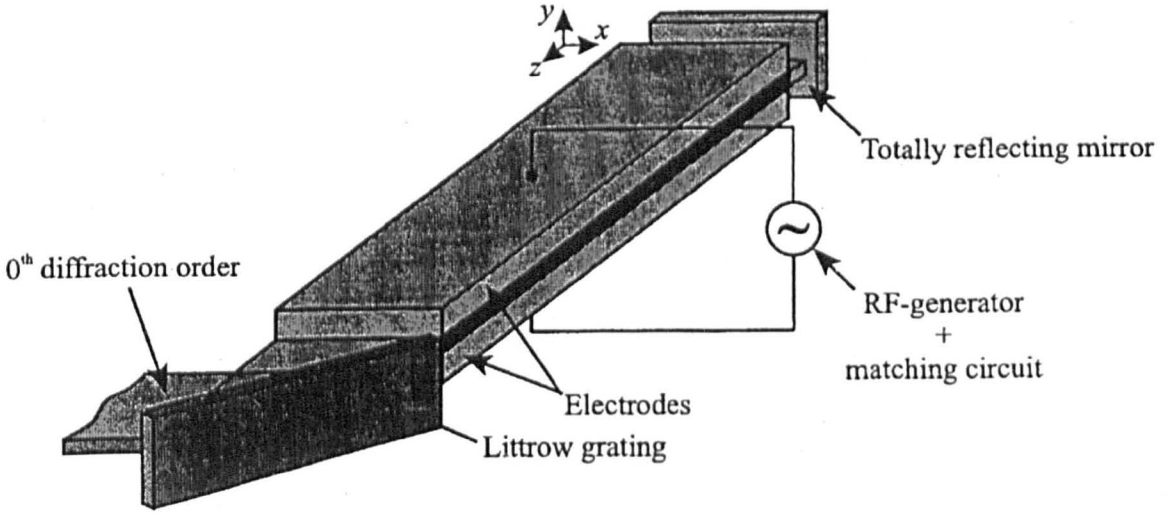

Figure 3.3 Line Selective RF-excited slab waveguide laser [3.3]

This laser was able to produce low power levels between 1 and 3 watts, on the 9P36 line of the CO_2 laser spectrum, and operated in both a stable and an unstable resonator

configuration. This work was driven by a need for a compact source for far infra-red lasers used in stratospheric experiments.

Several points should be noted about this design. Firstly for high efficiency, reflections from a diffraction grating must have their lines perpendicular to the electric field polarisation of the incoming light. To accomplish this the grating has to be orientated as shown in figure 3.3, leaving a large gap between the waveguide and the "mirror". It can be seen from section 2.4 that for low loss coupling the mirror should be very close to the waveguide. Therefore in this case coupling losses will be larger than for a generic *case I* resonator . As coupling efficiency depends upon the distance between the end reflector and the waveguide the amount of light coupled back into the guide will depend upon the position across the guide. This will lead to non-uniformities in the intensity across the guide.

Other factors also preclude the use of a grating to meet our requirements (see section 3.1). To maintain the desired unstable resonator, with the same mechanical layout, the grating would need to be constructed on a curved surface, which although possible is very costly. As well as this any grating would need to withstand the high power densities present in these devices increasing manufacturing costs. In addition the inclusion of a grating in the cavity would require significant modification to the laser tube, mirror mountings, alignment processes etc. A plain grating used in conjunction with a lens could be utilised in place of a curved grating. However this solution would also require that modifications be made to the mechanical layout of the device, and hence is unattractive.

3.3 FABRY-PEROT ETALONS

A technique often used to lock lasers to a single wavelength is the inclusion of a Fabry-Perot etalon. Fabry-Perot etalons consists of two parallel reflecting surfaces separated by a defined gap consisting of air or a suitable optical material. Such a device behaves as a narrow-band filter, the principal characteristic of which is a series of transmission peaks, dependent upon the etalon spacing, and that for most practical purposes are evenly spaced when expressed in frequency units. An etalon can be used as an optical filter in that it is capable of very high (and if necessary very narrow) peak transmission. However, the peak transmission can be degraded by absorption and scatter within thin film reflector coatings and substrates and by errors in surface flatness or parallelism.

Inclusion of an etalon within the cavity slab waveguide device as described in Chapter 2 would lead to a number of problems. Primarily the thickness, and hence transmission maxima, of the etalon seen by the incident radiation depends upon the angle with which the first surface of the etalon is struck. In an unstable resonator the angle at which light travels through the waveguide changes, depending upon which direction in the waveguide the light is travelling, see figure 2.9. Therefore if light were able to propagate in one direction through an in cavity etalon, in the other direction it would be stopped.

3.4 THIN FILM COATINGS

Thin film coatings are used in many modern applications, from anti-reflection coatings on display cabinet glass and camera lenses, to guidance systems for missiles. By applying coatings to surfaces of lenses or mirrors, the wavelength dependence of the transmission/reflection of these optics can be significantly varied. In laser cavities these coatings are used to both increase transmission at some wavelengths, and to reduce it at other wavelengths, allowing lasing at the wavelengths that are not surpressed.

Coatings are used in two CO_2 slab waveguide lasers available from Coherent. These devices operate at wavelengths of either 9.6 or 9.3μm. In the case of the 9.6μm laser, a coated mirror is used to increase the round trip cavity losses in the 10 micron band of the CO_2 spectrum, causing the strongest line in the 9 micron branch (9P20) to lase. In order to obtain the 9.3μm output the same coated mirror is used, but different isotopes of the constituent gases are used in the mixture enhancing the gain at 9R20 whilst reducing gain at 9P20. Figure 3.4 shows the reflectance curve for a coated mirror similar to those used by Coherent in their 9 micron lasers. For reference the positions of the traditional lasing lines for CO_2 are also marked.

From figure 3.4 it can be seen that mirror coating can be used to select which band of the CO_2 spectrum to lase, i.e. either the 9 or 10 micron band, but cannot select specific lines within these bands, thus making thin film mirror coating unsuitable for our particular problem. Another point to note, commonly used mirror substrates in of the CO_2 waveguide laser are aluminium or copper, neither of which readily accept coatings.

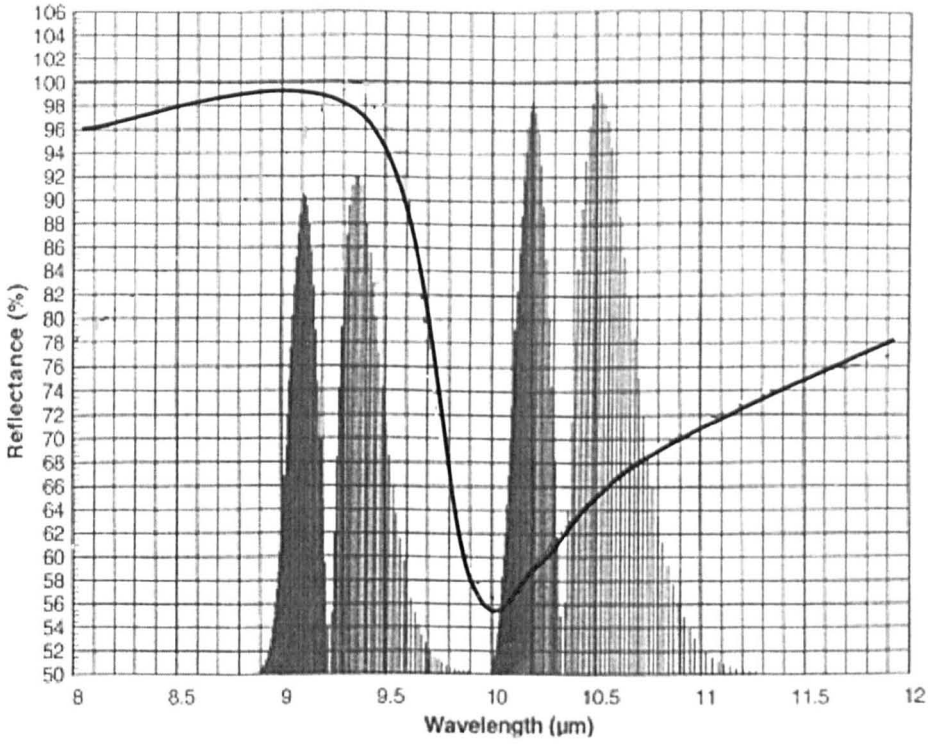

Figure 3.4 Reflectance vs. Wavelength for a coated mirror used t force a CO_2 slab waveguide laser to operate in the 9 micron band

3.5 BRAGG CAVITIES AND DFB LASERS

Bragg cavities and distributed feedback lasers employ similar resonator geometry to each other. Instead of utilising mirrors at either end of the cavity there is a stack of thin coatings, this is shown diagrammatically in figure 3.5. The main difference between a

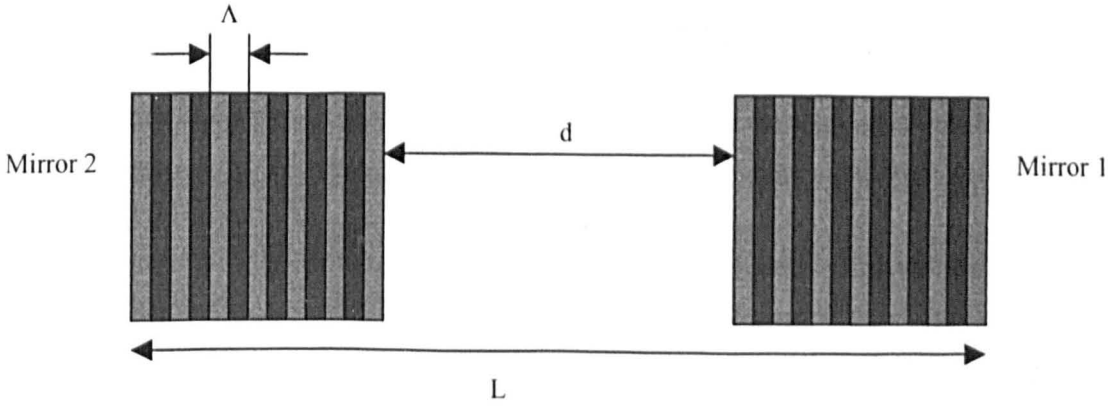

Figure 3.5 Schematic view of a distributed feedback laser

Bragg Cavity resonator and a DFB laser is that this periodic structure continues through the gain region (labelled d in figure 3.5) of the DFB device.

At each interface in the stack of thin coatings (with alternating refractive indices (see figure 3.6) a very small proportion of the incident radiation is reflected from each interface. If there are enough layers a large proportion of the light will be reflected. If the thickness of these coatings is such that the reflected rays are in phase then effectively, a very high reflectivity mirror can be formed.

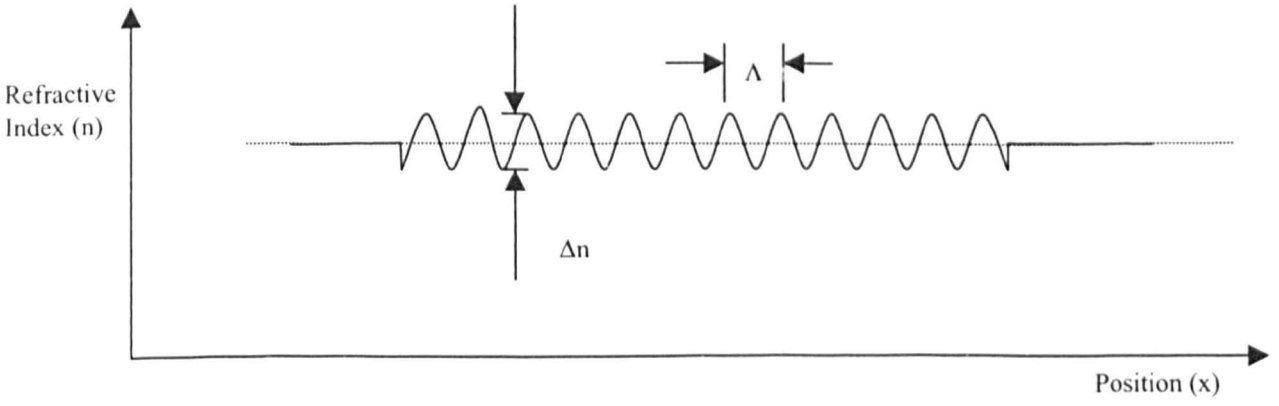

Figure 3.6 Refractive index profile in Bragg Reflector

As this feedback from a Bragg reflector is frequency selective, only wavelengths satisfying equation 3.2 can be reflected constructively

$$\Lambda = m\frac{\lambda}{2} \quad \text{with} \quad \lambda = \frac{\lambda_0}{n} \tag{3.2}$$

Where n is the index of refraction and m is an integer. Thus the permitted resonant wavelengths for any cavity can be selected during the construction of the semiconductor devices by simply altering Λ, the period of the layers.

This technology cannot be easily incorporated into the devices of interest in this thesis. Firstly any mirrors placed at the end of the resonator would be difficult to engineer, owing to the curvatures required and the need to withstand the energy densities present within this device. Secondly if a DFB laser geometry was used, a periodic medium would be required in the waveguide gap, leading to difficulties in excitation (possible γ discharge see section 2.5) and reducing the available gain area. A 1-D periodic media through the waveguiding region will also form the same directional dependence as described for Fabry-Perot etalons in section 3.3

3.6 PHOTONIC BAND GAPS FILTERS

Interest has recently been growing in the area of photonic band gap devices, especially their exploitation as filters, optical switches, laser cavities, and waveguiding devices.

The principle of photonic band gaps is best described by comparison with the movement of electrons in a crystal lattice. If an electron is moving through a lattice it will experience coulomb forces generated by the nuclei of the atoms in the crystal. This force leads to only electrons of certain energies being able to propagate through the crystal structure. Energy band gaps would form where electrons could not get through the crystal. If now instead of a crystal lattice we imagine that there is a piece of dielectric material containing a series air holes arranged in a lattice pattern, then to a

photon the refractive index changes in the dielectric caused by the air holes would be similar to the coulomb forces exerted on the electron by the nuclei. The photon would be confined to either the dielectric or the air holes, again leading to certain energy bands where no photons would be able to propagate, i.e. the so called photonic band gap. Reverting to the analogy with solid state physics, photons in the dielectric can be thought of as electrons in the valance band of an atom whereas photons in the air holes can be thought of as electrons in the conduction band.

Many groups have been investigating the use of photonic band gap devices as optical filters allowing certain frequencies to propagate whilst others are stopped or reduced. PBG devices have been constructed from a variety of different materials and in a number of different ways. The first experimental demonstration of PBG devices was in 1991 [3.4] using an array of holes drilled into a block of high index material. Since then numerous devices have been fabricated, mostly by various forms of etching [3.5, 3.6, 3.7], but also by drilling [3.4], and laser machining [3.8,3.9], in materials ranging from dielectrics to metals.

Many early PBG devices studied were considered in three dimensions, more recently two-dimensional devices contained within a waveguide have come under increased scrutiny. One example of this, which is of particular interest, is the work carried out by Krauss and De La Rue [3.10]. They have developed semiconductor waveguide devices with holes etched through the waveguiding layer as shown in figure 3.7. An optical pulse is used to excite quantum wells embedded in the waveguide, which in turn emits radiation over a large range of frequencies, some of which are coupled into the

waveguide. The transmission versus frequency of this device can then be monitored by inspecting the radiation emitted at the exit facet.

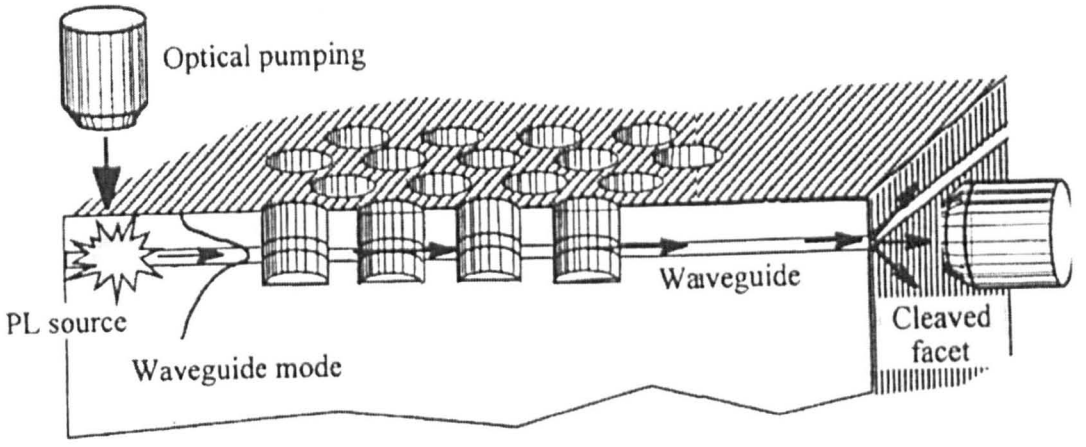

Figure 3.7 Semiconductor Waveguide with a triangular lattice of holes etched through the waveguide layer. [3.10]

The output from such a device is shown in figure 3.8 where it can be seen that there is a large region of frequencies where light cannot propagate through the waveguide.

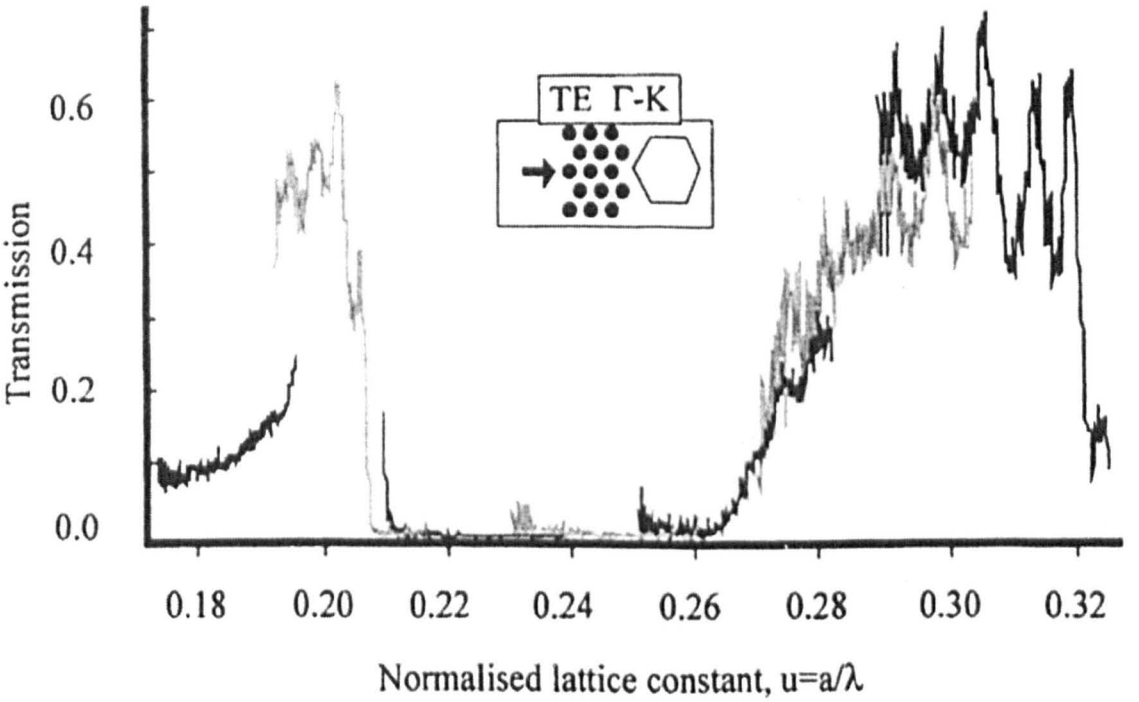

Figure 3.8 Spectral output of Waveguide shown in figure 3.7 [3.10]

Many of these PBG devices have been incorporated into waveguides, with rods, cylinders or holes spanning from one side to the other. In our CO_2 slab waveguide device the waveguide is hollow, unlike the case above, with generally only the gas mixture being present between the plates. Introducing a material between the electrodes, to form a PBG device, which projects out with the discharge sheath regions, may produce an unstable γ discharge, leading to possible electrode damage, see section 2.5. Aside from concerns with electrical instabilities, machining holes in a material to a depth of 1-2 mm (waveguide gap) with diameters of a few μm is difficult to achieve. Etching will cause the hole to spread over this depth, depth of focus issues will limit laser drilling, mechanical drilling would not be possible in this regime. Similar manufacturing difficulties would be present if rods were used in place of holes.

3.7 TUNING A CO_2 SLAB WAVEGUIDE – A POSSIBLE SOLUTION

As has been shown throughout this chapter, there are many ways to select a desired wavelength from a laser. The particular problem of interest in this work involves selecting a particular wavelength from a CO_2 slab waveguide laser.

The idea of using an in cavity device, such as the PBG devices described in section 3.6 is particularly attractive from a manufacturing perspective. If a method for wavelength selection could be incorporated internally within the waveguide, then modification of the remainder of the laser tube may be unnecessary.

As previously discussed, introducing a photonic lattice spanning the waveguide gap is undesirable. However in place of cylinders/rods bridging the waveguide, holes may be readily machined into one of the electrodes to form a lattice pattern. Such holes may have a similar effect to the radiation incident upon them as radiation passing through a photonic lattice as that described in section 3.6. Although producing a significantly smaller effect than a complete photonic band gap device, the effect may be large enough to stabilise the laser on one particular lasing line of the CO_2 spectrum, see section 2.2. The remainder of this thesis concentrates on the inclusion of these filters into a waveguide and finally into a laser cavity.

It is known that defects on the cavity wall reduce the transmission through the aluminium waveguide used in a slab waveguide laser. Including a lattice pattern or 2D grating in one of the walls introduces just such defects, thus reducing the transmission of the guide. It may however be possible to reduce this reduction in transmission at certain wavelengths by the choice of the period of the grating.

If the analogy with PBG devices is continued, maximum transmission peaks through such a device maybe be compared to the transmission through metallic filters constructed by Sigallis et al, where transmission with respect to frequency is modelled by equation 3.4 [3.11].

$$\nu_m = \frac{mc}{2d\sqrt{\varepsilon_0}} \tag{3.4}$$

where ν_m is the frequency at which the maximum transmission occurs, c is the speed of light in a vacuum and ε_0 is the dielectric constant of the material between the scatterers in the grating, in our case $\varepsilon_0=1$.

In terms of wavelength this can be rewritten as 3.5

$$\lambda_m = \frac{2d}{m} \tag{3.5}$$

Thus transmission through the patterned waveguide should be maximised for a given λ when equation 3.5 is satisfied. Note, this is the same period as for a Bragg Reflector, see equation 3.2.

It can be seen from 3.5 that the accuracy to which the period of the grating is manufactured is critical to enable the selection of the desired wavelength, thus the maximum allowable error in periodicity of these gratings which will still allow them to be effective must be known. This can be estimated by differentiating the equation for the expected transmission maximum equation 3.4:

$$\Delta\nu_m = -\frac{mc}{2d^2 n}\Delta d \tag{3.6}$$

Additionally the random variations in the scatterer position, likely to be produced during the manufacturing process, may act as a broadening mechanism for the transmission band of these filters.

3.8 CONCLUSIONS

There are many possible ways to wavelength tune lasers, however the methods commonly adopted for these purposes are not readily applicable to our CO_2 slab waveguide laser devices.

A new method has been suggested, based upon an analogy with a photonic band gap device, which may allow for wavelength selection by control of the periodicity of a lattice marked on to one of the two electrodes used to form the waveguide in this laser type.

3.9 REFERENCES

3.1 Eugene Hecht, "Optics", Second Edition pp 393 Pub: Addison-Wesley Publishing Company

3.2 Richardson Grating Laboratory, "Diffraction Grating Handbook" 2000

3.3 R.M. Hocke, "Lineselective CO2-Slab-Laser with spatial inhomogeneous reflecting Littrow Gratings", Doctoral Thesis in Electrical Engineering, Lehrstuhl für Hochfrequenztechnik (LHFT) of the University of Erlangen – Nürnberg

3.4 E. Yablonovitch, T.J. Gmitter, R.D Meade, A.M. Rappe, K.D. Brommer, J.D. Joannopoulos, Physical Review Letters 67 pp 3380-3383 (1991)

3.5 T.F. Krauss, R.M. DeLaRun, S. Brand, Nature 383 pp 699-702 (1996)

3.6 C.C Cheng, A. Scherer, R.C. Tyan, Y. Fainman, G. Witzgall, E. Yablonovitch, Journal of Vacuum Science and Technology B 15 pp2764-2767 (1997)

3.7 U. Gruning, V. Lehmann, C.m. Englehardt, Applied Physics Letters 66 pp3254-3256 (1995)

3.8 Hong-Bo Sun, Ying Xu, Saulius Juodkazis, Kai Sun, Junji Nishii, Yoshihisa Suzuki, Shigeki Matsuo and Hiroaki Misawa, "Photonic lattices achieved with high-power femtosecond laser microexplosion in transparent solid materials", SPIE Vol. 3888 pp131 (2000)

3.9 Hong-Bo Sun, Ying Xu, Masafumi Miwa, Shigeki Matsuo and Hiroaki Misawa "Photonic crystal structures with submicrometer spatial resolution achieved by high power femtosecond laser-induced photopolymerization", SPIE Vol. 3888 pp122 (2000)

3.10 Thomas F. Krauss, Richard M. De La Rue "Photonic crystals in the optical regime – past, present and future", Progress in Quantum Electronics 23 pp 51-96 (1999)

3.11 M.M Sigallis, C.T. Chan, K.M. Ho and C.M. Soukoulis, "Metallic photonic band gap materials" Physical Review B **52** pp11 744-11751 (1995)

Chapter 4

Precision laser processing of optical filters with slab waveguide CO_2 lasers

4.1 INTRODUCTION

In order to construct the optical filters described in chapter 3, features a few tens of μm wide, a few times the operating wavelength deep, spaced by around 100 μm, must be manufactured. The most crucial of these three being the spacing between the features, as this directly relates to the transmission wavelength. Another factor to be considered is the time taken to manufacture these filters; in order to allow for testing of many different filters it was necessary to have a technique allowing for fast prototyping.

For this work a CO_2 based laser-machining rig was used, allowing for fast prototyping times and construction of a wide variety of patterns. In a production environment alternative methods of construction may be more desirable. Once patterns and dimensions are set, fast prototyping is no longer a requirement, thus etching or ruling techniques may prove more beneficial and cost effective.

Experimental data describing the operation of these lasers is presented, focussing particularly on the beam pointing/steering issues typical of this type of laser (see chapter 1). The positional accuracy of mark made by the laser on this dimensional scale will be affected by the pointing errors present. Two methods were employed to reduce these errors. Firstly when marking samples, numerous lower energy shots were fired in place of single high energy pulses, leading to an averaging effect in hole position, reducing positional errors. Secondly if the system is perfectly aligned radiation can be reflected

from the sample directly back along the beam path to the laser. This has been seen to lead to changes in the output energy. A slight system misalignment has been found to reduce these energy discrepancies, removing retro reflections to the laser, without impacting upon beam quality on the sample.

Use of lasers to create optical filters has been carried out by other institutions. Short (femto-second) high power pulses have been used to form photonic lattices by Hon-Bo Sun et al. Sun reports 2 methods for the creation of photonic lattices. Firstly, the laser is tightly focused causing micro-explosions in a solid material, which in turn generates voids in the material [4.1]. Secondly, the tightly focused beam is used to induce photopolymerization of a resin, creating strands in the resin, with dimensions controlled down to the sub-micron scale. [4.2]

4.2 POSSIBLE CONSTRUCTION TECHNIQUES

There are several possible techniques for making devices with features as described in 4.1 above, notably etching, scribing and laser micromachining.

Etching structures such as those described above has several shortcomings, primarily the difficulty of etching a hole to a similar depth as its diameter. During etching a hole will tend to spread out sideways under the surface of the substrate. Also the process takes a considerable time, requiring different masks for different patterns/dimensions, excluding the possibility of rapid prototyping,

Scribing the above structures would be possible using a weighted scribe and an X-Y translation stage system. A similar technique is used for ruling traditional diffraction

gratings. Marks of the required size could be made easily. However if different mark thicknesses were required several scribes would be necessary. (This is not the case in the present work). Also changing materials may required scribes of different weights to obtain the same cut depth, leading to increased prototyping time whilst new scribes were obtained.

The possibility of laser machining optical filters is attractive for many reasons. A workpiece can be placed on a suitable X-Y translation stage and features down to the order of μm could be marked depending upon the laser used. Marking features of a few tens of μm in width should not present a problem. Computer control of the stages and the laser could allow for fast prototyping of filter devices, approximately at twice the speed of the scribe method., Lasers can operate in any direction where as a scribe can generally only be run in one direction. The spot size on the workpiece and hence the marked width can be altered easily by adjusting the position of the focusing lens of the laser beam delivery system. This type of system was chosen to manufacture the optical filters.

Several laser sources could provide the required optical power necessary for machining materials of interest here.

Excimer lasers could be used to machine these filters; having very short wavelengths would allow for machining of very small features. However the excimer laser is generally used in conjunction with a mask, which again would slow down prototyping times.

Very short pulse length lasers have been used to machine PBG devices [4.1,4.2]. Often working in the visible or near infra red region, they are able to produce very small feature sizes. However the removal rate per shot is very low, leading to increased production times, and initial costs are significantly higher than the other laser types mentioned here.

Nd:YAG lasers operate at a wavelength of 1.064μm or doubled to 532nm, and thus have a diffraction limited spot size of an order of magnitude smaller than that of CO_2. Q switched Nd:YAG lasers are routinely used for metals processing [4.3] and the high power pulse would allow for machining in ceramics. However one of the materials of interest here is Quartz glass, which is highly transparent at YAG wavelengths, and therefore cannot be machined.

The filters described in subsequent chapters of this thesis were all constructed in either aluminium, quartz, ceramic or silica, using a laser micromachining workstation, similar to the one described above. The workstation incorporates a commercially available RF excited hybrid resonator CO_2 slab waveguide laser [4.4] similar to that described in detail in chapter 2. As well as providing a mechanism to produce the desired filters, use of this type of laser presented us with an opportunity to evaluate its performance in this micro-machining regime.

The CO_2 slab waveguide laser was chosen to perform this task for several reasons. It is known to be used as a tool in the laser cutting of thin sheet metal and it is able to machine ceramic, which is often used as an alternative waveguiding material in the mid-infra red. It is also highly absorbed by many optical glasses, allowing for fast

machining. Thus all materials intended for use as optical filters could be machined using this type of laser.

This laser is particularly well matched to materials processing tasks in both the thermal and ablative regimes. The high gas pressure and high discharge power density within the narrow waveguide region gives a more rapid pulsed response than for other industrial CO_2 lasers. Pulses as narrow as 20 μs FWHM can be routinely produced at pulse repetition rates (PRF's) of up to 10 kHz. With RF excitation, the pulse width is particularly easy to control, without the need for high voltage modulators, allowing for control over pulse energy. Finally, these lasers have a beam quality of typically M^2 ~1.2, allowing for spot diameters as low as 20 to 30 μm to be attained at the workpiece using modern aspheric or diffractive lenses. However the previously discussed issues to do with stability in this type of laser are a concern. Although the small wavelength variations would not cause appreciable machining differences in these particular materials, the beam steering issues may cause problems. The magnitude of these beam steering effects will be discussed in later sections of this chapter.

One final advantage with the use of this type of laser was expedience. The majority of the equipment necessary to produce the laser micro-machining station described in section 4.3 was available within the group, reducing delays in ordering new equipment.

4.3 MICRO-MACHINING WORKSTATION

The compact size of the sealed-off slab waveguide laser allows the entire workstation to be accommodated on a desktop sized optical breadboard. The beam leaving the circularising optics is sampled using a diffractive optic beam-splitter[1], directing 0.25% of the beam to a fast pyroelectric detector (5μs risetime), enabling in-line monitoring of pulse energy and instantaneous pulse shape (See figure 4.1). This is cross-calibrated at a 1 kHz pulse rate against the average power from a conventional power meter. The

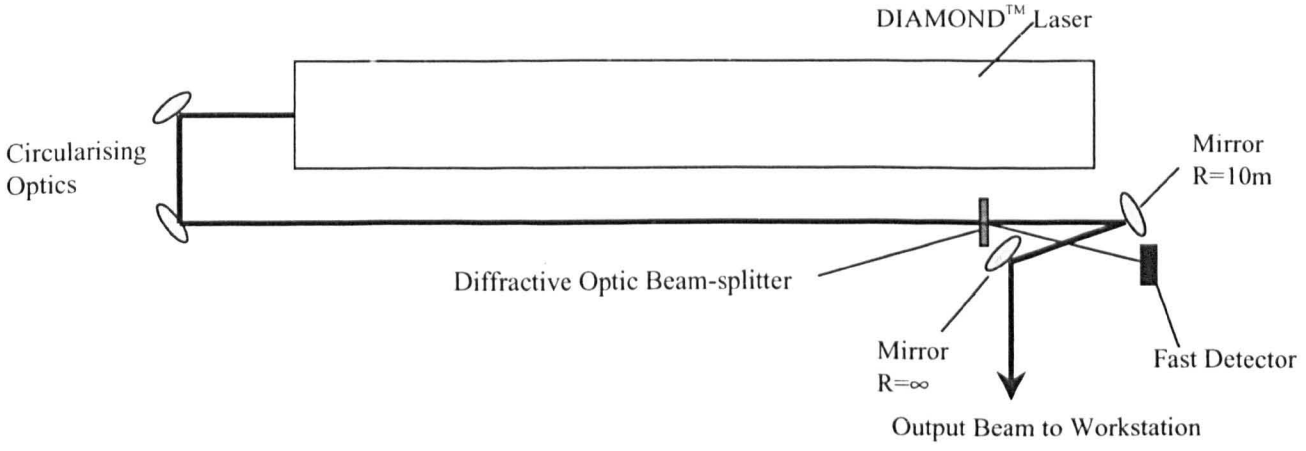

Figure 4.1 Beam Conditioning Optics

laser is capable of ~300 W average power in 50 to 60% duty factor pulsing, but is operated with much lower duty factor for the ablative micro-machining processes described here. The beam is expanded using a telescope of 2.5x magnification and focused on the workpiece by a 38 mm focal length, aspheric ZnSe lens, producing a spot radius of 15 μm ($1/e^2$ intensity point) and a depth of focus of ~100 μm. The aspheric lens is mounted on a motorised vertical translation stage to allow programmed variation in the focal height in 2.5 μm steps. The workpiece is positioned using an X-Y stage with a step size of 0.5 μm and an accuracy of 15 μm over 25 mm of travel. An additional workpiece levelling stage is adjusted to maintain the focal distance to ± 5 μm over the

[1] Beam splitter and high speed detector added by Dr. Gavin A.J. Markillie.

scanned area. Firing of the laser and motion of the workpiece is controlled through a PC running LABVIEW™. The design of the beam expansion and focusing optics, the mounts for the optics, the levelling stage and the software to control this laser and translations stages was undertaken by the author. The energy generated using a 60 μs RF pulse is typically 27 mJ, giving a peak fluence on the workpiece of ~7.6 kJ.cm^{-2}, well in excess of that required for shallow depth processing, but ideal for hole drilling and precision slit cutting. For some of the experiments described here, a 92% reflective attenuator is positioned in the beam line at a fixed angle to reduce the fluence. (See figure 4.2)

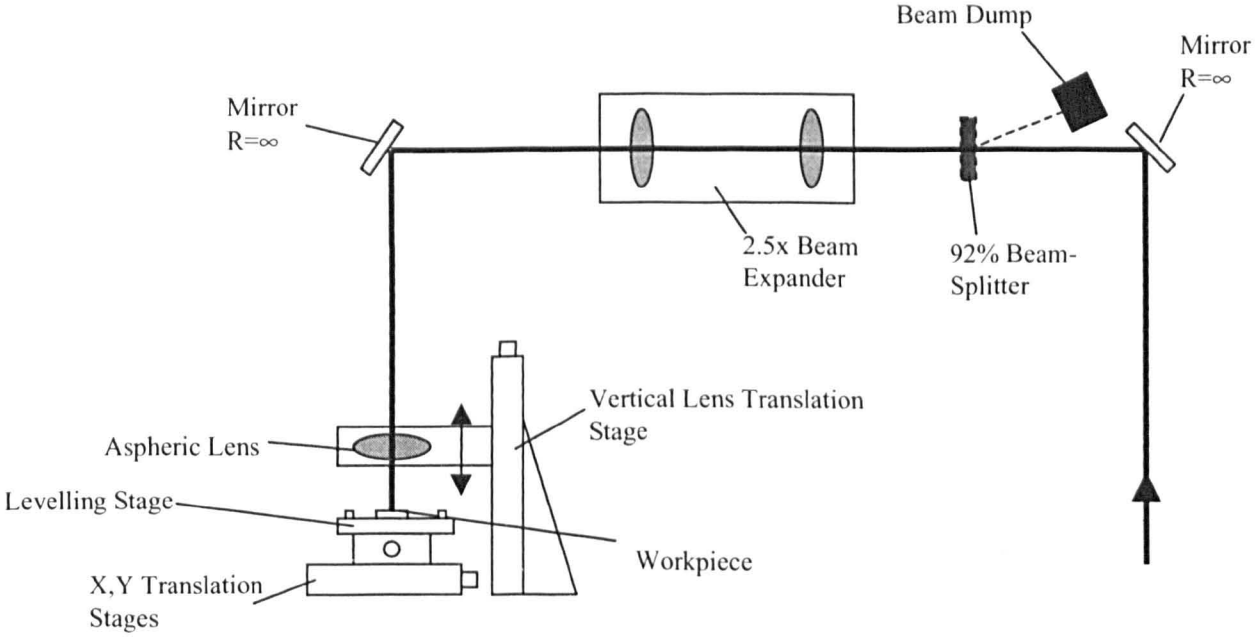

Figure 4.2 Workstation Layout

4.4 LASER BEAM PARAMETERS

The hybrid resonator incorporated in this laser is similar to the one described in section 2.5 with the waveguide mode defined by the electrode spacing in one dimension and a free space, negative branch unstable resonator mode in the other [4.5]. This design of resonator produces an asymmetric rectangular beam, which requires external

circularising optics. In this research, the proprietary beam correcting optics provided by the laser manufacturer is used [4.4]. In comparison with more conventional CO_2 lasers, this laser has a potential for unwanted beam artefacts, such as beam ellipticity and residual astigmatism. (Somewhat similar to the problems associated with diode lasers, and the presence of a significant non-Gaussian profile in some beam planes.) The response to resonator misalignment is different in the waveguide and unstable resonator planes. In addition, the relatively short cavity length of the laser leads to cyclical power drift as cavity length variations scan the laser mode through the gain spectrum. Early sections of this chapter discuss how these perceived or actual effects of the slab waveguide type of laser impact its use in precision processing, by studying the laser beam and pulse stability.

In order to determine whether the laser would be able to create uniform reproducible patterns in the materials to be used as optical wavelength filters it was necessary to determine the beam quality and stability characteristics.

Beam quality, ellipticity and pointing characteristics of this laser have been previously presented [4.6], a summary of which is given below.

Firstly the beam quality and ellipticity were measured to ensure that this specific laser tube had a well adjusted beam circularising system in comparison with the manufacturer's specification. The data was taken with an in-house rotating mirror beam scanner[2] with a resolution of 0.15 mm. A high PRF of 10 kHz was used to place several pulses in each scan, so that limited multi-sweep averaging could be used to produce a smooth profile of the laser beam. Different duty factors of 10, 20, 40 and 60 % were

used and the laser beam propagation factor, M^2 in both the unstable free space and stable waveguide regions was measured, using a sequence of scan planes. The M^2 value in both directions was stable at 1.1 ± 0.1, irrespective of duty factor. The values were found to be considerably better than the manufacturer's specification. Beam ellipticity was stable at < 1.05, with a divergence (full angle) in both directions of 2.0 ± 0.2 mrad and a waist diameter of ~7.0 mm at 0.5 m from the output coupler, in line with the manufacturer's specifications. In these trials, the beam maintained a good Gaussian appearance, fully consistent with the low M^2 values observed.

Secondly the rotating mirror scanner has also been used to measure the drift in beam pointing. Over the first thirty minutes of operation, the beam pointing showed a considerable drift of ~ 400 μrad in the free-space plane of the resonator. This is believed to be caused by differential expansion as the laser casing reaches thermal equilibrium with the internal electrodes and the external temperature of the cooling water. After thirty minutes, variations in the beam pointing were too small to be resolved using the rotating mirror beam scanner. These very small fluctuations were examined on a shot to shot basis during quartz glass machining trials described later in this chapter.

The excitation of the laser gas discharge is by an 81 MHz supply, which produces RF bursts at a fixed peak power of 4.8 kW. The laser has average power variations of ± 5% for RF pulse duty factors ranging from 20 to 60 % at 10 kHz, and shows the expected cycling with a period which increased with laser warm up time. The power drift is associated with the ro-vibrational line hopping caused by resonator length variations through expansion of the laser casing and also by the gas density variations in the resonator with varying duty factor. Use of a power stabiliser, which modulates the RF

[2] See section 6.2 for more information on Rotating Mirror Beam Scanner

pulse width or peak power, could compensate these variations. For the present experiments using low duty factor pulsing, the power stability is predominantly affected by the time taken for the laser casing to reach equilibrium with the cooling water, noted above. The pulse shapes recorded at low duty factor using the pyroelectric detector are shown in Figure 4.3 for RF pulse durations between 20 and 60 μs at a PRF of 125 Hz.

In the low duty factor regime, the laser pulse shape is determined by three processes. There is a delay of 10 μs produced by the discharge ignition time and build-up time of the optical flux, followed by a gain-switched spike which is not resolved by the present detector. The pulse then rises in power towards a quasi-cw level of ~600 W, but is cut off by the end of RF discharge pumping for all the time scales shown. The pulse fall time is approximately constant with a 90% to 10% fall time of 40 μs. In the pulse tail, it is common to see a second gain-switched pulse as the laser switches mode or line hops, and this has been reported previously for a similar type of waveguide laser [4.7]. This is believed to result from the mode frequency sweep produced by the heating of the laser gas during the discharge pulse, followed by an expansion which reduces the refractive index. The second pulse does not appear for every shot; however, its pulse energy is a small fraction of the total, as can be seen in Figure 4.3. For duty factors greater than

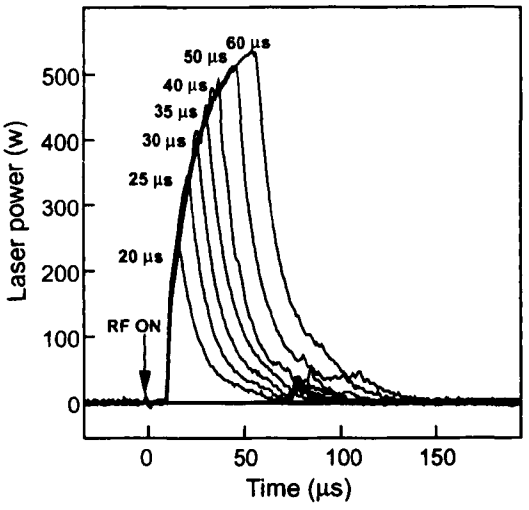

Figure 4.3 Laser pulse shapes for low duty factor pulsing with RF pulse widths between 20 and 60 μs.

10%, the line hopping seen in the tail disappears, due to an increase in the average discharge temperature.

For low pulse rates and the shortest discharge times there is an increase in shot-to-shot pulse energy fluctuation to ± 10%. This is associated with inadequate carry-over of ionisation from one pulse to the next for reliable discharge ignition. The UV pre-ionisation lamp provided with the laser does help in this region, but is not a complete solution. Without the lamp illuminated the laser fails to strike in this low pulse regime. Evidence of energy fluctuations is apparent in the glass machining trials reported in the next section.

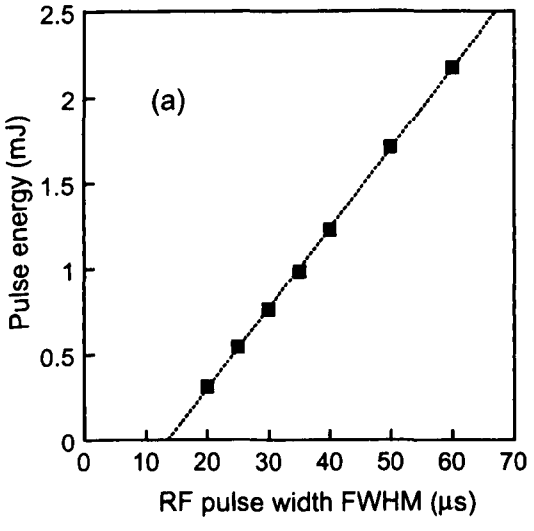

Figure 4.4 (a) Pulse energy versus RF pulse width in the low pulse rate region.

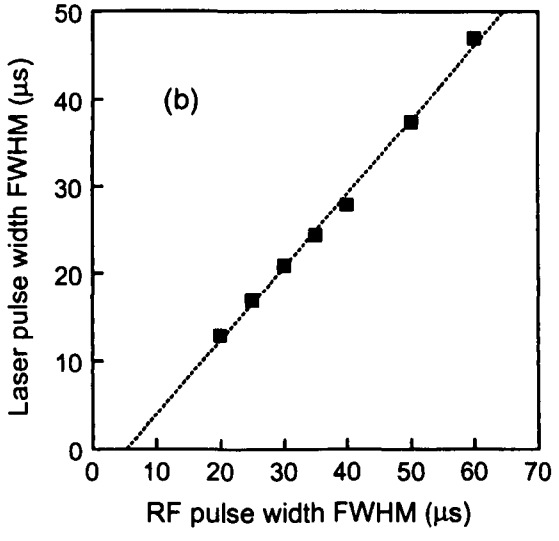

Figure 4.4(b) Laser pulse width (FWHM) versus RF pulse width.

RF pulse width provided a way of adjusting the fluence in machining trials. Figure 4.4(a) shows the relationship between pulse energy and RF pulse width. Figure 4.4(b) shows the pulse width as full-width at half maximum. Both in the low pulse rate region where these parameters are independent of pulse rate. Figure 4.4(b) shows the near-linear relationship between FWHM of the laser pulse and the RF pulse duration. This

pulse width variation may have an effect on machining mechanisms if large fluence adjustments are made in this way. The use of in-line attenuators is thus advisable for short pulse operation.

4.5 SHOT TO SHOT POINTING FLUCTUATIONS

Arrays of single shot holes were made in quartz and soda lime glass to allow for pointing stability fluctuations to be analysed. The slab waveguide CO_2 laser is an ideal device for this task as most optical glasses are strongly absorbing at the 10.6 μm wavelength and the pulse shape and energy combine to give a mass removal rate of nanograms per pulse, mainly by surface vaporisation. The relatively long pulse is a big advantage over other high repetition rate laser devices which usually work at much shorter pulse durations of ≤ 1 μs, giving higher irradiances which may cause micro-cracking when nanograms per pulse are being removed [4.8]. The 40 μs decay tail of the laser power shown in Figure 4.3 may aid in reducing residual stress which leads to micro-cracking [4.9] by prolonging the molten phase. However, the alternative of a discharge-modulated, DC excited, CO_2 laser produces pulses which are too long, giving reduced material removal by vaporisation and increased melt depths, reducing the accuracy of feature formation.

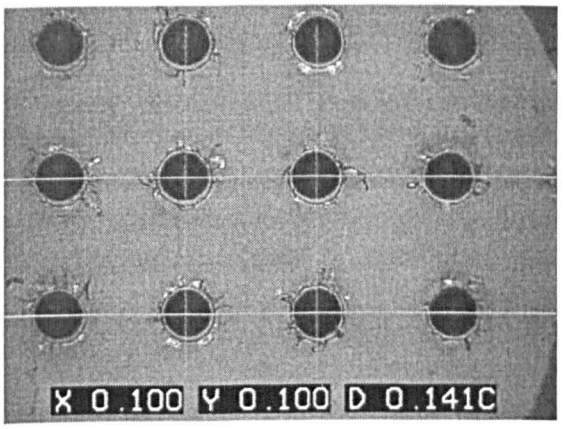

Figure 4.5(a) Craters machined in quartz glass at 0.47 mJ pulse energy, *x* and *y* crater pitch = 100μm.

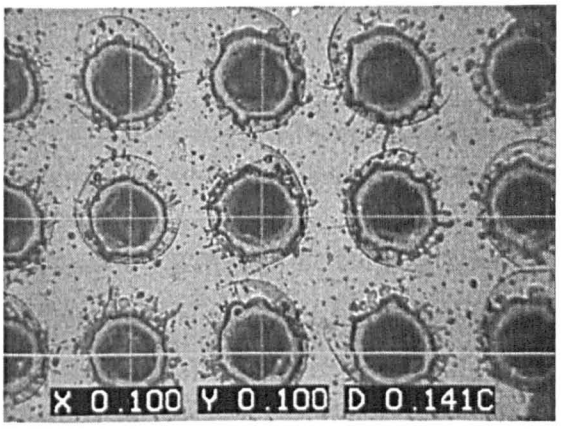

Figure 4.5(b) Craters machined in soda lime glass at 0.47 mJ pulse energy, *x* and *y* crater pitch = 100μm.

The test patterns filters are shown in figures 4.5 (a) and (b). Figure 4.5(a) and (b) show normal incidence micrographs of an array of craters on a 100 μm square grid, produced in quartz and soda lime glass respectively using an average energy of 0.47 mJ and a measured energy standard deviation of 0.036 mJ (calculated from around 20 energy readings taking throughout each test pattern run). These energies were produced by operating the laser with 25 μs RF pulse duration and 8% transmission attenuator. Each crater was formed by a single laser pulse with the workpiece stationary when the laser was fired. Test pieces of this type have been analysed to give statistical data on the variation of beam landing position and crater diameter caused by effects in the laser. The positional variation of the holes relative to a grid aligned to the mean central position of the holes in the vertical and horizontal directions was measured. The deviation from this grid was then calculated, allowing for the pointing stability in both the free space and laser waveguide resonator planes to be determined. The positional standard deviation of the centre of the crater divided by the 38mm focal length of the lens measures the pointing stability of the incoming beam. This was observed as 13.5 μrad (0.49μm positional variation) in the axis corresponding to the waveguide

direction in the laser resonator and 55.5 μrad (2μm positional variation) for the free space direction. (These values are measured after the beam has passed though the expanding telescope, so will be 2.5 times larger at the laser) Whilst some of this pointing error may be associated with room vibrations. There is a clear difference between the two axes with the unstable resonator direction showing the largest pointing stability error. Nevertheless, the statistical component of the beam pointing error is substantially less than the contribution caused by the drift associated with the laser reaching thermal equilibrium, discussed in Section 4.2. This residual drift may be reduced further by operating the laser at a higher duty rate.

Figure 4.5(a) shows that machining quartz glass at 0.47 mJ produces no signs of micro-cracking and only small amounts of spatter on the substrate surface, making this pulse energy suitable for machining these patterns. An important factor in producing such an excellent result is the temporal pulse shape of the CO_2 slab waveguide laser. A previous study of the marking of soda lime glass by Allcock *et al.*[4.10] using a TEA-CO_2 laser has concluded that micro-cracking occurred resulting from residual stresses left within the substrate upon cooling. Figure 4.3 shows that a considerable part of the energy in a pulse from the present device is contained within the tail. This exponential reduction in irradiance at the workpiece is believed to reduce the rate of solidification of the molten material and hence anneal the surface of the crater, reducing the amount of residual tension upon cooling and leading to very low instances of micro-cracking.

It can be seen from Figure 4.5(b) that significant amounts of spatter are formed on the surface of soda lime glass, thus these samples were inappropriate for use in the above pointing stability measurements and consequently were not used.

4.6 DIRECT WRITING IN ALUMINIUM

The first set of filters to be tested were constructed by directly writing a uniform array of scatterers in an aluminium substrate. Both grooved lattices and arrays of drilled holes were made, with structures up to 50 μm in depth (within the depth of focus capability of this workstation) with a separation between scatterers of ≥ 50 μm.

Numerous different filters have been constructed with lattice spacing varying from 100μm up to 143 μm. Figures 4.6 (a) and (b) show two structures marked in highly polished Aluminium. The first is a simple array of circular holes and the second is a lattice formed by intersecting grooves.

Prior to drilling all samples of aluminium were prepared in a similar manner to the laser electrodes for inclusion in the laser were. The surface was first skimmed flat by a mechanical process before being polished by hand with wet and dry sandpaper. The surface was then polished with various grades of polishing compound to remove all marks greater than 1 μm in size. After this polishing the samples were cleaned with water and iso-propanol to remove any remaining polish along with any grease or other contaminants.

Initial results from machining aluminium showed uneven cuts. In the case of an array of circular holes some holes appeared considerably larger than others, even though the pulse energy remained the same. This was attributed to two main factors. Firstly the non-uniformity of the aluminium substrates; impurities in the aluminium led to differing

machining rates at different points on the same material. The same was seen if the material was not adequately cleaned prior to machining possibly a result of contaminates on the surface. The second cause for this non-uniform machining was debris left on the surface from a previously marked section. This small amount of material led to a larger plasma being formed on the surface of the substrate, damaging the surface. Both these problems could be overcome by firstly using higher grade aluminium substrates (see section 4.7) and secondly by using a gas assist over the machining site. The gas assist had the effect of removing any debris from the machining area and by the use of an inert gas, i.e. nitrogen, reduced the possibility of a damaging plasma forming on the surface of the metal.

The preferred substrate material for these filters is aluminium, as this material produces excellent hollow waveguide walls owing to its high reflectivity. Also this is the material currently used as electrodes in RF excited CO_2 waveguide lasers. The high reflectivity of aluminium in this wavelength region leads to poor coupling of CO_2 radiation into the surface. However, in Section 4.2, the peak on target fluence of the workstation is given as 7.6 kJ cm^{-2}, allowing an absorbed energy density up to 150 Jcm^{-2}. In aluminium this is sufficient to produce material removal. (Assuming 98% reflectivity from the aluminium surface, this reflectivity does however decrease for aluminium once in a molten state), For a square array of holes, multi-shot drilling at each site is used, with interleaved table motion. To reduce the distortion of the holes by melting, the laser is operated with no attenuator and with a short RF pulse width of 20 to 25 μs (corresponding to 3.7-5.9 mJ per pulse). Very little material is removed per shot and the required depth is built up by multiple shots. For this mode of production, the utilisation factor of the laser is very low and much of the production time is taken by table

movement cycles. However multiple pulses average out the effect on hole position on the shot-to-shot beam pointing fluctuations. The pointing error can be described by the normal distribution [4.11], thus discrepancies in lattice spacing when drilling arrays of holes will scale as $N^{-1/2}$, where N is the number of shots per hole. In Figure 4.5 (a), 100 laser shots are used per hole, thus the positional accuracy in the lattice spacing for a specific direction is 10 times better than the positional accuracy of a single pulse. Thus the main issue of concern is that of slow scale drift in beam pointing during the long machining period, typically 3 hours for a 10 x 10 mm^2 array. This may produce a small modulation of the lattice spacing as machining progresses across the several centimetres of workpiece. The worst case drift for the workstation corresponds to the holes being displaced by 6 μm from the required position, but after laser temperature stabilisation the effect is much less than this, typically giving an uncertainty of 2 μm, somewhat worse than the positional accuracy achieved by the X-Y table.

As previously mentioned two basic patterns were machined in aluminium, the hole array as shown in Figure 4.6(a) and the lattice pattern as shown in Figure 4.6(b). The grooves are formed using continuous table motion in a raster type manner, allowing production of a much larger 15 x 40 mm^2 area in ~ 45 minutes. In this case the laser was operated at around 1kHz with pulse durations of between 30 and 75μs depending upon the individual aluminium sample. This corresponds to energies of between 10 and 35 mJ per pulse and an average power of between 10 and 35W. The tables were run at around 10 mm/s leading to 10μm positional steps between individual shots. In Figure 4.6(b), 14 laser shots define each wall of the unit cell of the lattice, and the uncertainty of the wall position may be then approximated by $(14)^{-1/2} . \Delta x.$, where Δx is the uncertainty in the spot centre caused by shot-to-shot beam pointing fluctuations. In this particular case

the effective positional accuracy of the lattice spacing is 2.6 times the positional accuracy of the laser.

Grids provide a number of benefits over the dot patterns. Production times are significantly smaller as the raster scanning technique is faster than the stationary drilling used in the hole drilling pattern. In addition the grid pattern leads to a higher fill factor, leading to a higher scattering efficiency than would be expected from the hole pattern.

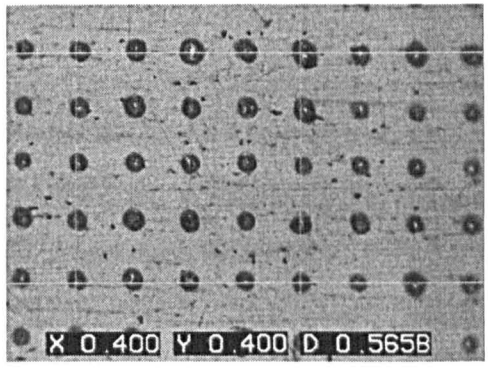

Figure 4.6 (a) Hole array on the aluminium wall of a hollow planar waveguide.

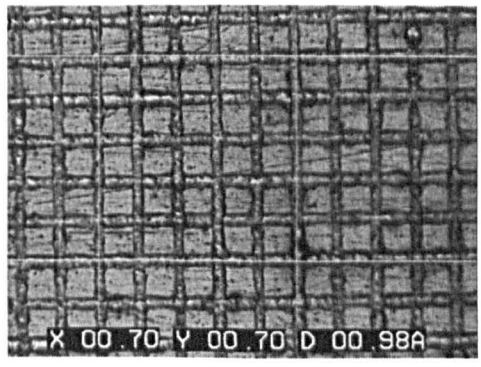

Figure 4.6 (b) Lattice pattern formed by crossed grooves with 143 μm pitch on the aluminium wall of hollow planar waveguide.

4.7 ALUMINUM REMOVAL FROM PRE-COATED MIRRORS

It was found that drilling different samples of aluminium required significantly differing laser characteristics, one sample may be significantly machined by one set of characteristics (i.e. pulse duration/repetition) whereas another would not be marked. This had the effect of drastically slowing production of prototypes as for each sample a new set of laser operating conditions had to be found. Various samples of aluminium supplied by the same supplier as the same material were found to have differing machining properties.

In order to try and minimise this delay in prototyping a different approach to the construction of filters was taken. Aluminium coated glass mirrors were used as the waveguide walls. It was found that the aluminium coating could easily be removed from the glass using the CO_2 laser workstation, and patterns similar to those demonstrated in section 4.5 could be constructed. There was no difference found in the required machining characteristics between different mirrors.

The mirrors used were commercially available aluminium coated glass mirrors, each 5x5cm in size. In order for the two mirrors to form a waveguide the Fresnel condition (see section 2.2) had to be satisfied. For this to be the case 'a' the half waveguide spacing had to be less than 0.7mm.

The depth of the grooves made in the mirrors was not as crucial as with the aluminium filters since if all the aluminium coating were removed it exposed the glass below. The glass, which acts as an almost perfect absorber, next to the almost perfect reflecting patches of aluminium led to the possibility of a device with very high scattering capabilities..

It was found that grooves with good edge quality, see figure 4.7, could be made using a laser pulse of 21μs with a lasing frequency of 1KHz (Pulse Energy ~ 3.8mJ, Average Power ~ 3.8W). A constant problem when constructing grooved patterns was the acceleration time of the translation stages. Although not causing a great effect in the solid aluminium filters, significant differences were seen when machining the mirrors. During the acceleration time the shots from the laser were closer together, resulting from the slower velocity of the laser spot on the mirror surface, leading to more damage

to the mirror, for both glass and aluminium. This was stopped by attaching a copper mask to the surface before machining, the acceleration of the translation stage movement was then timed to occur whilst the beam was directed at the mask, allowing the tables to move with a constant velocity of 10mm/s whilst cutting the mirror.

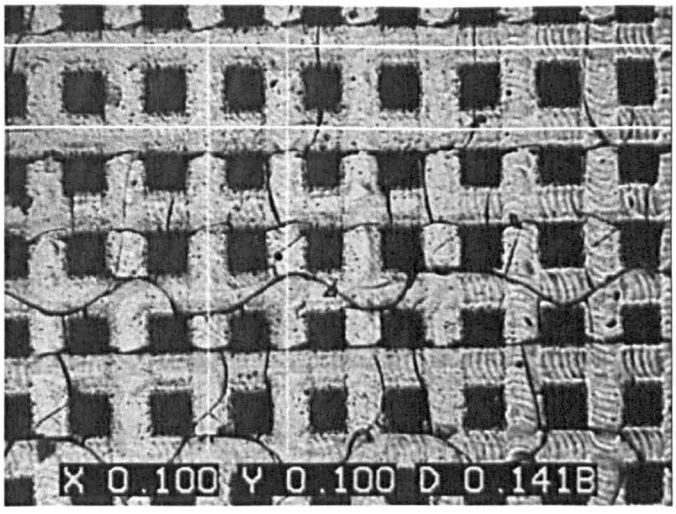

Figure 4.7 Micrograph of grid pattern with spacing 100μm made in an aluminium coated mirror

At these low pulse energies it was found that the beam did not always remove the aluminium coating when it first hit the sample. Once the laser had broken through the aluminium coating it would continue to cut, however it did not always break through at the start of the run. This issue was overcome by making a mark/scratch around the edges of the pattern, just inside the mask, with a scalpel.

4.8 MACHINING OF LASER ELECTRODES

To allow for simple incorporation of the 2-D filters into a laser cavity, patterns were directly machined into the laser electrodes. It was found that the high grade, pre-stretched aluminium used to construct the waveguide electrodes was readily machined, even when highly polished.

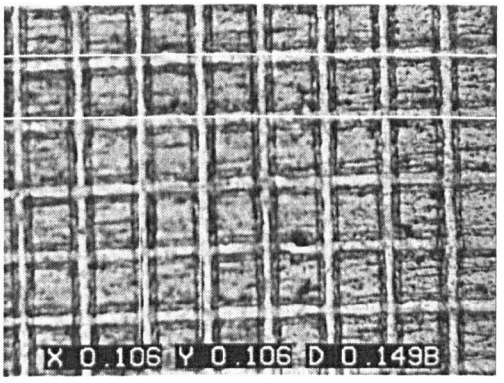

Figure 4.8(a) Micrograph showing patterned section of a laser electrode, with pattern period of 106μm

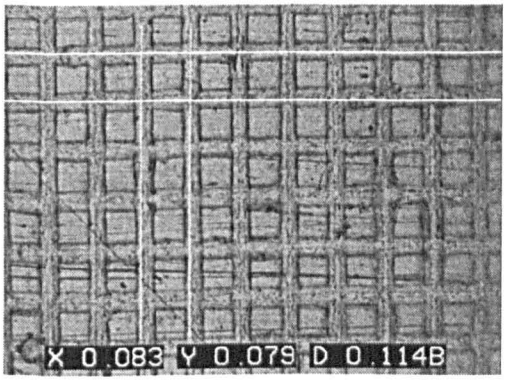

Figure 4.8(b) Micrograph showing patterned section of a laser electrode, with pattern period of 82μm

The ease of machining gave the ability to construct significantly finer grids (with smaller lattice spacings) than had been previously produced in aluminium. A greater depth could be attained from a single pass than in previous samples.

The first pattern drilled in an electrode was a grooved pattern with a lattice spacing of 106 μm see figure 4.8(a). All subsequent patterns were again grooved but with a lattice spacing of 82μm see figure 4.8(b). These patterns were drilled with the same laser characteristics of 22μs pulse duration at a PRF of 1.44KHz. This corresponds to an energy of 4mJ an average power of 5.8 W. The cutting was assisted by a 0.9 bar nitrogen gas jet directed on to the workpiece via a 2mm diameter nozzle. This jet removed any debris created by the cutting process and also reduced plasma forming on the surface of the electrode which has been found to produce uneven cuts in aluminium. All different electrode samples were machined with the same laser characteristics to produce the patterns. The 106μm pattern took around 1.5 hours to machine with the 82μm pattern taking around 1.9 hours, both with the tables travelling at 6mm/s.

It is thought that the marked improvement in drilling these electrodes as compared with previous samples of aluminium is because of the lower impurity levels found in the material used for the electrodes. These impurities are machined by the beam to a greater or lesser extent than the normal aluminium which leads to uneven cuts/holes being formed, see section 4.6.

4.9 CONCLUSIONS

The CO_2 slab waveguide laser has been used to produce the optical waveguide filters suggested in Chapter 3. These filters have been successfully machined in several different materials, soda-lime glass, quartz glass, ceramic, aluminium coated glass mirrors and aluminium. The laser proved to be a versatile source for the high precision workstation, offering a wide range of pulse duration and PRFs suitable for the optimisation of micromachining of both the highly absorbing quartz glass and highly reflecting metals. Beam quality, ellipticity, drift and instability in beam pointing all show measurable residual effects related to the source being an asymmetric laser resonator, but none of these is found to be a limitation on the use of the laser in the micro-machining application discussed here.

The large peak power, up to 600W with this CO_2 slab waveguide laser, is of particular use in machining aluminium, where much of the light is reflected when the process is operated with short pulses in an ablative regime to limit melting. Machining depths particularly depend upon the quality and uniformity of the sample used. Some samples can be easily drilled to depths exceeding the required 50μm, whereas others can only be uniformly drilled to lesser depths. The characteristics of the laser must be varied significantly to obtain uniform cutting on different samples of aluminium. Uniform

cutting is not always possible with low grade/purity samples. Care must also be taken to avoid back reflections into the laser, which leads to laser stability problems.

For future work, machining of larger areas than are available in this project may lead to an increase in the effect of these optical filters. In order to accomplish this translation stages with greater travel would be required. Producing gratings with a finer spacing may also have a marked improvement on filter performance. The current system is not affected by the beam steering effects, present in this type of laser device. Positional fluctuation can be controlled to an acceptable level by utilising a multi-shot process; working at smaller spacing, especially in aluminium, led to unacceptable defects being produced and also significantly longer production times. Moving to smaller feature sizes would be hard to achieve satisfactorily with this micro-machining set-up, however if an alternate laser source were used, with a shorter operating wavelength, possibly a Nd:YAG or doubled YAG, finer features could be produced in aluminium or ceramic.

4.10 REFERENCES

4.1 Hong-Bo Sun, Ying Xu, Saulius Juodkazis, Kai Sun, Junji Nishii, Yoshihisa Suzuki, Shigeki Matsuo and Hiroaki Misawa, "Photonic lattices achieved with high-power femtosecond laser microexplosion in transparent solid materials", SPIE Vol. 3888 pp131 (2000)

4.2 Hong-Bo Sun, Ying Xu, Masafumi Miwa, Shigeki Matsuo and Hiroaki Misawa "Photonic crystal structures with submicrometer spatial resolution achieved by high power femtosecond laser-induced photopolymerization", SPIE Vol. 3888 pp122 (2000)

4.3 S.S. Kudesia, W.S.O. Rodden, D.P. Hand, P. Solana, J.D.C.Jones, "Suitability of Laser Drilling Models Containing Melt Eject Mechanisms", Section B-ICALEO 2000

4.4 DIAMOND™ 84 Laser datasheet, Coherent Inc., Laser Group, CA.

4.5 P Jackson, H J Baker, and D R Hall, "CO_2 large area discharge laser using an unstable-waveguide hybrid resonator" Appl. Phys. Lett., **54**, 1950-1952, (1989).

4.6 H J Baker, G A J Markillie, P Field, Q Cao, C Janke, D R Hall, "Precision laser optical microstructures with slab waveguide CO2 lasers" International Conference of Laser Ablation, Osaka (1999)

4.7 E F Plinski, B W Majewski, A S Bednarczyk, and K M Abramski, "Pulse mode operation of RF excited CO_2 waveguide laser" Proc. GCL/HPL 1998, ed A S Boreisho and G A Baranov, SPIE Proc. **3574** , 500-503 (1999).

4.8 P E Dyer, I Waldeck, and G C Roberts "Fine-hole drilling in Upilex polyimide and glass by TEA CO_2 laser ablation" J.Phys. D: Appl. Phys., **30**, L99-L21 (1997).

4.9 H Batteh, "Effect of surface relaxation on stress failure in laser-irradiated glass" J. Appl. Phys., **54**. 3769-3776 (1983).

4.10 G Allcock, P E Dyer, G Elliner and H V Snelling, "Experimental observations and analysis of CO2 laser-induced microcracking of glass" J. Appl. Phys., **78,** 7295-7303 (1995).

4.11 Suwas K. Nikumb and Mahmud U. Islam, "High-Precision Machining of Materials for Manufacturing Applications Using Diode Pumped Solid State Laser", International Conference of Laser Ablation, Osaka (1999)

Chapter 5

Wavelength Selective Waveguide Transmission

5.1 INTRODUCTION

In this chapter, the transmission and diffraction of the filter patterns described in Chapter 4 are investigated. The way in which incoming radiation is affected by the different samples is recorded, including details on the proportions transmitted and scattered for each of the different materials. Other factors affecting the scatter and transmission, such as the incidence angle of the incoming radiation and the diffraction pattern itself are studied. In a waveguide laser the incidence angle is very small, however the angle at which the light strikes the pattern in the horizontal (waveguide) plane can vary significantly, and this is also investigated within this chapter. The initial experiments are non-wavelength specific, and are aimed purely at characterising the scattering effects. The amount scattered from the patterns will have a direct relation to the transmission changes in the final experiments in this section. The final section describes a series of experiments showing how transmission through a waveguide with one patterned wall varies with incoming wavelength.

5.2 MATERIAL DEPENDENCE ON SCATTERING & REFLECTION

As described in Chapter 4, several different materials had patterns machined in them, including quartz glass, alumina/ceramic, aluminium coated glass and aluminium. Results from scattering experiments from all these materials are described below.

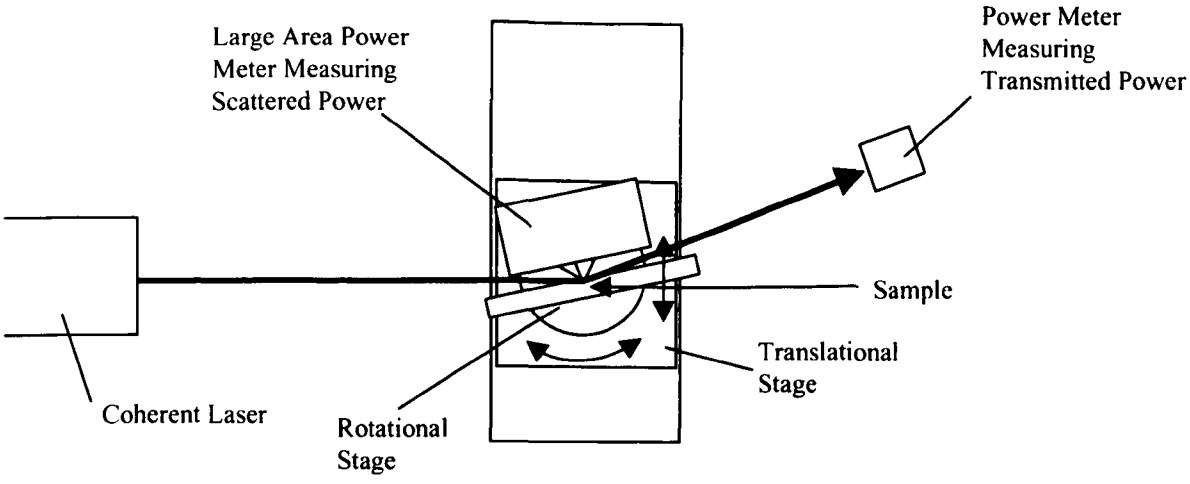

Figure 5.1 Apparatus to measure scattered and transmitted power from patterned sample.

The set-up shown in figure 5.1 was designed and constructed by the author. In this set-up the amount of radiation scattered by the diffraction pattern, rotated by 5° from the plane of the input beam, and the amount of radiation unaffected (i.e. which reflects from the sample as if the sample were unpatterned) was measured. By substituting the various samples into the beam the scattering and transmitting properties of these samples could be obtained. All these samples had a square lattice pattern drilled in them similar to the one shown in figure 4.6 (b), in this case with a lattice spacing of 106μm. Results are shown in table 5.1. The input beam was provided by a commercial CO_2 slab waveguide laser produced by Coherent, powered by a 120 MHz RF generator pulsed at 900Hz with a 30% duty cycle.

From table 5.1 it can be seen that the amount scattered and transmitted from the various different materials varied significantly. The glass and glass backed mirror appeared to absorb more of the incoming radiation, which would be expected owing to their high absorption at 10.6μm. This absorption led to problems when taking results for the glass

backed mirror at powers similar to those used for the aluminium samples as the large intensity present on the sample led to the glass fracturing. It can also be seen from table 5.1 that the radiation scattered and transmitted by aluminium and alumina is very similar, with an extra 1.4% being scattered by the aluminium and the same amount transmitted by the two materials.

Material	Scattered (%)	Transmitted (%)
GLASS	20	40
ALUMINIUM	6	86
ALUMINA	4	86
MIRROR	10	51

Table 5.1 Percentage of radiation scattered and transmitted from diffraction patterns marked in various materials.

It can be seen that the glass or mirror samples would provide the best diffraction, and hence the largest effect on wavelength variations through the proposed waveguide filters, however the attenuation added by such filters would be high. This attenuation would certainly reduce the power attainable from any laser, possibly even prohibiting the laser from operating. Aluminium and alumina are both commonly used inside current CO_2 slab waveguide lasers so the high transmission observed was to be expected. They also exhibit a usable level of scattering, of the order of 5% per pass at these incidence angles, and thus, could possibly be used as a diffraction mechanism within the proposed waveguide filters.

5.3 PATTERN DEPENDENCE ON SCATTERING AND REFLECTION

As in section 5.2 different samples constructed as described in Chapter 4 were subjected to illumination from a laser source. Samples had either grids or holes drilled in them, see figures 4.6 (a) and (b) for similar examples.

The apparatus shown in figure 5.1 was used again, with both samples being constructed from aluminium and having lattice spacings of 106μm. Results from the experiments are shown in table 5.2. From this we can see that the grid pattern diffracts light to a significantly greater extent than the hole pattern. This could be predicted as a far larger percentage of the surface is marked in the grid pattern as opposed to the hole pattern. Also from table 5.2 it can be seen that the reduction in diffraction from the dot pattern leads to a slightly increased transmission.

Pattern	Diffracted (%)	Transmitted (%)
GRID	6	86
DOTS	3	95

Table 5.2 Percentage of incoming radiation scattered and diffracted from 2 diffraction patterns marked in Aluminium

5.4 INCIDENCE ANGLE DEPENDENCE SCATTERING

In the actual laser the angle of incidence with which the passing radiation strikes the diffraction pattern will be very small as a consequence of the plane-plane resonator geometry used in the waveguide direction of the laser. It is therefore important that we evaluate the operation of these grating devices with very small angles of incidence. As this angle decreases, the spot size created by any incident beam will increase. A circular

beam would form an oval where it struck the sample. Thus a very large area would have to be patterned to allow for the study of the diffraction from these devices at small incidence angles. If the spot size is greater than the patterned area then the over-spill leading to reduced scattering must be taken into account.

In this section the scattering is measured at various incident angles for both polarisations of the incoming light. The set-up shown in figure 5.1 is again used, with an aluminium sample marked with a grid pattern, again with a lattice spacing of 106μm, being illuminated. The sample was illuminated in 2 areas, the first being an unmarked section

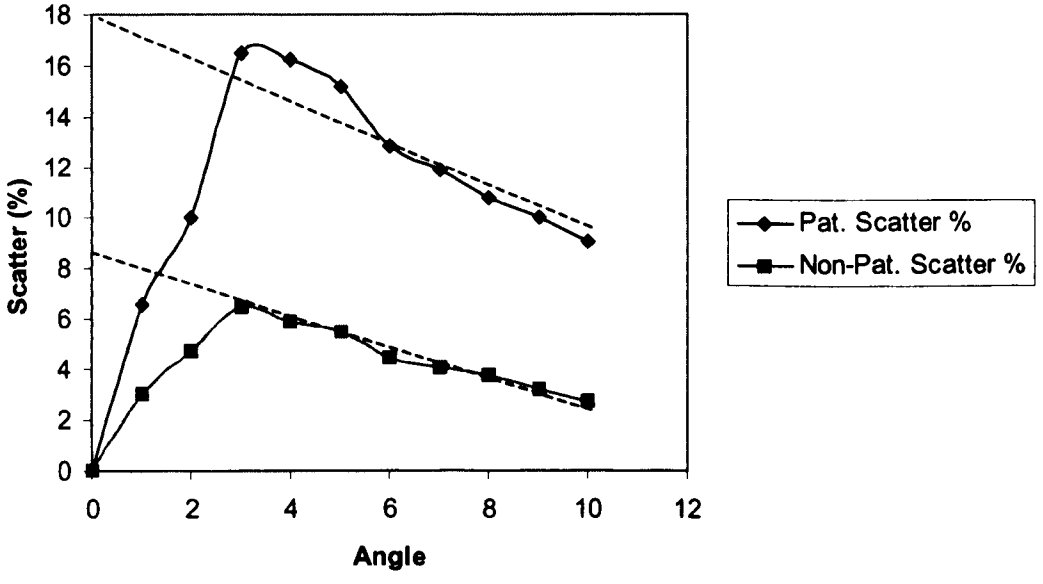

Figure 5.2 Percentage of s polarised radiation scattered from diffraction pattern in aluminium at various incidence angles.

and the second a patterned section. This allows for a truer picture of the patterned area's effect on scattering to be found. Readings were taken for the sample at incident angles from 1° to 10°, results are shown in figure 5.2 for the s polarisation and figure 5.3 for the p polarisation. In figure 5.2 the expected percentage scatter at lower incident angles has been extrapolated, this is shown by the dotted line.

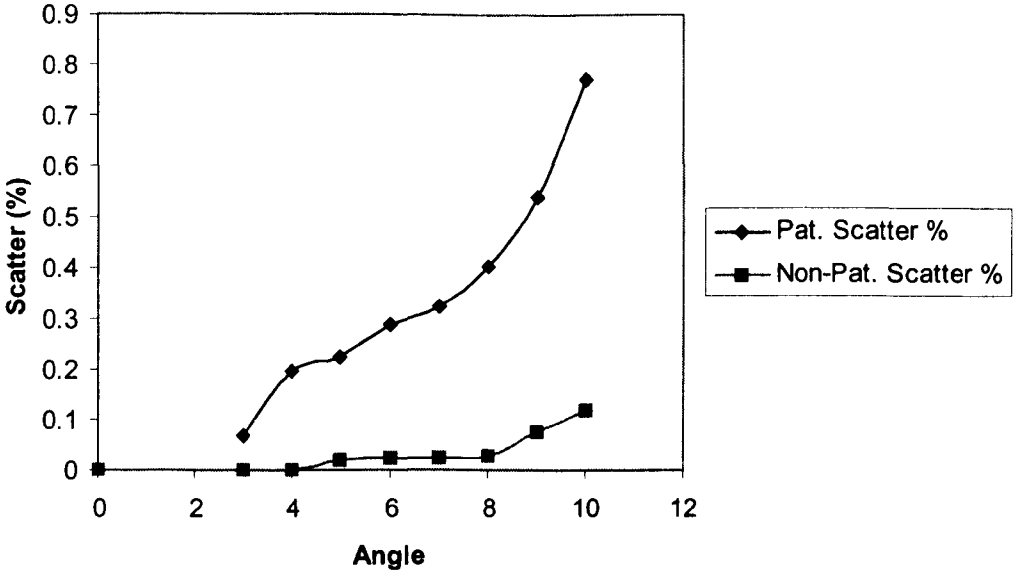

Figure 5.3 Percentage of p polarised radiation scattered from diffraction pattern in aluminium at various incidence angles.

It can be seen that for the p polarisation the scattering level increases as incident angle increases, whereas for the s polarisation it actually decreases as incidence angle increases. The drop off shown in figure 5.2 towards the small angle end is a result of the spot size projected on the sample being larger than the marked area on the sample. It can also be seen that significantly more radiation is scattered when the incoming radiation is s polarised.

5.5 HORIZONTAL ANGLE DEPENDENCE ON SCATTERING

Inside the laser cavity some of the radiation incident on the patterned area is not parallel with the central axis of the cavity in the horizontal direction. Figure 2.7 shows that in one direction of a negative branch unstable resonator the radiation is parallel to this central axis, however the returning radiation forms a focus. Therefore, some of the radiation incident on the patterned area will not be parallel with the horizontal axis, as

has been the case in all results reported previously in this chapter. Results below describes what happens to the proportion of the incoming light diffracted and transmitted as the horizontal incidence angle is altered. This was recorded by using a similar set-up to that shown in figure 5.1 with the sample able to rotate in the horizontal plane rather than in the vertical plane. The sample was held at a vertical incident angle of 4°, using incoming radiation with an s polarisation. This is where the maximum viewable diffraction is found, see figure 5.2.

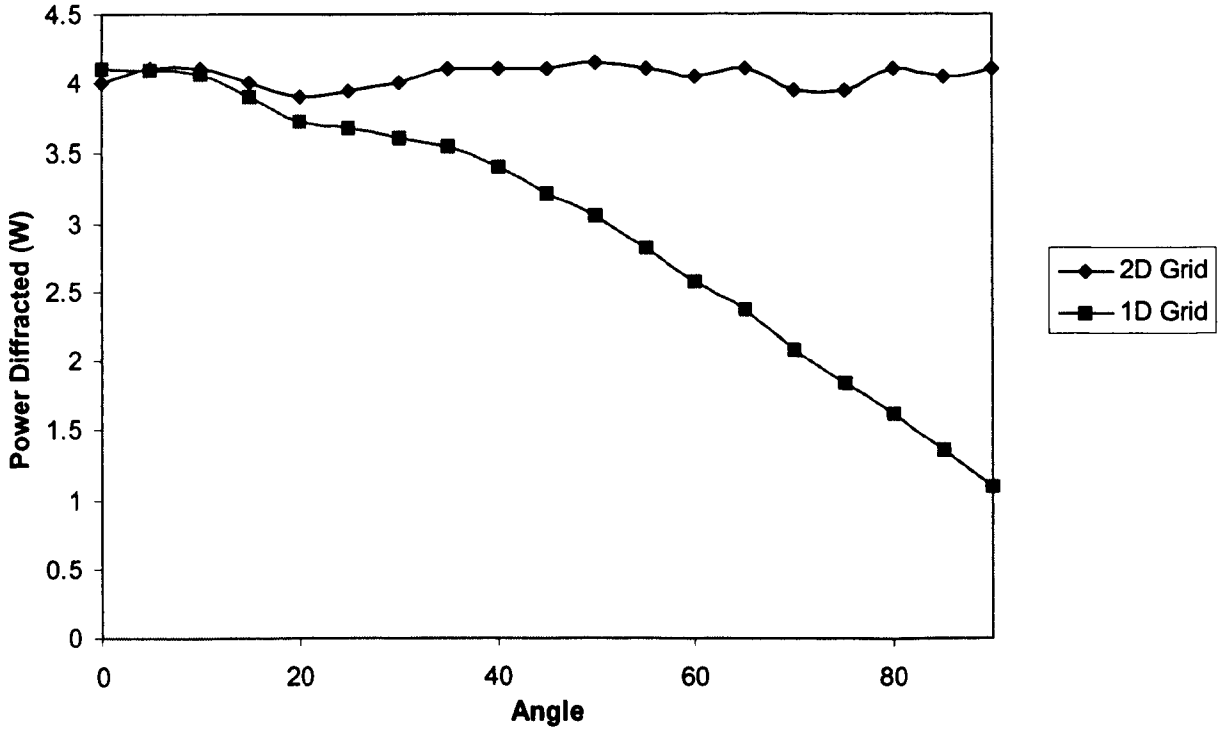

Figure 5.4 Percentage of radiation scattered from diffraction pattern in aluminium at various horizontal input angles, for 2 different grid patterns.

Figure 5.4 shows how the proportion of incident radiation scattered for two patterns, both marked in mirrors, alter with horizontal incident angle. The first pattern is a 1D pattern made up of a series of lines in a traditional diffraction grating layout, the second

pattern is a 2D grid of lines as shown in figure 4.6b. It can be seen from figure 5.4 that when the 1D pattern is normal to the incoming radiation it behaves in the same manor as the 2D grid. However when the 1D pattern is parallel with the incoming radiation it has the same effect on the radiation as an unmarked surface, (when compared with scatter from unmarked waveguide in figure 5.4). Between these two extremes, the amount of diffracted radiation appears to follow a cosine dependence on incident angle. The amount diffracted by the 2D pattern does not appear to be affected by the incident angle of the incoming radiation.

5.6 WAVEGUIDE TRANSMISSION

In order to see how the diffraction patterns whose construction was described in Chapter 4 acted as filters it was necessary to construct waveguides from machined samples. Transmissions of numerous waveguides were tested with respect to the wavelength of the incoming radiation.

The very first experiment carried out on a waveguide was purely exploratory and designed to see if the pattern would have any effect on transmission at certain wavelengths. A test piece, drilled by an external company, was incorporated into a waveguide and light from a tuneable Edinburgh Instruments Laser passed through it. The beam was not matched into the waveguide so the majority of the incoming radiation was scattered by the waveguide walls. Differences in transmission between modulated and unmodulated portions of a waveguide as a function of wavelength were measured. At most wavelengths the transmission through the modulated section is lower than that through the unmodulated section, however at certain wavelengths, those predicted as

transmission maxima by equations 3.4 and 3.5, the transmission drop between modulated and unmodulated sections of waveguide was smaller than in other regions.

Following these initial crude experiments a more elaborate procedure was devised to provide a better understanding of the throughput of the patterned waveguide with respect to wavelength. The apparatus shown in figure 5.5 was constructed. This set-up, which is the author's expansion of a matching set-up initially designed by Dr. Q Cao, allows for the matching of a TEM_{00} beam into a waveguide mode with efficiencies of up to 99.5%. In order to successfully match to waveguide the beam must have a waist radius ω as given by equation 5.1. Differing waveguide spacings can be accommodated for by either repositioning the curved mirror in figure 5.5 or, for larger waveguide spacing variations, by replacing the mirror with one of a different curvature.

$$\omega = 0.69a \tag{5.1}$$

In addition to the vertical movement shown for the waveguide in figure 5.5 it was also possible to move the waveguide horizontally allowing transmission through different regions of the waveguide to be studied. Hence if the patterned area was to one side of the waveguide, transmission through an unmodulated section of waveguide could be compared with that through a modulated section of waveguide by simply sliding the waveguide across the beam path, either manually or by computer control via a translation stage.

The output from the 2 detectors was fed into an A-D converter in a computer running a LABVIEW™ program, written by the author specifically for this task, which calculated

and returned to the user an average percentage transmission over a user defined (usually 50-100) number of readings. Code within the software also allowed for the differences between the power meters to be calibrated out giving an accurate transmission value.

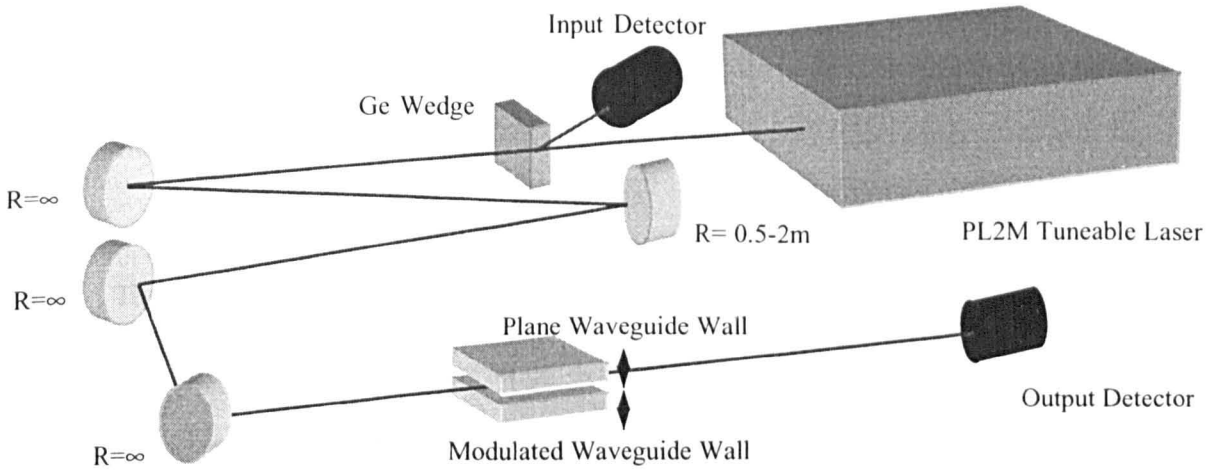

Figure 5.5 Optical set-up for coupling TEM00 mode to slab waveguide mode enabling transmission of waveguides to be found.

Matching the output beam from the source laser proved a particular challenge. A number of factors had to be considered. Possibly the most critical factor to achieve repeatable readings for transmission through the waveguide is the stability of the source laser. The initial laser used in these experiments was an Edinburgh Instruments' PL2 laser. This was found inadequate for our needs, the output beam shape was not reproducible or predictable, leading to vastly differing transmission measurements between readings (keeping all other variables constant). The second laser used for these experiments was again from Edinburgh Instruments, but this time the PL2M model, which offered far greater wavelength/mode stability and reproducibility, along with a higher output power. Use of this source did allow for repeatability between readings.

When altering the output wavelength from the source, care had to be taken to ensure the correct matching conditions remained at the new wavelength. The spot size emitted from the laser altered with wavelength. The size alterations were small enough that no significant changes in matching, and hence transmission, could be seen within each branch of the CO_2 spectrum. However when switching to differing branches the setup had to be checked to ensure that the input beam was correctly mode matched to the waveguide.

The absolute transmission through a 15cm long waveguide with a gap of 1.2mm was measured. Previous experience within the group has enabled in excess of 99% transmission through a waveguide for an input beam well matched to the fundamental waveguide mode. The transmission was maximised, and burn patterns taken some distance from the waveguide output to assess how well coupled the input beam was to the fundamental waveguide mode. As perfect coupling can not happen, a small percentage, say 0.5-2% of the power incident on the waveguide is likely to be coupled into higher order modes. Although only accounting for a very small amount of the transmitted power these modes cannot be ignored. The effect we are looking for is only a few percent in size, therefore loosing the power from the higher order modes could be critical. For an accurate transmission measurement these modes must be detected. As these higher order modes have a larger divergence than the fundamental mode, a larger spot will be produced than if these modes were not present. To ensure that all these modes were recorded a detector, with an active area of 19mm diameter, was centred on the fundamental mode never more that 15cm from the output of the waveguide..

All transmission results reported further in this chapter are relative as opposed to absolute. Where transmission through a patterned section of waveguide is compared with a result through an unpatterned section both readings were taken one after the other thus reducing experimental errors. The only change required in optical set-up between these two readings was the horizontal movement of the waveguide allowing the incident radiation to see either the patterned or the unpatterned region of the waveguide. This relative process along with the multiple readings taken, allowed us to view accurately the small changes in transmission levels reported here.

Figure 5.7 shows the reduction transmission caused by the diffraction pattern vs. wavelength for a waveguide made of two mirrors, separated by 0.7mm. This narrow gap was necessary in order to obtain a Fresnel number of less than 1 as is required for any device to act as a waveguide, see equation 2.6. The lattice constant of the diffraction pattern was 100μm. This figure shows a marked increase in transmission at

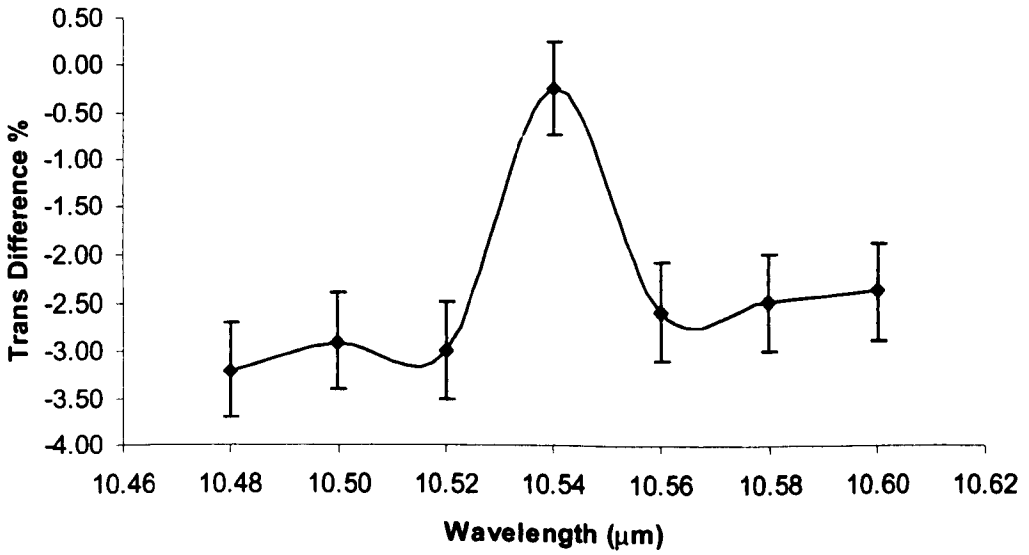

Figure 5.7 Transmission reduction caused by diffraction pattern in waveguide made of 2 mirrors

the expected wavelength, 10.54 μm (10P14) (as predicted by equations 3.4 and 3.5). As with all following wavelength transmission curves, the transmission shows the reduction in transmission caused by the pattern on the electrode, i.e. if the transmission difference is zero then the patterned waveguide has the same transmission as an unpatterned waveguide would.

Figure 5.8 shows the same data as in figure 5.7, this time for a device of the same physical dimensions, made of aluminium. The transmission through the aluminium waveguide was higher, at ~90% transmission compared to the ~80% through the mirror waveguide. However the height of the maxima is larger in the mirrored waveguide case. By comparison with the results shown in table 5.1, this was expected.

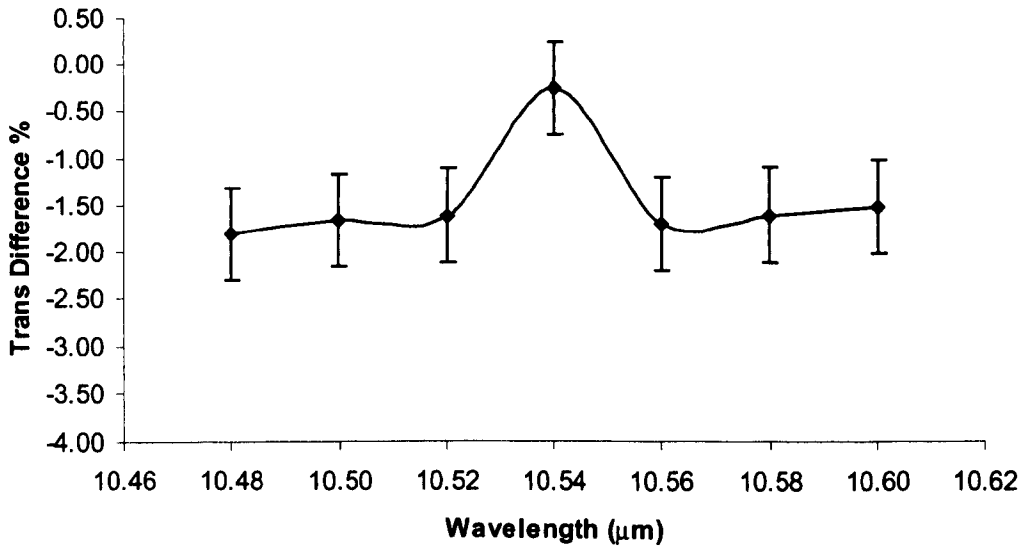

Figure 5.8 Transmission reduction caused by diffraction pattern in waveguide made of 2 aluminium pieces

Figures 5.9 shows transmission vs. wavelength data for two different portions of a waveguide, made from pre stretched aluminium measuring 150 x 250mm, with the plates separated by 1.1 mm, (in order to satisfy the Fresnel condition the spacing had to

be less the 1.25mm). One portion of the waveguide had a grid pattern, similar to that shown in figure 4.6(b) and the other a dot pattern similar to that shown in figure 4.6(a). A measurement of transmission through an un-patterned area was again taken to use as a reference. As was predicted in section 5.3, the transmission through the system is similar for both patterns however the grid pattern leads to a greater transmission at the maxima than the dot pattern.

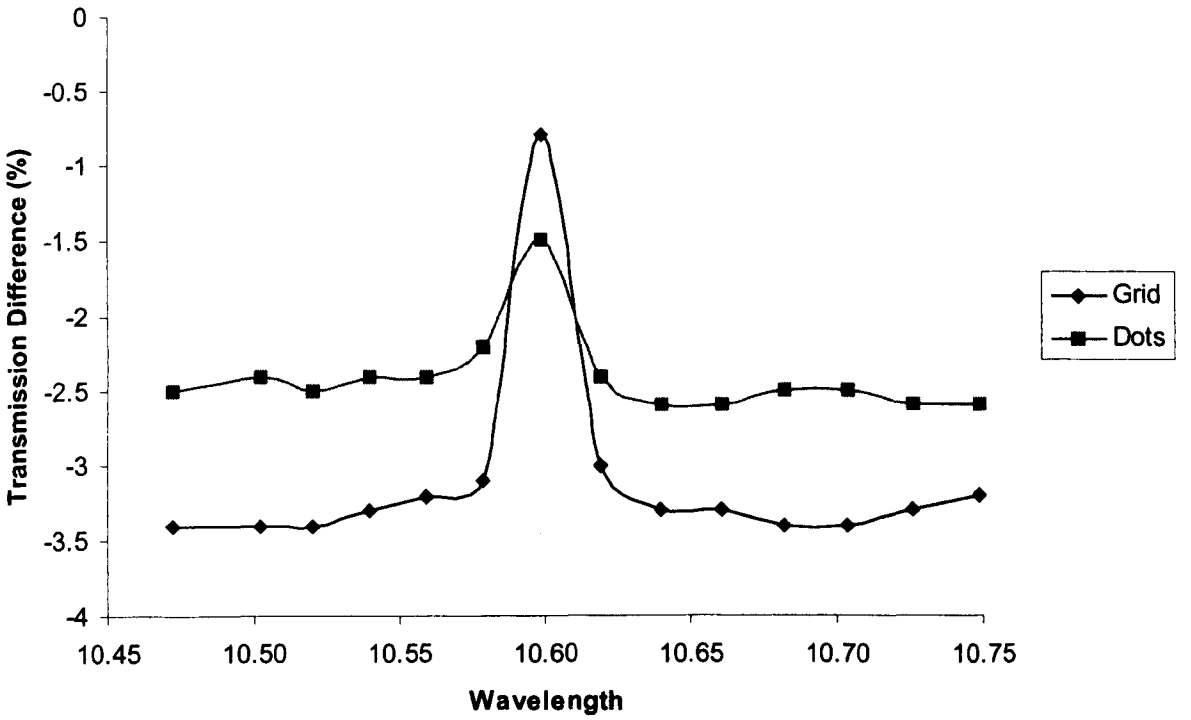

Figure 5.9 Transmission reduction caused by diffraction pattern in 2 waveguides made of aluminium each containing different diffraction patterns

The final tests were carried out on the electrodes constructed for incorporation into the laser described in chapter 6. Extensive testing was carried out so that the exact transmission characteristics of the laser waveguide could be found. The electrodes were constructed of pre stretched aluminium, measuring 45 x 365 mm, with patterns machined in the positions shown in figure 6.8. The lattice constant of the patterns was

106μm. This positioning allowed for reference transmission vs. wavelength through an unmarked portion of waveguide in the 15mm between the pattern and the waveguide wall. Transmission reduction owing to pattern vs. wavelength was again studied, this time for the four main lasing wavelength regions of the CO_2 spectrum. Also the transmission though the patterned area at various input angles was investigated.

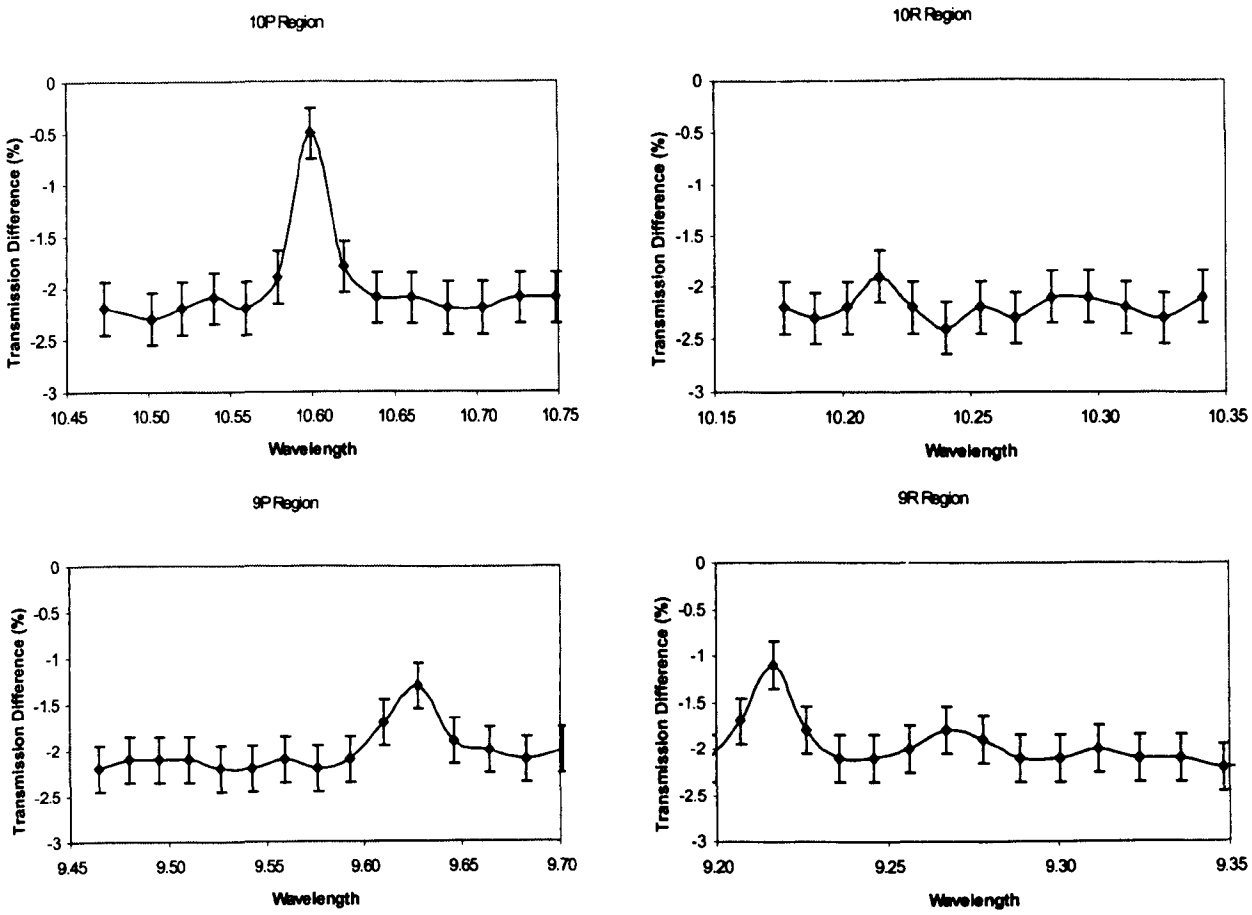

Figure 5.10Transmission reduction caused by diffraction pattern with a lattice constant of 106μm in a waveguide made of 2 Laser Electrodes for the 9P, 9R, 10P and 10R regions of the CO_2 lasing spectrum.

Figures 5.10 shows the reduction in transmission vs. wavelength for the, 9P, 9R, 10P and 10R regions of the CO_2 emission spectrum. According to equations 3.4 and 3.5 There should be transmission maxima at 10.6μm (10P20 line), 9.636μm (~9P30), and

9.217μm (~9R34). All these maxima can be seen in the in figure 5.10, the relative strength of the 10P20 maxima is considerably larger than the other lines which are all present at significantly weaker regions of the CO_2 spectrum, therefore less power is available from the laser and consequently less difference seen.

Figure 5.11 again shows transmission vs. wavelength data but this time several curves are shown corresponding to different launch angles, only the 10P region of the CO_2 spectrum was analysed. No significant difference can be seen for transmission with respect to wavelength, this is a result of the 2D pattern incorporated into the waveguide as shown in section 5.5.

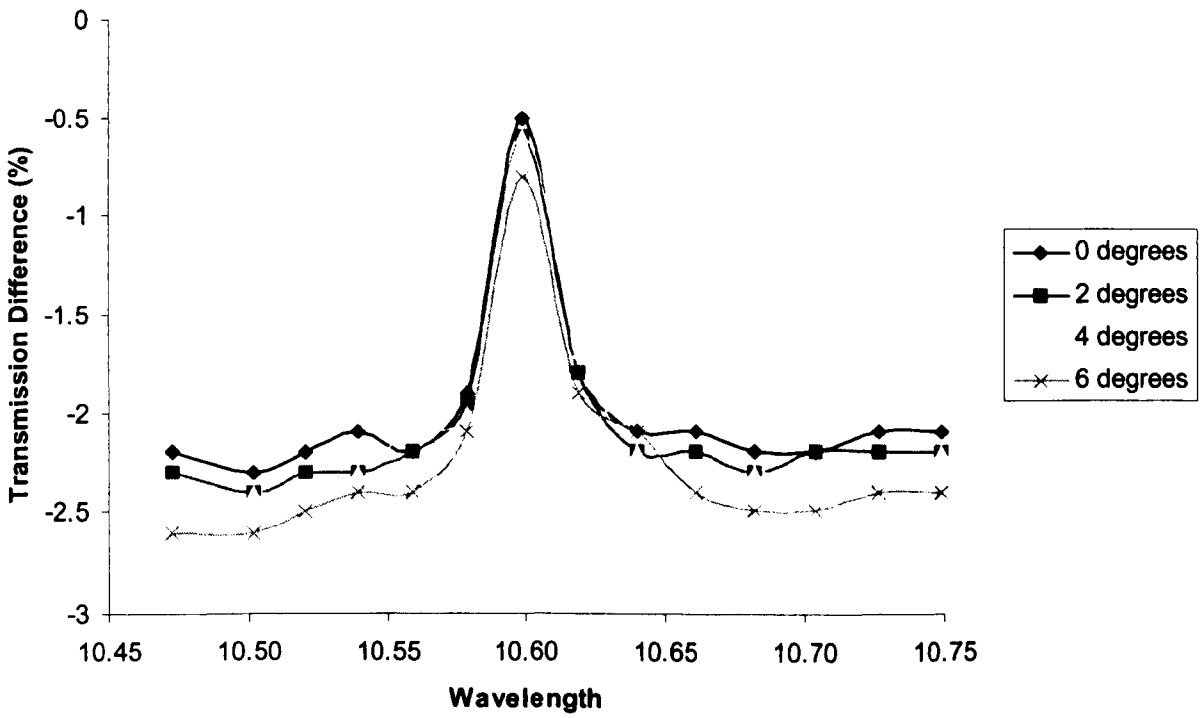

Figure 5.11Transmission reduction caused by diffraction pattern with a lattice constant of 106μm in a waveguide made of 2 Laser Electrodes for the 9P, 9R, 10P and 10R regions of the CO_2 lasing spectrum at various horizontal input angles

Finally the second laser electrode constructed was tested. Transmission reductions vs. wavelength curves are plotted in figures 5.12 corresponding to the four main lasing region of the CO_2 spectrum. This electrode had a lattice spacing of 82μm, with expected transmission maxima at 10.25μm (10R20), 9.647μm (9P30) and 9.11μm (~9R38). Once again all maxima can be seen however as with the previous electrode only the intended output (10R20) can be easily seen as this is the only maxima close to a wavelength with a high gain coefficient.

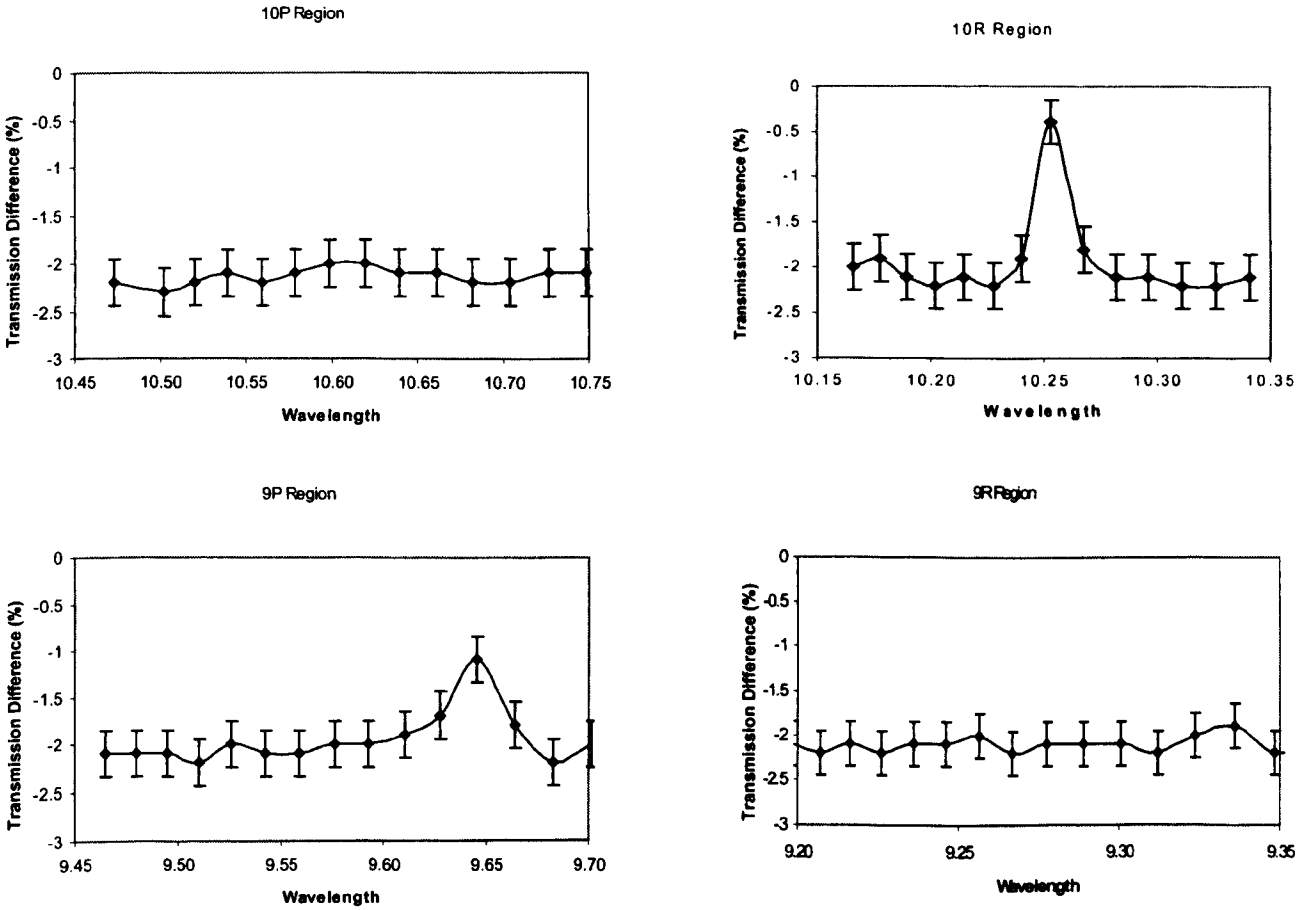

Figure 5.12 Transmission reduction caused by diffraction pattern with a lattice constant of 82μm in a waveguide made of 2 Laser Electrodes for the 9P, 9R, 10P and 10R regions of the CO_2 lasing spectrum.

5.7 CONCLUSIONS

It has been shown that the optical filters proposed in Chapter 3 and constructed as described in Chapter 4 do indeed alter the transmission of the radiation passing through them dependent on the wavelength of that radiation. The maxima of the transmission are in agreement with predicted values as modelled in equations 3.4 and 3.5. The reduction in transmission away from these maxima is between 2 and 3% per pass for an all aluminium waveguide as used in a CO_2 slab waveguide laser.

These waveguide filters can be made out of many different materials, each giving different variations in transmission with wavelength. Those with a low reflectivity for CO_2 radiation diffract more and transmit less, and vice versa. The pattern can also be altered, a pattern containing more marked surface (i.e. grid pattern compared with dot pattern) diffracts a larger proportion of the light, consequently transmitting a smaller proportion.

Filters constructed using a 1D pattern would have the same effect on the transmitted radiation as a 2D pattern if this radiation enters with a horizontal incidence angle normal to the pattern. However if non-normal incidence or multiple incidence angles are present the use of a 2D pattern is advantageous.

Chapter 6

Line Selective Slab Waveguide Laser

6.1 INTRODUCTION

In this chapter, results from incorporation of two waveguide wavelength filters, as described in chapter 5, into a RF excited CO_2 slab waveguide laser are discussed. The first of these filters aims to stabilise the laser to operate solely on the most probable lasing line in the CO_2 spectrum, the 10P20 line, lasing with a wavelength of 10.59μm. Under normal conditions these lasers operate over a few possible lasing transitions from around 10P16 to 10P28, (corresponding to wavelengths of between 10.56μm and 10.68μm).

The second filter aims to move the operating wavelength of the laser to another branch of the CO_2 spectrum, namely to the 10R branch. The specific line chosen was the most probable transition to occur in the 10R branch, which is the 10R20 transition, with the corresponding wavelength of 10.25μm.

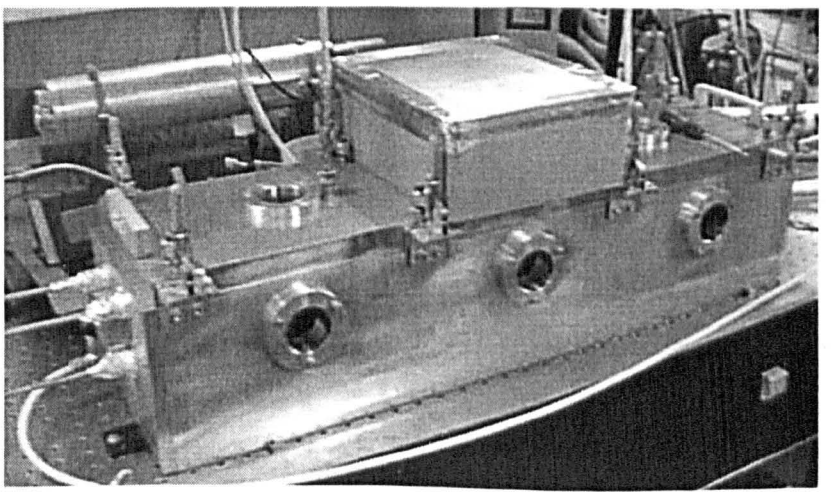

Figure 6.1 A photograph of the laser used in the line selective experiments

The laser used has electrode sizes, mirror spacings, positionings and radii as described in the patent [6.1] held by Coherent Inc. As can be seen in chapter 5 the effect of these filters is very small, thus to reach a reliable conclusion experiments must be carried out with a high degree of precision, and all possible data from each experiment must be obtained.

6.2 LASER AND BEAM ANALYSING APPARATUS

The experimental set-up consists of two main sections the laser and the beam analysing section. The patented [6.1] laser electrodes and mirrors were enclosed in a "research" vacuum box of internal dimensions 150x150x600mm^3, the area of the electrodes is 45x365mm^2. The laser operates with a hybrid stable/unstable confocal resonator configuration with the front mirror having a radius of 384mm and the rear with a radius of 420mm. The laser is shown in figure 6.1 with an internal schematic in figure 6.2. The cavity mirrors are adjusted with kinematic mounts held in lateral position by an invar rod along the base of the cavity. Piezo translators also allow for fine adjustment of the rear mirror.

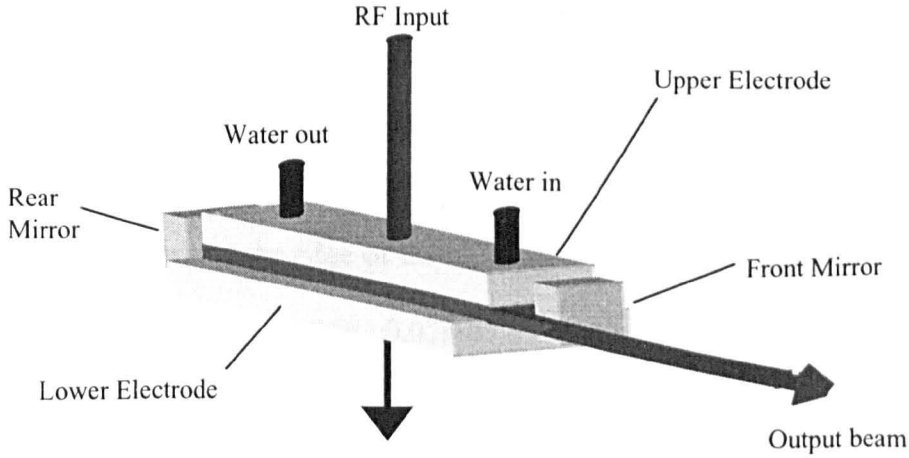

Figure 6.2 Internal Laser Schematic

Power into the discharge is provided by a water cooled 81MHz RF generator. The laser electrodes are also water cooled. The maximum output power seen from the laser was around 110W average, with a 3:1:1, $He:CO_2:N_2$ gas mixture. The overall laser efficiency was 11%. The 3:1:1 gas mixture was supplied from a premixed bottle which also contained 5% Xenon. Other mixtures used (1:1:1) were mixed from separate gas bottles in a vacuum vessel.

For these experiments, it was essential to be able to remove and reposition the electrodes in an identical location, relative to the mirror cavity. This led the author to alter the water cooling pipe geometry, allowing for the removal of the electrodes without disturbing the optical cavity alignment. This was accomplished by re-routing all the cooling pipes through the lid of the vacuum chamber, cooling the electrodes in series rather than in parallel as with the original laser. Once the lid was removed the two electrodes could be removed as one assembly, without effecting the cavity alignment.

The 2 electrodes were mounted parallel to each other outside the vacuum chamber. This was accomplished using an in group technique where a glass cone is inserted between the two electrodes, the length of the cone able to enter the waveguide being proportional to the spacing between the electrodes. If the cone is inserted into the waveguide at various locations around the edge of the electrodes it is possible to adjust the gap across the entire electrode to within 0.02mm. The spacing between electrodes was altered/maintained by positioning bolts on threaded shafts, one at each corner of the assembly. Once mounted together the electrodes, with water pipes connected could be re-inserted into the vacuum chamber in an identical position. Sockets on the base of the

lower electrode rested on a three point mount attached to the base of the case. This process allowed for several patterned and un-patterned electrodes to be tested in the cavity under almost identical optical conditions.

The beam analysing system[1] allows for simultaneous measurement of vertical (waveguide) far and near field mode patterns along with the spectral (wavelength) output and power output. Only the waveguide mode was of interest here, as the filter

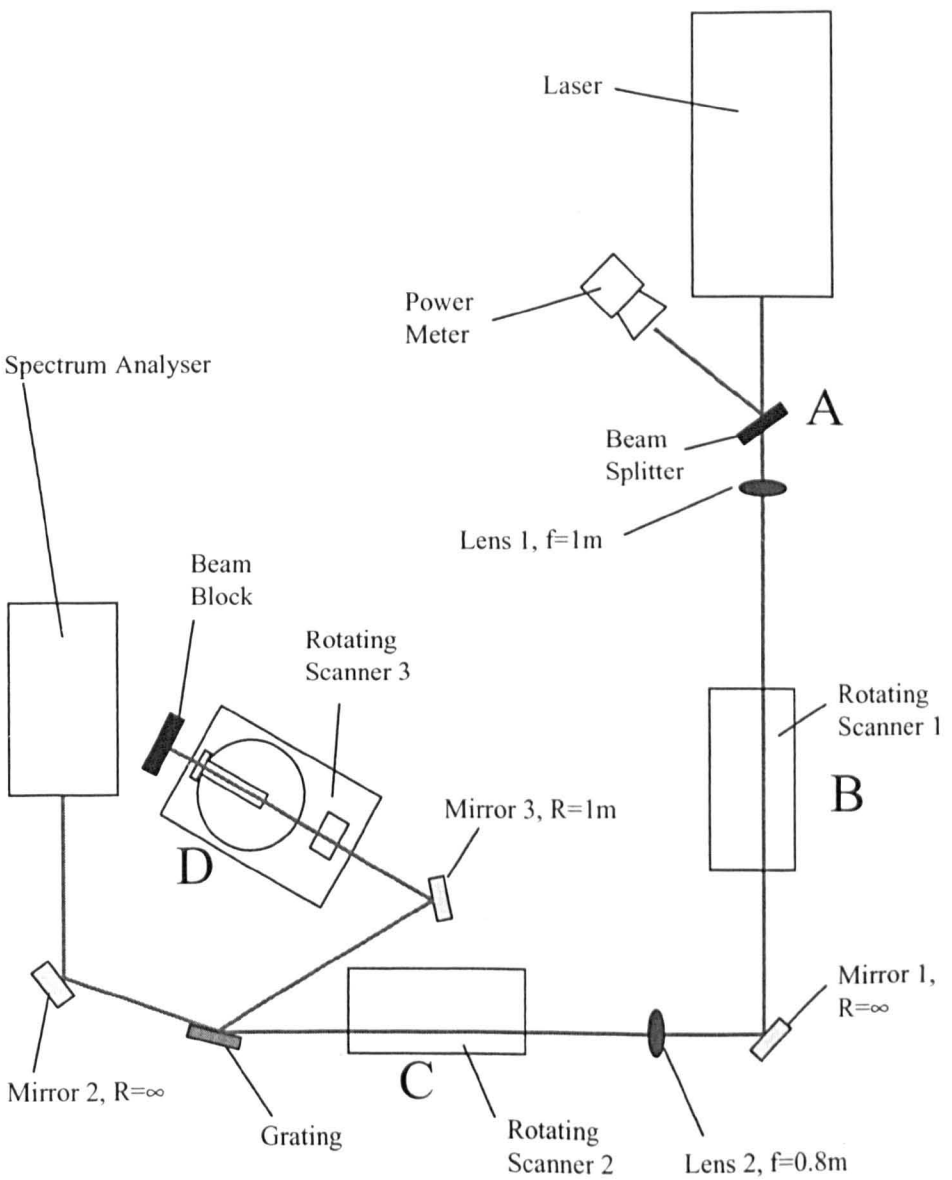

Figure 6.3, Layout of Beam Analysing System.

[1] Beam analysing system designed by Dr. F. Villarreal, Heriot-Watt University

only affected that mode, the free space (horizontal) mode would not be affected by the pattern marked in the electrodes. Recording both near and far field beam profiles allowed for the entire beam to be analysed. These readings were fed to various computers running data logging software, written in LABVIEW™. This allowed for the laser output to be continuously monitored over periods of several hours. Figure 6.3 shows an overall schematic of the beam analysing system. We believed that any effect seen would be very small, and to ensure that the effect would be seen it was necessary to monitor the experiment completely, recording as much information about the laser output characteristics as possible.

At point A, 56% of the laser power was diverted via a beam splitter to a power meter, the output of which was in turn fed to a computer for data logging. The far field (waveguide) beam pattern of the laser was logged at point B, one focal length from lens 1, by the rotating beam scanner described below. A real image of the laser exit aperture was formed at point C where the near field pattern was taken, by a second rotating mirror scanner.

After point C the beam then passes to a diffraction grating ruled 150 lines per mm. The zeroth order from the grating passes off mirror 2 and enters a commercial spectrum analyser to discern the laser wavelength. The first order from the grating passes to mirror 3 and a far field image is again formed at the focus (50cm) point D. Here the horizontal output is scanned by a third rotating scanner to allow the position of the diffracted beam to be recorded. This position could be converted to wavelength by comparison with wavelength noted from the spectrum analyser.

As discussed above the near and far field beam profiles along with the spectral output of the laser were all recorded using rotating mirror scanners. The scanners take a sample of the beam at set intervals (every tenth of a second in this case) by chopping the beam with a rotating mirror and reflecting the beam to a detector after first passing through a 200μm pinhole. The detector can be moved vertically by means of a stepper motor to sample different portions of the beam. The scanner is shown schematically in figure 6.4 and 6.5.

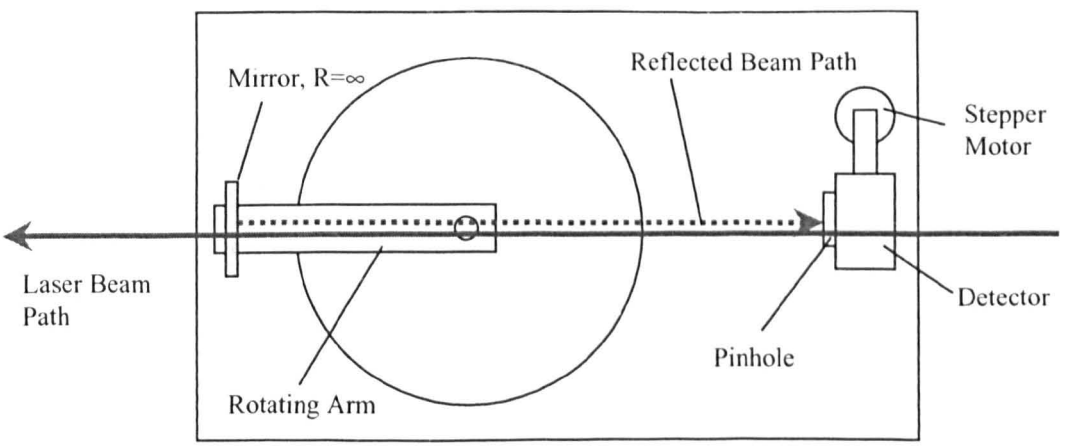

Figure 6.4 Schematic of the Rotating Mirror Scanner as seen from above

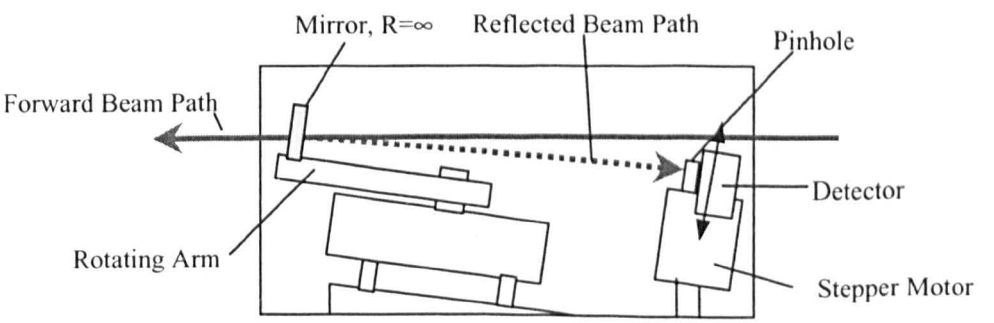

Figure 6.5 Schematic of the Rotating Mirror Scanner as seen from the side

As the scanners are in line, if two scanner mirrors pass through the beam at the same time there will be a null reading at the second scanner, the beam having been blocked by

the earlier scanner. However this does not cause a significant problem as the scanners are not operating at exactly the same frequency (10±0.2Hz) thus the beating phenomenon only affects results for short periods of time during an experimental run.

6.3 WAVELENGTH CHARACTERISTICS DURING STANDARD OPERATION

Initial experiments were conducted to measure the wavelength and mode behaviour of the RF excited CO_2 slab waveguide laser with unpatterned electrodes. These measurements could later be used in comparison with the laser operating with wavelength selective patterned electrodes The laser operating parameters were defined during these initial baseline experiments and maintained for all following experiments. The input RF pulse was modulated at a frequency of ~160Hz with a 50% duty cycle. The power input to the laser was around 1kW with reflections from the matching circuit minimised for each run. Gas pressure inside the cavity was set to 85 torr. The optical cavity was aligned to produce as close to the fundamental mode as possible, with this resonator geometry the fundamental mode produces the maximum power

Figure 6.6 shows the power of the laser and the line that the laser was operating on with respect to time for a 2½ hour run of the laser with un-patterned upper and lower electrodes. The marks in the upper section of figure 6.6 records which wavelengths were present at a particular point in time, with the lower section recording the power.

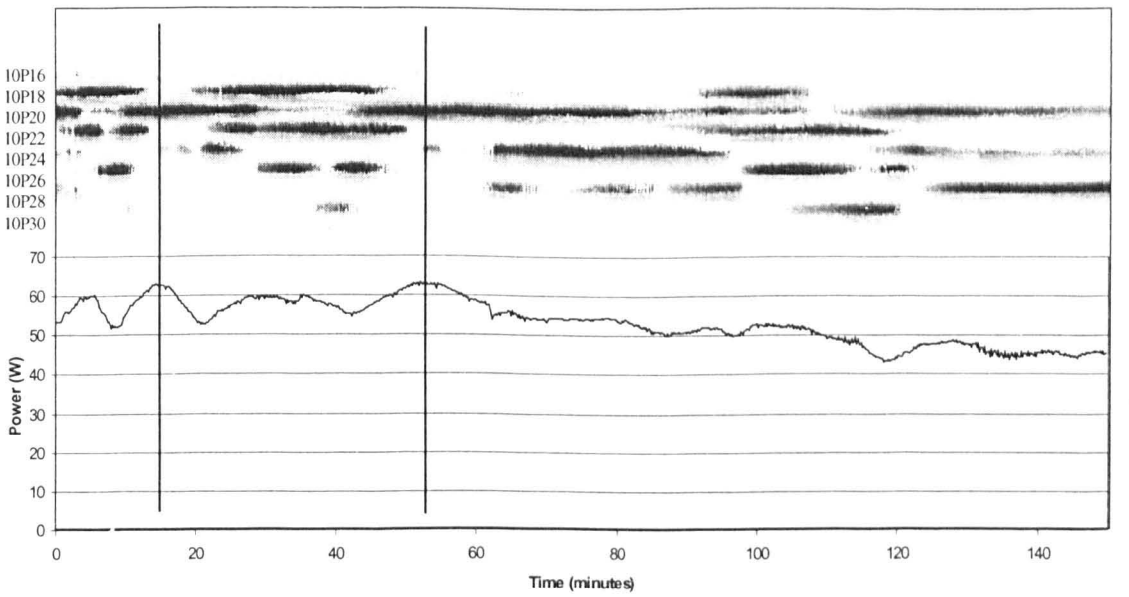

Figure 6.6 Power and Wavelength characteristics during standard operating conditions

It can be seen from Figure 6.6 that the wavelength and power of the laser vary considerably. This is primarily a result of the thermal expansion of components inside the laser altering the cavity length and alignment. Although the mirror mounts are held in place by an invar rod (with a very low thermal expansion coefficient) the mounts themselves will move as they are heated as will the rest of the laser box which could alter the position of the electrodes relative to the resonator mirrors. The electrodes themselves will reach a thermal equilibrium relatively quickly, between heating by the gas discharge (and to a much lesser extent resistive losses in the electrode) and cooling from the water flow though them. Changes in wavelength and spectral output of the laser are a result of the fluctuations in the resonator length and the lateral position of the mirrors, whereas any change in the spatial mode of the laser output can be accounted for by a tilting of the mirror mounts.

Under normal circumstances thermal tuning would be highly undesirable, however in our case it allows us to attempt to counteract these effects by incorporation of our waveguide filtering patterned electrodes.

By closer inspection of figure 6.6 the effect of signature scanning can be seen. It can be seen that a pattern of wavelengths and power fluctuations is scanned through whilst the laser heats up and stabilises. The beginning of two possible repetitions is shown by the vertical lines marked on the diagram. One method for viewing any alteration in operation of this device after the inclusion of the wavelength filters would be to view the change in this signature.

Along with power and wavelength measurements for standard operating conditions, near and far field beam patterns were taken. Generally the far field showed a single fundamental mode being produced by the cavity. However as the cavity reached thermal equilibrium the far field pattern also occasionally changed, which may have been caused by the laser operating on higher order waveguide modes. The output beam may contain the third order mode, causing the shoulder, and the second order mode, causing the asymmetry. This can be seen by a shoulder forming on the side of the fundamental mode in the far field beam profile. Figures 6.7 (a) & 6.7 (b) show the far field pattern at several times during the experimental run.

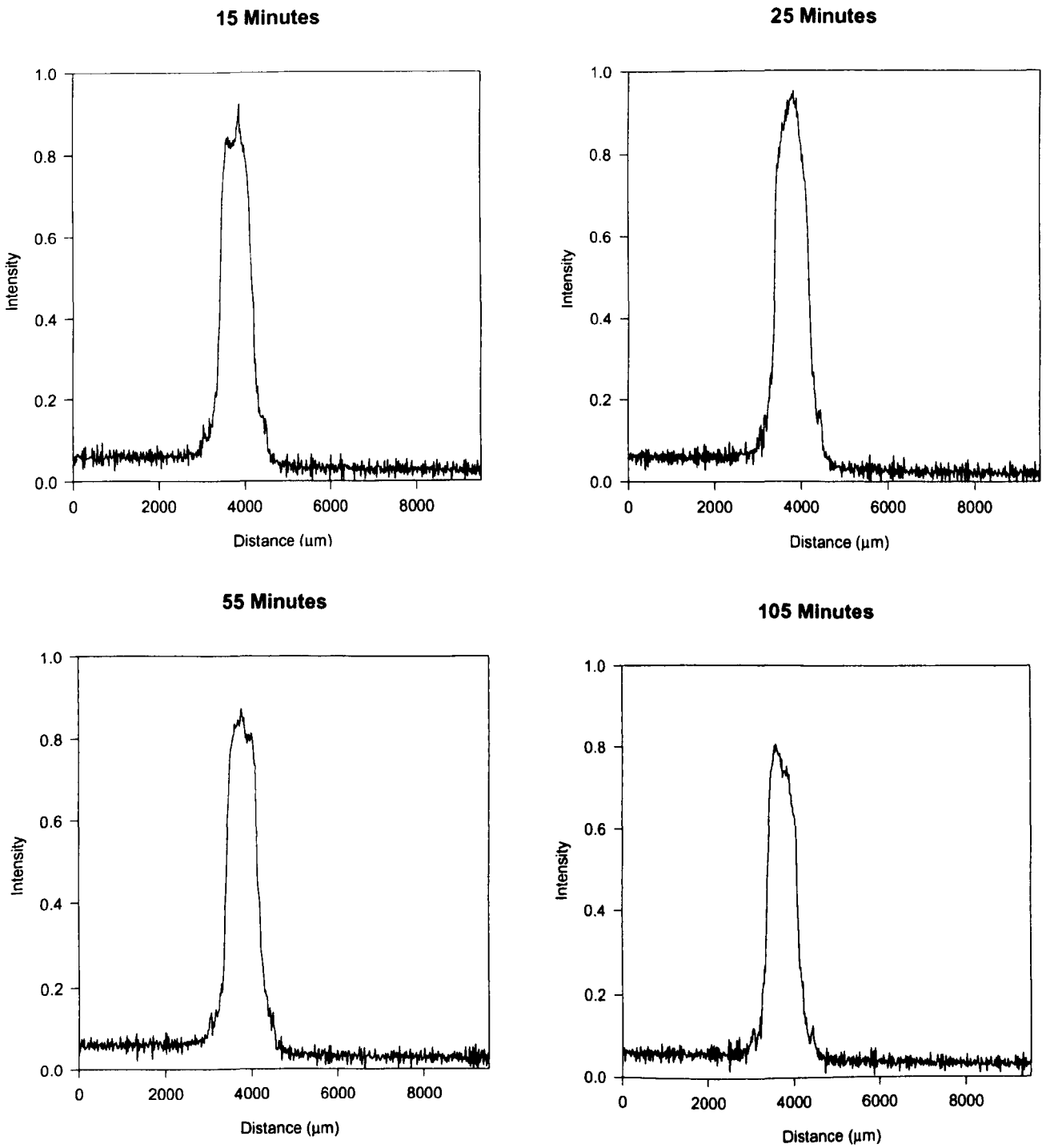

Figure 6.7 (a) Normalised near field beam profiles in the waveguide direction of a standard RF excited CO_2 slab waveguide laser at various times

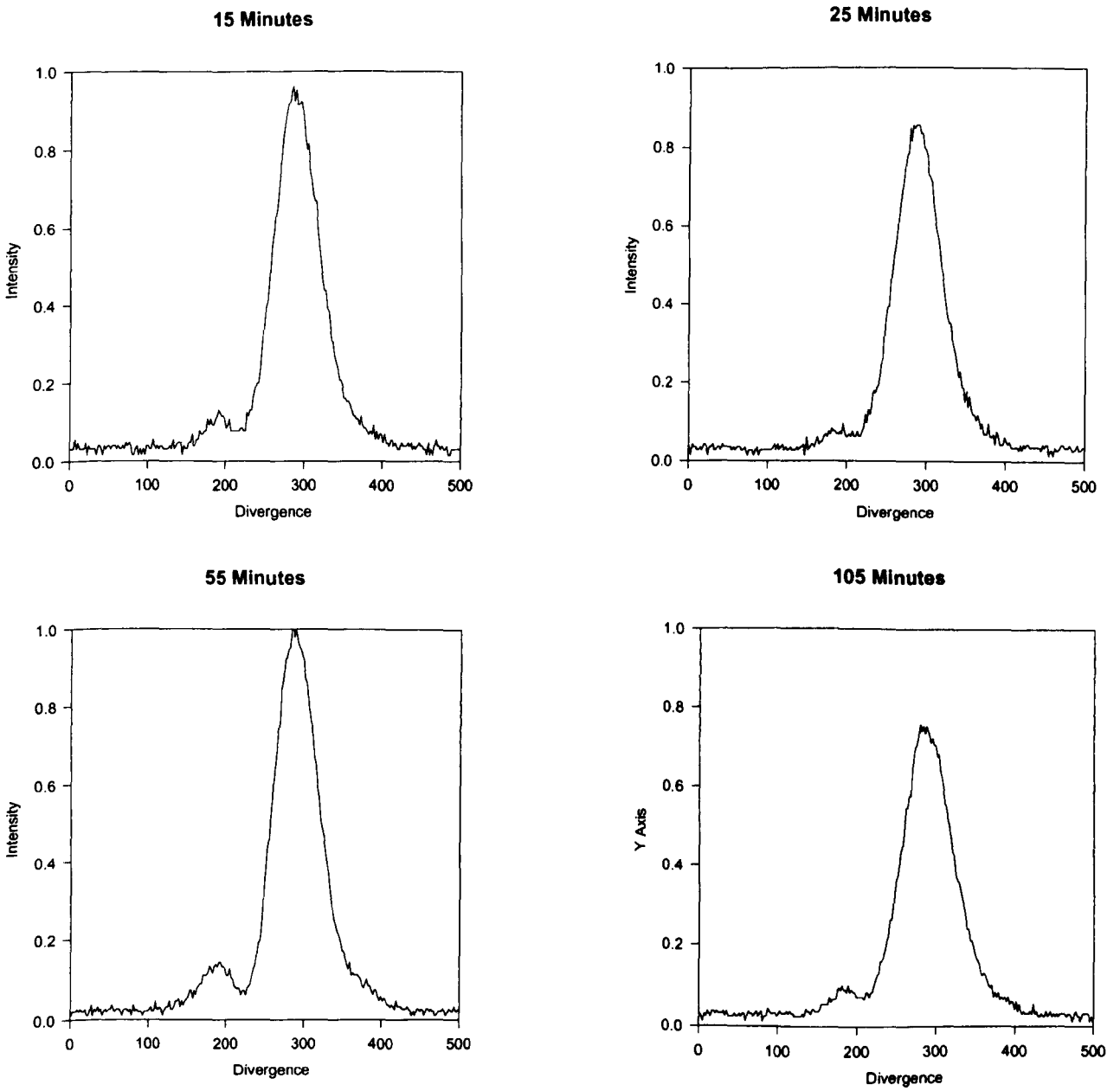

Figure 6.7 (b) Normalised far field beam profiles in the waveguide direction of a standard RF excited CO_2 slab waveguide laser at various times

Up to this point the piezo actuators on the rear mirror had been used solely to allow for fine alignment of the cavity alignment. They could also be used for manually adjusting the resonator length, by translating the rear mirror, in a similar way that thermal expansion had altered the resonator length previously. This allowed us to adjust the laser very quickly throughout all the possible longitudinal modes seen during the laser warm up period. With this manual length tuning it was possible to get the laser to operate purely on one line. However after a matter of a few minutes it began to cycle through the various wavelengths shown in figure 6.6. This was tried after the laser had been running for over 120 minutes to allow thermal equilibrium to be reached.

6.4 10P20 LINE SELECTION IN A SLAB WAVEGUIDE LASER

In this next section, data has been recorded with the upper electrode replaced with a patterned electrode in order to achieve wavelength selection. To maximise the effect that the pattern would have on the line selected, the pattern was machined where the beam path crosses in the cavity, i.e. at the focal points of both of the mirrors. All the radiation in the cavity must pass this point at least once per round trip, allowing for the largest levels of interaction between available radiation and patterned area.

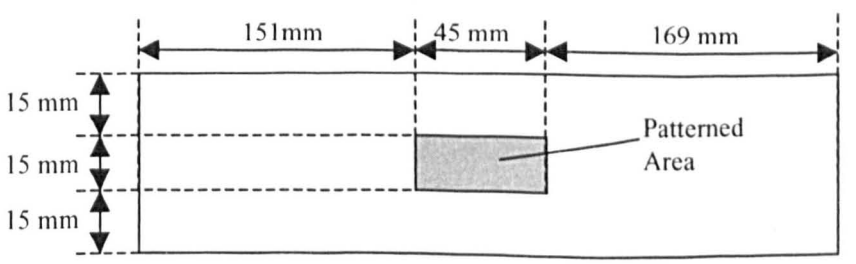

Figure 6.8 Position of the electrode pattern on the upper electrode.

The pattern on the electrode consisted of a perpendicular grid with 106 μm spacing between adjacent lines in both x & y directions. This filter will, according to equations 3.4 and 3.5, have pass bands at 9.22 μm, 9.64 μm, 10.01 μm, 10.59 μm, and 11.15 μm. 9.22μm corresponds to 9R30 and 9.64 μm corresponds to 9P30, both of which have a far lower probability of lasing than 10P20, see section 2.2. The remaining transmission maxima lie outside the range lasing transitions in the 9R & 9P and 10R & 10P branches of the CO_2 laser spectrum (for the standard C12 and O16 isotopes used here.) Thus the patterned electrode should preferentially choose the 10.59μm, 10P20 line above all other lasing lines.

As in the previous section the laser was again left to run for 2½ hours. The power and wavelength output is shown in figure 6.9, every effort was made to maintain identical cavity alignment conditions, waveguide spacing, mirror alignment, mirror to waveguide alignment, as were used in the previous baseline experiments.

It can be seen by comparison between figures 6.6 and 6.9 that the laser is now far more inclined to operate on the 10P20 line, the one preferentially transmitted by the patterned electrode.

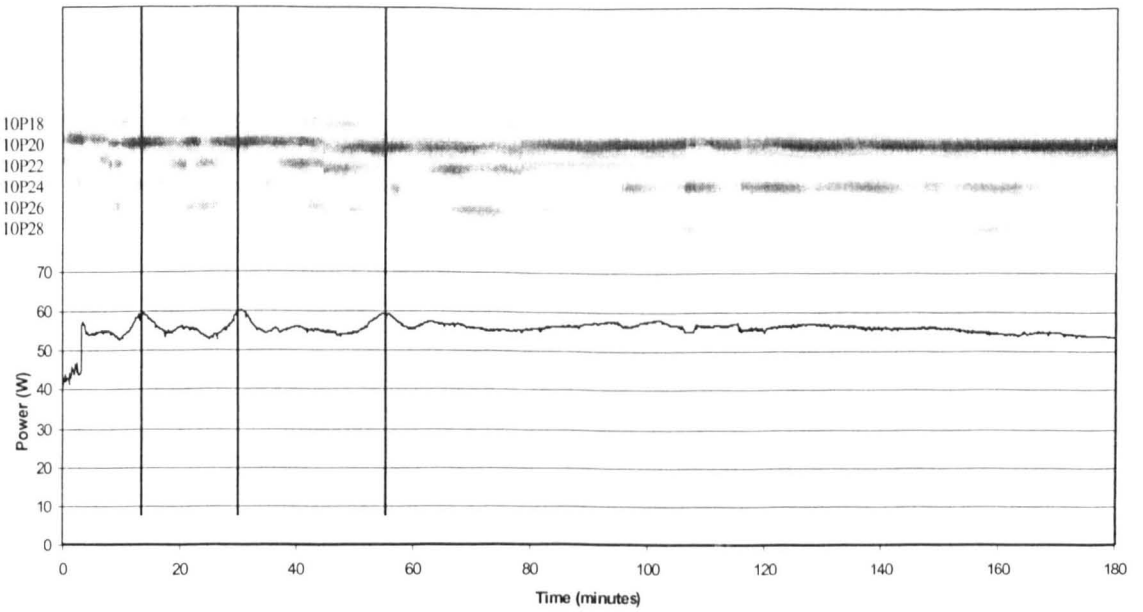

Figure 6.9 Power and wavelength spectrum for a slab waveguide laser containing a patterned electrode optimised for 10.6μm transmission with cavity aligned as for a 'normal' unpatterned use

The corresponding near and far field patterns of this run are shown in figure 6.10 (a) & 6.10 (b) respectively. They show that higher order modes are propagating in the waveguide direction more than in the case of the un-patterned electrode. Side lobes have appeared on the fundamental mode suggesting that the path through the waveguide is trying to avoid the patterned region of electrode, the region with greater loss.

A signature scan can again be seen in figure 6.9, with the repetition again shown by vertical lines. By comparison with figure 6.6 it can be seen that there is a marked change in signature, again showing that the inclusion of the patterned area of the electrode has had a noticeable effect on laser output. The change in signature could also be partially a result of errors in realignment of the upper electrode.

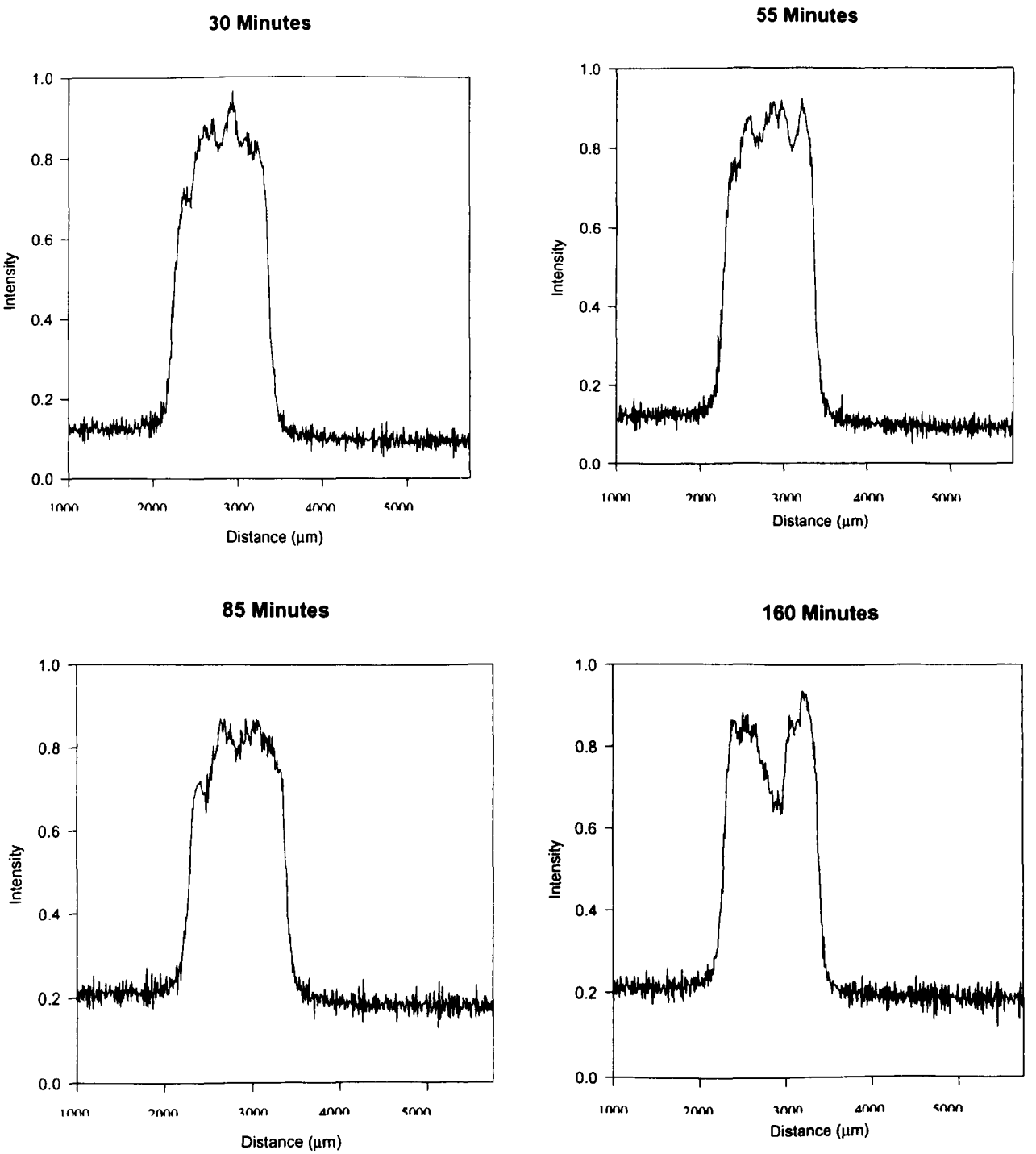

Figure 6.10 (a) Normalised near feeld beam profiles for a slab waveguide laser containing a patterned electrode optimised for 10.59μm transmission with cavity aligned as for 'normal' unpatterned use, at various times

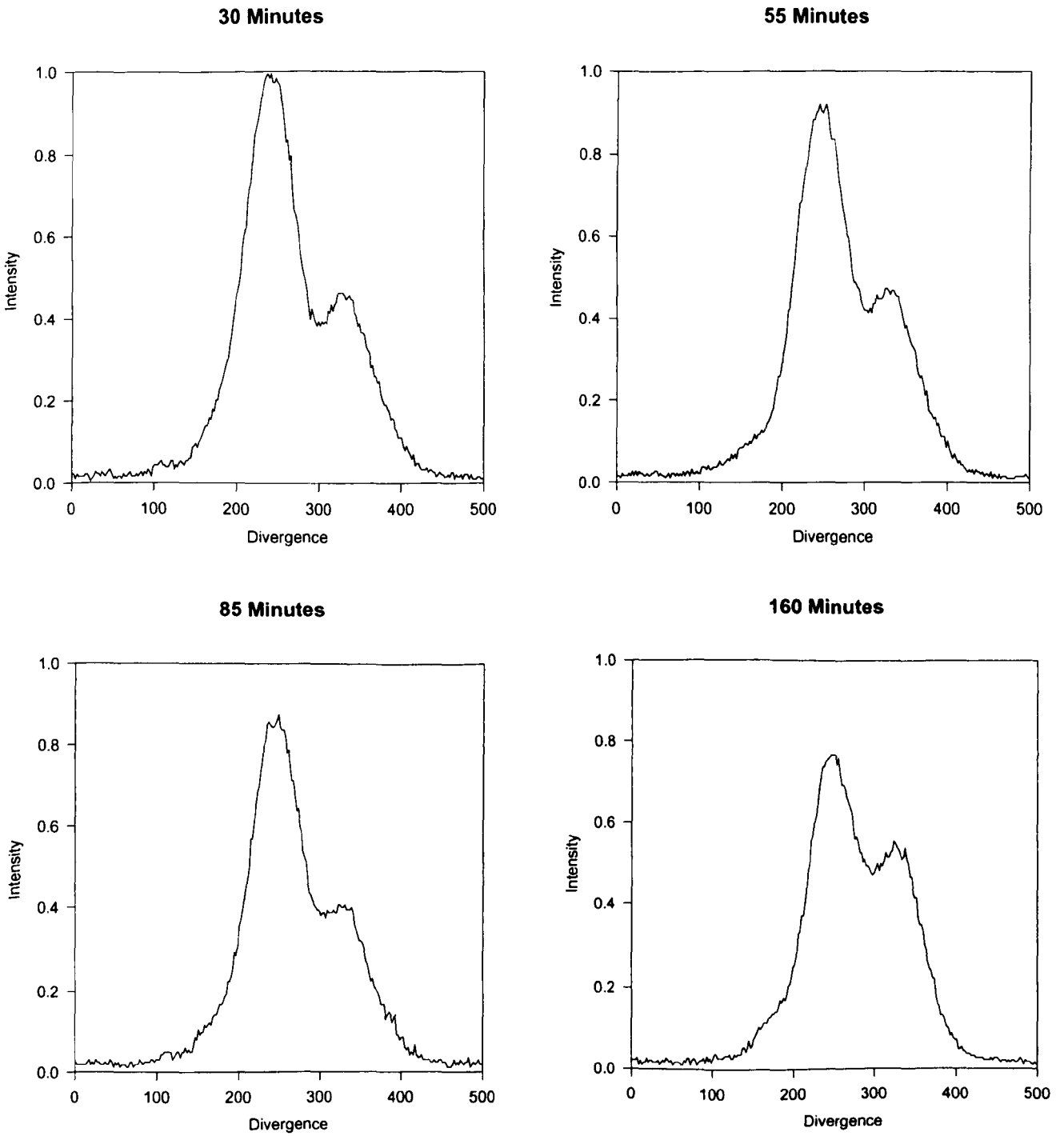

Figure 6.10 (b) Normalised far field beam profiles for a slab waveguide laser containing a patterned electrode optimised for 10.59μm transmission with cavity aligned as for 'normal' unpatterned use, at various times

After these initial results had been obtained the cavity was realigned to produce once again an output close to the fundamental waveguide mode; only a minor mirror adjustment was required to return the cavity to a fundamental mode output. The realigned laser was then run again, power output and wavelength were very similar to those shown in figure 6.9. The far field patterns obtained showed that the laser was indeed operating in the fundamental mode.

After a period of 120 minutes the laser was fully warmed up. With manual adjustment of the length of the cavity, by means of the piezo electric mounts on the rear mirror, it was possible to choose a cavity length where the laser transition remained constantly on the 10P20 line. This was never possible when using the un-patterned electrode even after a warming up period. Adjusting the cavity length allowed wavelengths ranging from 10P16 to 10P24 to be seen. Figure 6.11 shows wavelength and power for the laser operating in this tuned mode. The far and near field beam profile remained constant over this period. Near and far field beam profiles are shown in figure 6.12(a) and 6.12 (b).

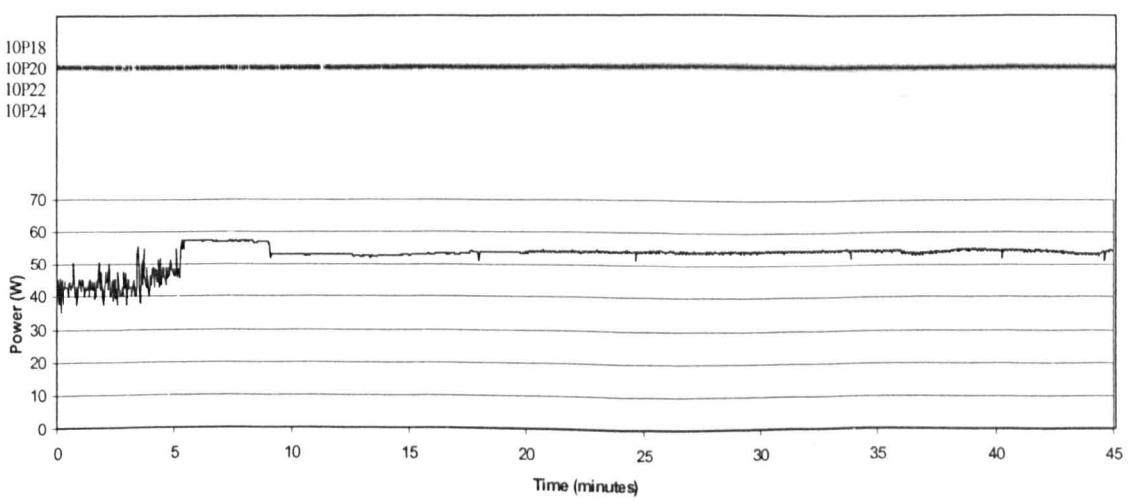

Figure 6.11 Power and wavelength spectrum for a slab waveguide laser containing a patterned electrode optimised for 10.59μm transmission after cavity realignment for fundamental mode output, with 10P20 line initially selected by length tuning with piezo translators

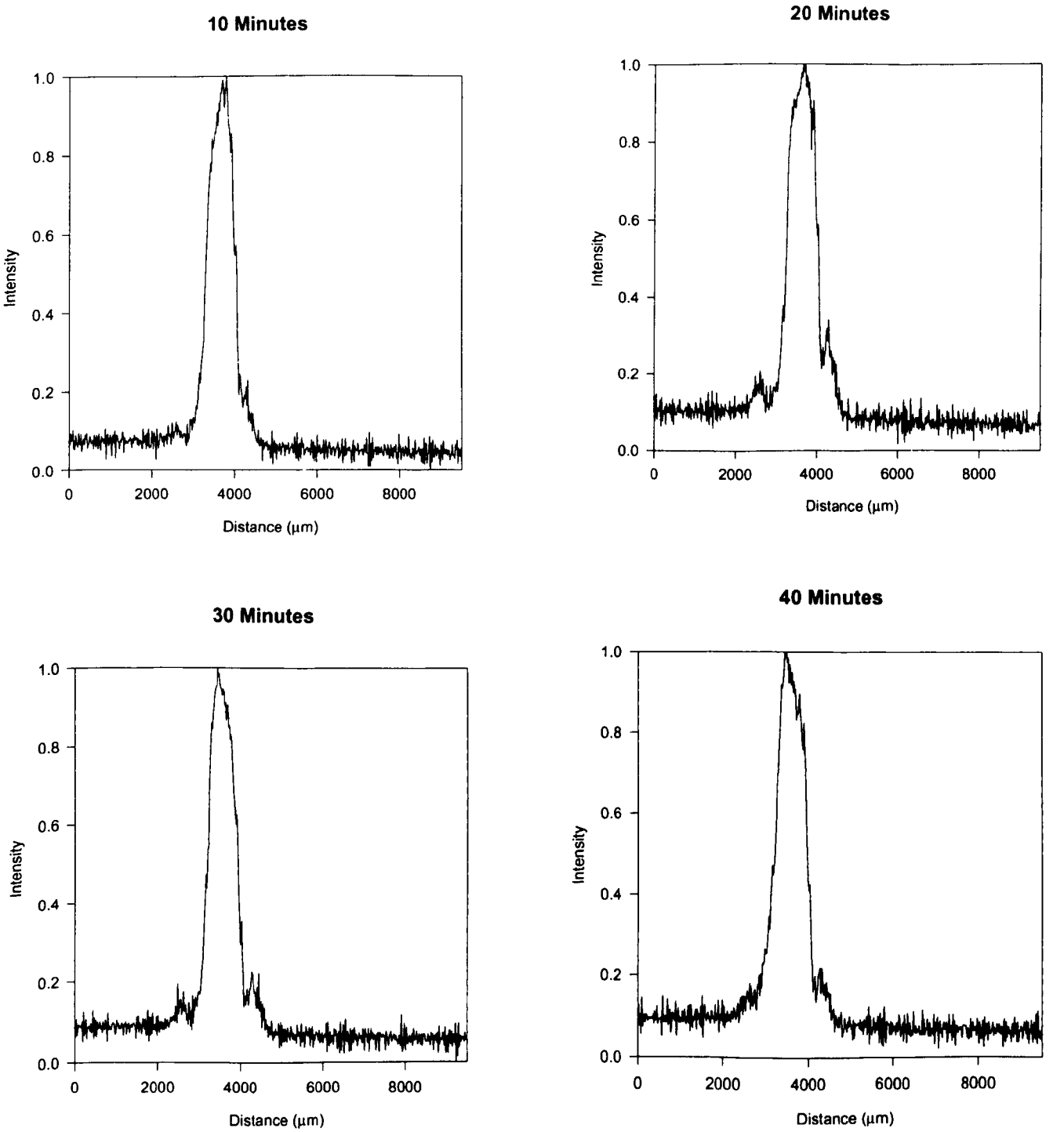

Figure 6.12 (a) Normalised near field beam profiles in the waveguide direction for a slab waveguide laser containing a patterned electrode optimised for 10.59μm transmission after cavity realignment for fundamental mode output, with 10P20 line initially selected by length tuning with piezo translators, at various times.

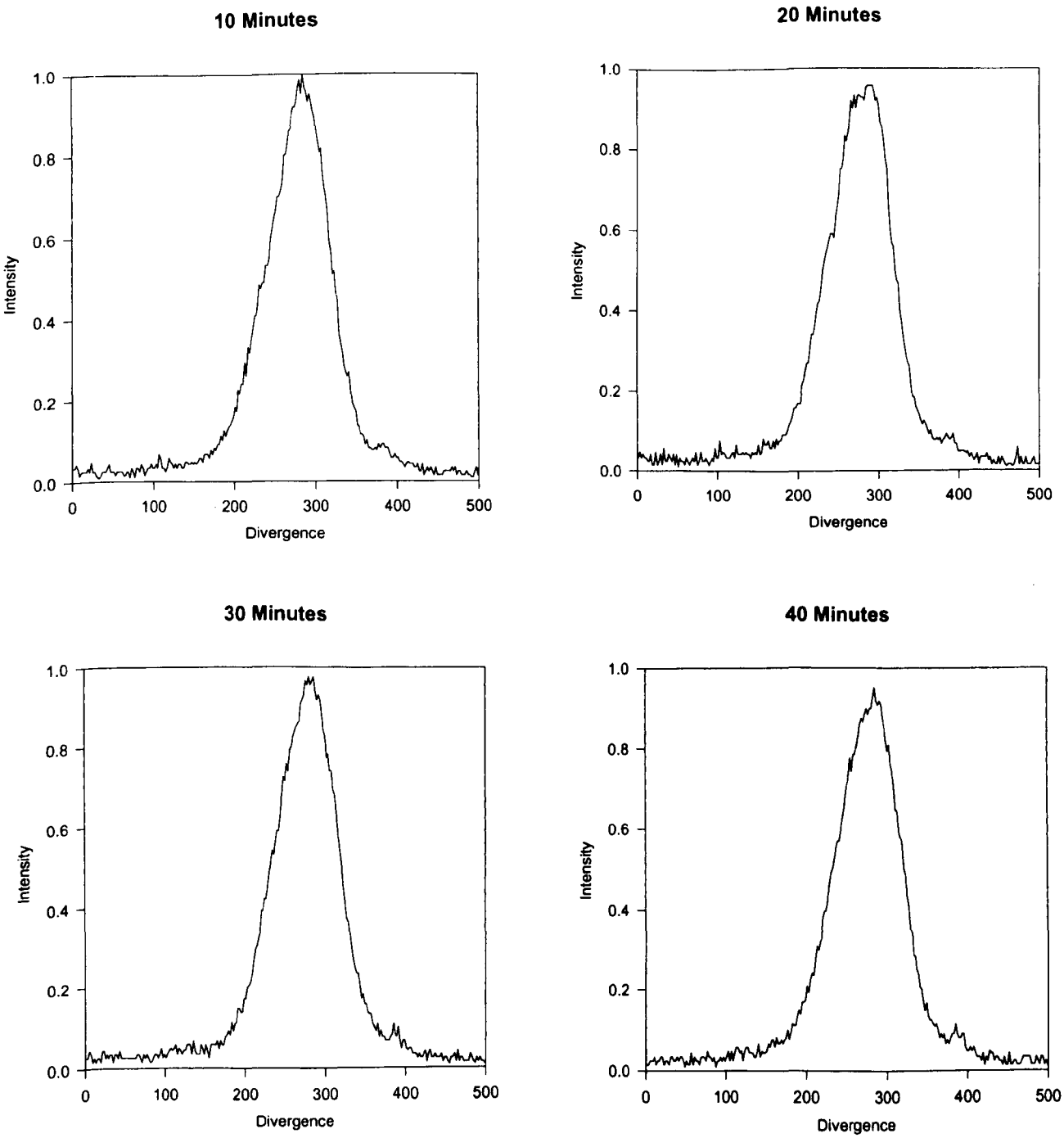

Figure 6.12 (b) Normalised far field beam profiles in the waveguide direction for a slab waveguide laser containing a patterned electrode optimised for 10.59μm transmission after cavity realignment for fundamental mode output, with 10P20 line initially selected by length tuning with piezo translators, at various times.

6.5 10R20 SELECTION IN A SLAB WAVEGUIDE LASER

In this section, results are presented for incorporation of a second waveguide wavelength filter into an RF excited CO_2 slab waveguide laser. This case utilises a filter designed to have a peak in transmission at 10.25μm, corresponding to the 10R20 laser transition. It was initially decided to try to operate the laser in a different branch of the CO_2 laser spectrum from the standard 10P branch. The branch chosen was the next most probable branch, or the branch with the next highest small signal gain, which is the 10R branch (see section 2.2), the most probable transition in this branch is at the 10R20 line.

Initially the upper electrode was again replaced with a plain unpatterned electrode, and as in section 6.3 the laser realigned to give the best modal behaviour. When tested the output of the laser was very similar to those shown previously in figures 6.6 and 6.7.

After base line measurements had been completed the top electrode was substituted for an electrode with a patterned region, again marked at the "cross-over" position as shown in figure 6.8. The pattern was of the same layout as for the 10P20 selective grid but with a new spacing of 82 μm in x & y directions. According to equations 3.4 and 3.5 this will give rise to transmission maxima at 9.11 μm, 9.64μm, 10.25μm, and 10.93 μm. The 10.25μm maxima corresponds to 10R20 the desired wavelength. The 9.64 μm maxima being the only other wavelength corresponding to a line in the standard CO_2 spectrum, namely the 9P30 line, which has considerably lower probability of occurring than 10R20. Therefore 10R20 should be favoured by this filter.

As in previous sections the laser was left to run for a period of 2½ hours. Figure 6.13 shows the wavelength and power output of the laser. It shows that the laser did not tune to 10R20, but retained a varied spectral output operating on as many lines as in the unpatterned electrode case. By comparison with figure 6.6 it can be seen that the signature of the device with this pattern in the cavity has been altered. The 10R20 line was within the viewable range of both the rotating scanner and the spectrometer. The laser occasionally jumped to operate in the 10R branch but not for more than a few seconds. Also an important feature to note is that the laser did not tune to 10P20. Commercial RF excited CO_2 slab waveguide lasers are often produced with a rough finish to the electrodes, as it has been found that the roughness of the electrodes can assist in stabilising the laser to operate at 10P20. Therefore any loss in gain introduced by roughness of the electrodes caused by the pattern being present in the waveguide may have caused the laser to tend towards the 10P20 line. However in this case loss in gain caused by the pattern does not lead to lasing on the 10P20 line. Therefore it can be concluded that grid spacing of the pattern, and not the roughness of the electrode, is the main line selection device.

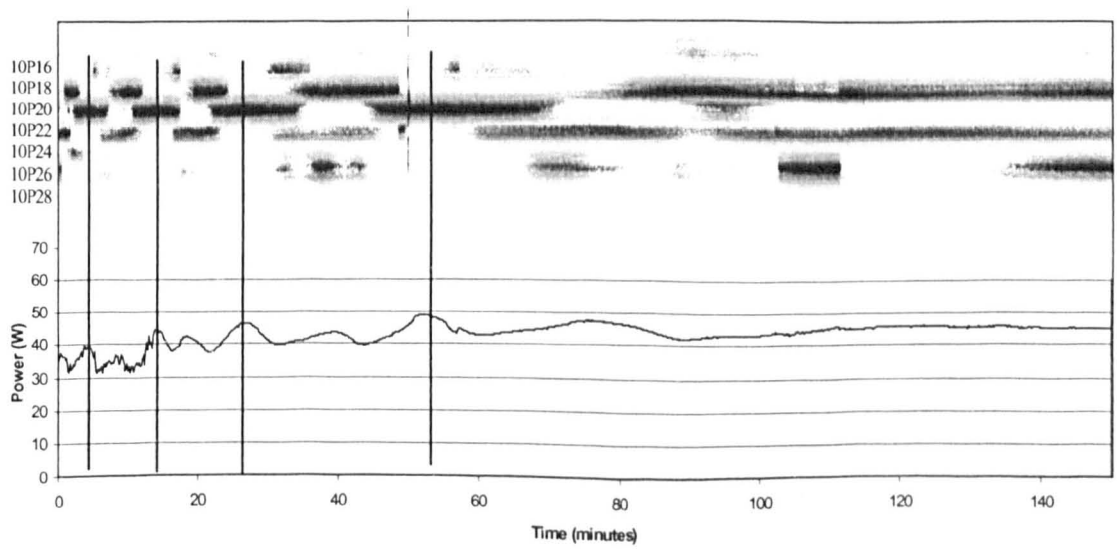

Figure 6.13 Power and wavelength spectrum for a slab waveguide laser containing a patterned electrode optimised for 10.25μm transmission

This null result in itself was not surprising; the pattern would have to make a considerable difference to the transmission of the waveguide that was much larger than that demonstrated in chapter 5 to cause the laser to operate on 10R20. Therefore in order to increase the effect of the filters more regions of the waveguide were patterned. Limitations in the available movement of the translation stages led to the largest reproducible pattern being only 5cm long. To increase the pattern area would require marking two patterns next to each other. The patterned area could be increased if we marked two patterns adjacent to one another; but in order to keep any phase variation between patterns within acceptable limits the electrode would have to be repositioned on the translation stage to within a few μm of the required position. Difficulties in repositioning the electrode led to the decision to mark two further two regions at either end of the electrode. This maximised the spacing between the patterned areas and reduced the need for the patterns to be in phase. Figure 6.14 shows the positions of the patterns.

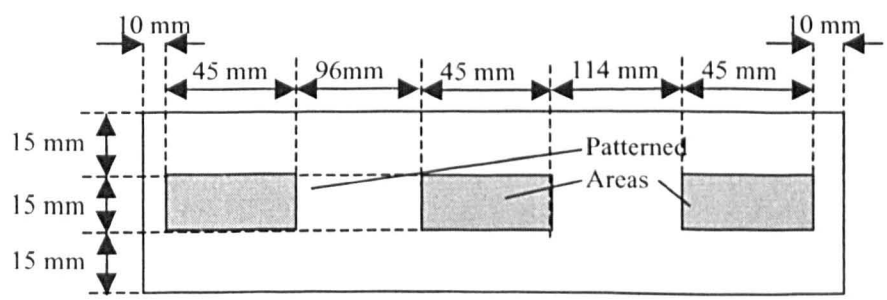

Figure 6.14 Position of Electrode Patterns for increased wavelength selection

The laser was again run with this newly machined electrode, however the laser did not operate in the 10R20 region of the CO_2 spectrum, but operated with a similar signature to that shown in figure 6.13.

In order to have a larger effect it was decided to try and reduce the gain present in the laser. If this gain, as shown in figure 2.4, were reduced then the probability of each line lasing would be reduced by the same percentage, thus causing the probabilities (and small signal gain) of different lines lasing to be moved closer to each other. This reduction in gain was accomplished by reducing the helium content of the gas mixture down to 1:1:1 (He:N:CO_2). A reduction in helium led to a decrease in the cooling of the lower lasing level and consequently a reduction in the population inversion and the gain, (see section 2.2). With the probabilities of the lines being closer together one of the weaker lines may begin lasing, in turn reducing gain on all other lines even further, as described in section 2.2. In addition to the reduction in gain, the gap between the electrodes was reduced to 1mm. This had the effect of increasing the interaction to the patterns marked in the electrodes. The resultant output still showed no tendency to lase in the 10R branch.

6.6 CONCLUSIONS

We have devised a method that can be incorporated into a slab waveguide laser configuration that allows for the selection of the laser wavelength. This has enabled us to line lock a CO_2 laser to its most probable wavelength, namely the 10P20 transition lasing at 10.59μm. As far as the author is aware this approach has not been tried before, this experiment can be seen as a first step towards a possible new technology in this area of research.

However the selection effect is, at present, very small, and we are not able to line lock the laser away from the principle wavelength, even after attempts to increase the size of the effect through an increased number of pattern or a reduction in gain. The small nature of this effect, has led to a requirement for a high level of precision and accuracy during experiments to obtain reliable results.

In order to increase the size of this effect, and consequently the level of wavelength selection, several options may be possible.

Firstly the area of the electrode which was marked could be increased. Not, as described in this chapter where separate regions of the electrode are marked, possibly leading to phase errors between regions, but by marking one larger area, possibly the entire electrode area. This would be possible by incorporating translation stages with greater travel into the laser workstation described in chapter 4.

Using filters with smaller features may increase the diffraction efficiency , effectively using a lower order grating. In order to accomplish this an alternative marking method would be required. If laser machining were still used an alternative laser source, such as the Nd:YAG, would be required.

6.7 REFERENCES

6.1 US Patent no. 5,123,028 "RF Excited CO2 Slab Waveguide Laser" Assignee, Coherent Inc., Palo Alto, Calif. (1992)

Chapter 7

Conclusions and Future Work

Many uses have been found for high power CO_2 slab waveguide lasers, in both industry and manufacturing. They are used for amongst other things welding, cutting and marking. This laser is generally well suited to these applications, however where output wavelength or beam position is of critical importance this laser can falter.

This thesis has aimed to address this stability issue, offering one possible solution which fulfils a number of criteria namely; maintaining the general layout of the existing laser, loosing not more the 10% of the available power, and being able to operate the laser solely on one predetermined line. These criteria have been met by the inclusion of a periodic grid pattern on one of the electrode walls.

Processes have been demonstrated to allow this patterning of aluminium plates, to a standard and with the speed which would be acceptable for use in a manufacturing environment.

The passive transmission of a waveguide containing such patterns has been found to be wavelength dependent, with transmission maxima located as expected. Two dimensional patterns have been shown to provide an optical wavelength filtering device capable of accepting incoming radiation over a range of incident angles, not just with normal incidence as in the case of a 1D device.

The final section of the thesis described for the first time, the inclusion of patterning on the electrode used within a laser cavity. One of the electrodes from a standard laser, constructed to industrial specifications, has been replaced with an electrode patterned with a periodic grid pattern at the focal point of the cavity. The period of this pattern was chosen to lock the output wavelength to the 10P20 transition. The output from the laser was consistently maintained at 10P20 with a stable beam shape, an output state long sort after by manufacturers and users of this type of laser.

However this solution offers only an intermediate outcome for this problem, the ability to choose wavelengths away from the central wavelength of the laser is not yet possible. In order for this research to be carried forward the strength of the effect investigated throughout this thesis has to be increased.

The next step which must be taken in this area of research is to construct a theoretical model of the scattering processes present in these optical filters. This model could then be used to plan future work, some possibilities for which are listed below.

- The area covered by of the grating could be increased. Recently the group has purchased equipment which allows for greater areas to be marked, resulting from greater travel in translation stages.
- Varying the dimensions of the grating may lead to an increased effect, either altering the spacing to allow for lower order grating, changing the fill factors or machining grooves to greater depths.
- The electrodes could possibly be coated with a polymer that is then removed to leave a pattern of rods/dots above the surface, scatterers projecting into the

waveguide gap may have a larger effect than those in the waveguide wall. One polymer that could be used for this is polyimide, recent machining trials in polyimide have shown it to be very resistant to CO_2 radiation, with a low absorption coefficient at the 10.6μm wavelength. Thus it may be possible to incorporate polyimide coated electrodes into a cavity without damage being caused to either the electrode or the coating.

- The pattern could be machined in a tilted section of grating protruding into the waveguide gap. The tilted area of the electrode would cause the path of the waveguide mode to be altered, this could be corrected for by an adjustment in mirror alignment. To minimise any alteration in mode difference from the waveguide, it would be desirable to have the tilted region close to the end of the guide.
- If a true PBG were to be created the possibility exists to include rods, possibly made from ZnSe across the entire waveguide gap. Obvious considerations of discharge instabilities would have to be carefully considered in this case, as would possible methods for construction of such rods.

This preliminary study has shown great promise for future use of patterned electrodes in hollow slab waveguide devices. With further research this new area of research could provide a method of wavelength selection and stabilisation techniques for not just CO_2 lasers but for other types of hollow slab waveguide lasers.